The Role of m^{6}A RNA methylation in chikungunya virus Replication

Veronica Anne DeJesus

Submitted in accordance with the requirements for the degree of
Doctorate of Philosophy

The University of Leeds
Faculty of Biological Sciences

February 2024

The candidate confirms that the work submitted is her own and that appropriate credit has been given where reference has been made to the work of others.

Acknowledgements

Many thanks to the Wellcome Trust for funding this PhD and providing a programme that allowed me to experience different areas of structural biology before starting my PhD project.

First and foremost, thank you to my supervisors. To my primary supervisor Dr Andrew Tuplin thank you for encouraging my interests, being open to discussion, and for allowing me to grow as an independent scientist. Thank you to Dr. Julie Aspden for all of your scientific advice throughout my PhD and for your invaluable help in applying for post-docs. I am very grateful for the time you spent preparing me for my interview and the encouragement to apply for a role that really excited me. Thank you to Professor Adrian Whitehouse for your support and scientific advice throughout my PhD it has been a great help.

Thank you to the members of the Tuplin Lab, including those who have since left the lab: Dr Marietta Mueller, Dr Oliver Prosser, and Magdalena Karwatka. Thank you to Kaiwen Sun for being a helpful and kind lab mate. Thank you to Dr Kate Loveday for the laughs even when we were going through it and for being a friend as well as a supportive lab mate. Thank you to Fran Appadoo for always being there to digest our sometimes confounding results and chatting dogs and life. Thank you to Dr Grace Roberts for throwing candy at me and Anya Morrison for morning TV debriefs. Thank you to members of the Whitehouse group, Dr Oliver Manners and Dr Belinda Baquero for your guidance on the m^6A methods.

Thank you to Katie Allott. Your work on the trans replicon in Huh7 cells was extremely helpful in developing the story of this project. You were an utter joy to work with.

Thank you to Sarah Menzes. You did so so so much in such a short time with me! You were persistent and intensely hardworking. You are curious and motivated and I am excited to see what you do. Your project using the trans replicon in mosquito cells provided an interesting dimension to this project.

Alright. Guys, you five have been just something else. I could not have asked for a better bunch of friends to go through this process with.

Dr Amy Turner, I am just so glad we met, I absolutely adore you and am eternally impressed by your intelligence and silliness in equal exuberant abundance.

Dr Ben Lane, you are an absolute angel. You so often have the correct answer and the soundest advice around. Thank you for being my friend. I value your opinion so highly because I know it will always be considered and with my wellbeing in mind.

Dr Chris Smith, you have been a familiar face and I have always appreciated our impromptu catch ups.

Dr Fran Chandler you are always so up for adventures! Walking, concerts, travels, excited for more with you! I feel very lucky to have you in my corner. You are such a powerhouse.

Dr Molly Gravett, you are simply a star. Strong, caring, and extremely thoughtful. I am so excited to see all that you do! You have been a great support in both career and personally.

Thank you also to Dr Michaela Agapiou (WOOOOO *high five), Alex Flynn (my intensely fun and smart friend), Rachel Tran (a beautiful blue soul), and Dr Jaimie Pitts (roller on!).

Thank you to Zoe Rand and Ariela Schnyer for all the love and support from the other side of the Atlantic. Our synchronized yoga sessions and group chat sustained me.

Thank you finally to my family. To my mom, Gillian McMillan, you have been a massive support throughout my entire academic journey. I just simply could not have done this without you. You made all the difference. To my dad, Yady DeJesus, you are always there without question, always putting my best interests even above your own, and I am so grateful I could make you proud. *Estoy nadando en estos aguas para nosotros dos*. To my brother, Neil DeJesus, I am so lucky to have such a caring and lovely brother. Thank you for your balance and perspective.

Contributions

My own contributions, fully and explicitly indicated in the thesis, have been: all live CHIKV work, MeRIP development, all experimental design, shRNA knockdowns in human cell lines, c3Ado work, and in-silico analysis.

Some research contained has been carried out as part of a team. The other members of the group and their contributions have been as follows: Katie Allott (under my direct supervision) the *trans* replicon experiments in Huh7 cells, including c3Ado and $96^{A>G}$ experiments. Sarah Mendes (under my direct supervision) *trans* replicon experiments in C636 cells, including c3Ado and $96^{A>G}$ and $11749^{A>G}$ experiments. Kate Loveday performed nanopore sequencing of the $96^{A>G}$ ICRES plasmids and RNA isolated from cells transfected with that RNA.

Abstract

Chikungunya virus (CHIKV) is an emerging human pathogen transmitted through the mosquitoes *Aedes aegypti* and *Aedes albopictus*. CHIKV has a widening distribution due to the impact of globalization, including changing land use and international travel and trade. Infection with CHIKV in humans can present as severe fever and chronic arthritis, with the virus showing a tropism for the joints. Viruses manipulate hosts cells in a variety of ways including through gene expression at the level of RNA. N^6-methyl-adenosine RNA modification (m^6A) is a common and dynamic RNA modification, which involves the reversible addition of a methyl-group to an adenosine. m^6A has been implicated as an important regulatory signal for replication of other RNA viruses, including Zika virus (ZIKV). This work sought to build a more comprehensive understanding of CHIKV biology and its lifecycle, including viral genome transcription in both human and mosquito cell line systems. Huh7 cells, a human liver cell line, and C636 cells, a mosquito cell line, were primarily used in this study. This work sought to investigate the role of m^6A methylation on CHIKV replication. A small molecule inhibitor, c3Ado, previously used in other studies of m^6A was used to treat human and mosquito cell lines. c3Ado reduces the amount of the methyl donor in the m^6A reaction, SAM, leading to lower levels of methylation in the cell. Treatment with the small molecule inhibitor resulted in decreased viral replication and viral genome transcription in both Huh7 and C636 cells. Knockdown of proteins in the m^6A pathway, Fat mass and obesity-associated protein (FTO) and Wilms' Tumor 1 Associated Protein (WTAP), and site-directed mutagenesis of potential m^6A sites in the CHIKV genome were also performed. These results showed that knockdown of WTAP in Huh7 cells resulted in a decrease in viral replication. This work also suggested the importance of an adenosine (A) at nucleotide position 96 in the CHIKV genome to overall viral replication in mammalian and insect cells. While the importance of 96^A to viral genome replication was shown in a human cell line this could not be conclusively shown in a mosquito cell line. This work adds weight to the hypothesis that 96^A and potentially m^6A

methylation of that position has a pro-viral effect, through an increase in viral genomic transcription in human cells.

Table of Contents

List of Tables

List of Figures

List of Appendix Figures

List of Abbreviations

°C - degrees celsius

3'- three prime

5' –five prime

Ad5 – adenovirus type-5

ALKBH5 – ALK homolog 5

APS – ammonium persulfate

BHK-21- baby hamster kidney cells

c3Ado - 3- deazaadenosine

cDNA - complementary DNA

CHIKV – chikungunya virus

Cryo-EM – cryo electron microscopy

DC-SIGN - DC-specific intercellular adhesion molecule-3-grabbing non-integrin

ddH_20- double distilled water

DENV – dengue virus

DMEM- Dulbecco's Modified Eagle Medium

DMSO - dimethyl sulfoxide

DNA – deoxyribonucleic acid

dsRNA- double-stranded RNA

D.melanogaster - Drosophila melanogaster

EBV - Epstein-Barr virus

ECSA - East/Central/South African strain of CHIKV

EV71 – Enterovirus 71

E. coli - *Escherichia coli*

FBS- foetal bovine serum

GAPDH - glyceraldehyde 3-phosphate dehydrogenase

gvRNA - genomic viral RNA

HBV - hepatitis B virus

HCV - hepatitis C Virus

HIV-1 - human immunodeficiency virus 1

HMPV - human metapneumovirus

hpi- hours post infection

hpt: hours post transfection

IAV – influenza Virus A

IC - infectious clone

IgG - immunoglobulin G

ISGs - interferon stimulated genes

KIAA1429/VIRMA - vir like m^6A methyltransferase associated

KSHV - Kaposi's sarcoma-associated herpesvirus

lncRNA - long non-coding RNAs

Mxra8 - matrix remodelling associated 8

MDA-5 - melanoma differentiation associated gene-5

METTL14 - methyltransferase 14, N6-Adenosine-Methyltransferase Subunit, KIAA1627

METTL16 - methyltransferase 16, N6-methyladenosine

METTL3 - methyltransferase 3, N6-adenosine-methyltransferase complex catalytic subunit

MOI - multiplicity of infection

MOPS- 3-N-morpholinopropanesulfonic acid

m^6A - N^6-methyl-adenosine RNA modification

ncRNA - non-coding RNAs

nts - nucleotides

ORF - open reading frame

PBS- Phosphate Buffered Saline

PCR- polymerase chain reaction

PEDV - porcine epidemic diarrhoea virus

PFU/mL - plaque forming unit per millilitres

RD - human rhabdomyosarcoma

RdRp – RNA dependent RNA polymerase

RIG-1 - retinoic acid inducible gene I

RNA – ribonucleic acid

RISC - RNA induced silencing complex

RNAP - RNA polymerases

RBM15B - RNA-binding motif protein 15

RSV - respiratory syncytial virus

RT-qPCR - reverse transcription quantitative real-time polymerase chain reaction
SAM - S-Adenosyl methionine
SARS-CoV2 - severe acute respiratory syndrome coronavirus 2
SDS-Page- sodium dodecyl sulphate–polyacrylamide gel electrophoresis
SFV - Semliki Forest virus
SHAPE - selective 2′-hydroxyl acylation analysed by primer extension
siRNA - single stranded complementary sequence
ssRNA - single-stranded RNA
SINV - Sindbis virus
SL- stem loop
SLC - Slc6a19
SV40 - simian vacuolating virus 40
TIM-1 - T-cell immunoglobulin and mucin 1
TEMED - tetramethylethylenediamine
Tris-HCl - Tris hydrochloride
TBS - Tris Buffered Saline
UTR – Untranslated Region
VEEV - Venezuelan equine encephalitis virus
vRNA – viral RNA
VSV – Indiana vesiculovirus
WAF - West African strain of CHIKV
WTAP - Wilms' tumour 1-associating protein
WNV – West Nile virus
YTH - YT521-B homology
ZIKV – Zika virus

Chapter 1
Introduction

Chikungunya virus (CHIKV) is an enveloped positive stranded RNA virus within the Alphavirus genus and family Togaviridae[1]. This major public health threat, with epidemic potential, is an arbovirus, meaning that it is transmitted by an arthropod vector. CHIKV is transmitted by the mosquito *Aedes aegypti* and due to adaptive mutations and expansion of host-range, is now effectively transmitted by *Aedes albopictus* [2]. Due to the impact of globalization, including changing land use and international travel and trade, the range and reach of mosquito-spread viruses are expanding[3]. This makes the search for tools to tackle infection imperative. Infection with CHIKV in humans can present as severe fever, rash and chronic arthritis with the virus showing a tropism for the joints[3]. The virus was given its name for the disease it causes in human patients, commonly presenting as debilitating arthritis. “Chikungunya” means “that which bends up” in the Makonde language of Mozambique/Tanzania [4,5]. With no specific antivirus drugs available current treatments are limited to palliative care of symptoms[6]. On November 9, 2023 a vaccine, named IXCHIQ, developed by the biotechnology company Valneva Austria GmBH was approved as by the US FDA for use in specific populations[7,8]. This is an excellent and exciting development in the potential prevention of CHIKV but continued study will help improve treatment and further development of vaccines in the future. This study aimed to build a more comprehensive understanding of the molecular biology and interactions essential to controlling CHIKV’s replication within both their human and mosquito host cells to inform the development of targeted therapeutics and vaccines for this re-emerging threat.

1.1 CHIKV Epidemiology

1.1.1 Transmission and geographic range

CHIKV circulates in tropical and subtropical regions of Africa, Asia, and The Americas through *Aede*s species mosquito vectors[9], with the geographical range of the virus having expanded in recent decades. CHIKV was first isolated by Lumsden et al. (1955) in 1952-1953 during an outbreak in present-day Tanzania [10]. It was described as a dengue-like fever that was likely primarily spread by *Aedes aegypti* mosquitoes and afflicted between 13-95% of the local human population, depending on the specific location in the Makonde Plateau[10]. Prior to laboratory tests, the severity of the arthralgia associated with CHIKV infection was the main feature that distinguished it from infection with Dengue virus (DENV)[11]. Reclassification of historical epidemics is fraught with potential misclassifications. However, it is becoming increasingly apparent that a number of past epidemics classified as DENV outbreaks, such as in the Americas in 1827-1828, may have been associated with CHIKV infection[11]. According to phylogenetic analysis, CHIKV has likely been circulating for hundreds of years, with the disease symptoms being treated and studied in Asia and Africa[9, 12].

There are three distinct genotypes of CHIKV, based on the amino acid sequence of the envelope protein (E1), and which are named for their historical geographic distribution: The West African (WAF), East/Central/South African (ECSA), and Asian genotypes[12,13]. Volk *et al.* 2010 describes the two transmission cycles of CHIKV as enzootic/sylvatic and urban/endemic/epidemic[12]. The two African genotypes WAF and ECSA CHIKV maintain this likely ancestral sylvatic/enzootic cycle with non-human primates acting as a reservoir [14]. The virus circulates in primate populations through primatophilic species of *Aedes* spp. mosquito and spills over into human populations periodically **(**Figure 1) [14].

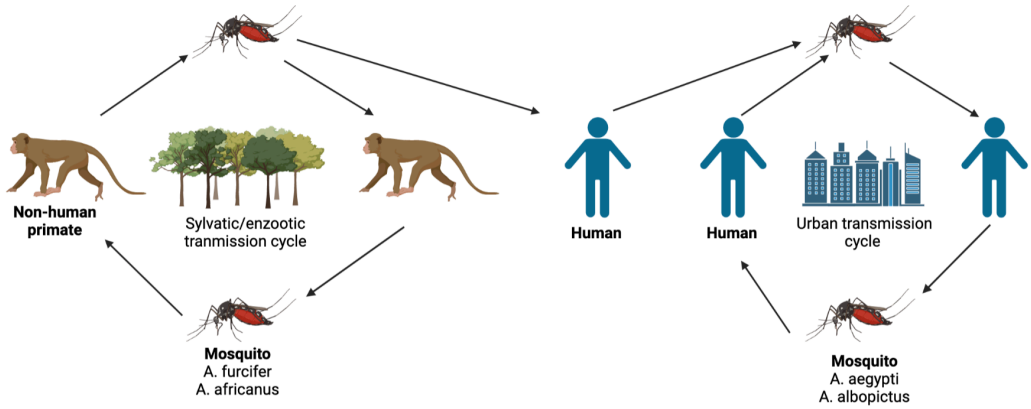

Figure 1. CHIKV transmission cycle

Model of CHIKV transmission showing the sylvatic/enzootic transmission occurring between non-human primates transmitted primarily by primatophilic mosquitoes *Aedes fucifer* and *Aedes africanus*. When one of these infected mosquitoes transmits to a human this can introduce CHIKV into the urban transmission cycle primarily cycling through *Aedes aegypti* and *Aedes albopictus*. Adapted from Madariaga et al. 2016 [14].

created using BioRender

From a study in Senegal, the arboreal mosquito *Aedes furcifer* has been proposed as the vector of enzootic spill over into humans, based on landcover and mosquito behaviour [15]. Under the urban transmission model Volk *et al.* 2010 estimate higher levels of nucleotide substitution, suggesting higher mutation rates in the urban transmission cycles than the enzootic cycles [12].

The ECSA genotype is also endemic in urban transmission networks in many areas both within and outside of Africa, and has given rise to what is known as the Indian Ocean epidemic lineage, which is responsible for many recent outbreaks [16]. Specifically, there was the $226^{A>V}$ mutation in the E1 envelope protein (E1 will be introduced in greater detail later in this chapter, Section 1.3.3) of an ECSA lineage CHIKV, which allowed the virus to be transmitted by *Aedes albopictus* with greater efficiency [17]. For the Indian Ocean lineage, the primary method of transmission within the human population is endemic spread. However for instance in areas like India

where it is not believed to be endemic, antibodies detected in the population suggests a possibility of enzootic spread [16].

The expansion of CHIKV endemic regions closely follows that of its primary vector hosts, *Aedes aegypti* and *Aedes albopictus* [9]. *Aedes albopictus* is aggressively establishing itself in a spread west and north into more temperate regions across the Americas, Africa, and Asia[18]. *Aedes. albopictus* continues to spread outside of its historical range through passive transport by humans, notably international shipment of used tyres[18]. Once the mosquito has been transported they adapt to colder winters by: lying dormant, utilizing high levels of protective larval lipogenesis, and opportunistic choice of host to thrive[18]. Increased travel by viraemic patients who are bitten by mosquitoes also spread CHIKV in new locations.

CHIKV re-emerged in Kenya in 2004, before epidemic spread into the Southwest Indian Ocean (2005) and Indian subcontinent (2006) [19]. Outbreaks of imported Asian genotype CHIKV in the Caribbean and Central America (2014) have supported the continued global spread of this virus [16,19,20] (Figure 2.A). In their review of published CHIKV outbreaks Bettis *et al.* 2022[21] show CHIKV prevalence increasing steadily with time, most prominently in the Americas and Asia (Figure 2.B). Coinfection of CHIKV and DENV is on the rise in North Western India, where both viruses circulate regularly, and has been leading to significant cases of arthralgia and thrombocytopenia in coinfected patients[22].

With the spread of the virus intrinsically linked to the spread of its vectors, another consideration is CHIKV's evolution into new hosts species of mosquito, through mutation and/or location opportunity. In 2019, it was reported that the native European *Aedes genicultus* mosquito was both susceptible to CHIKV and able to transmit the virus[23]. This indicated at least one new potential vector, and consequentially new avenues for viral transmission and possible continued global spread of CHIKV. When considering CHIKV it is important to consider the adaptability of the virus and lifecycle in both of its hosts, because the vector plays a major role in its global spread and epidemic potential of the virus.

A

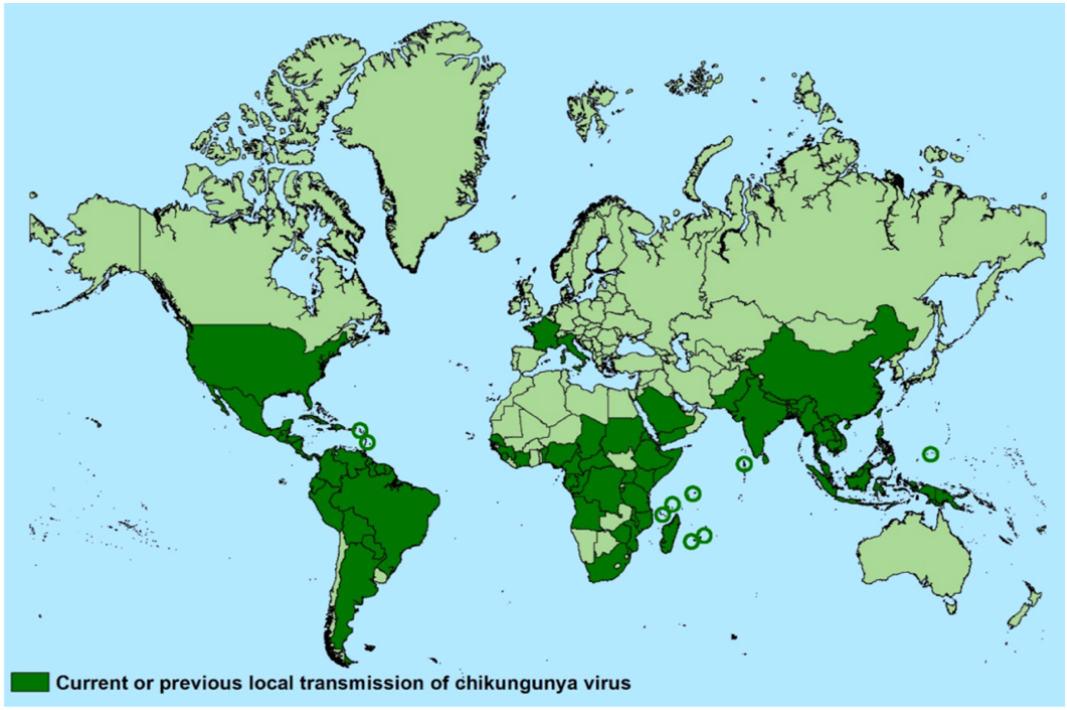

B

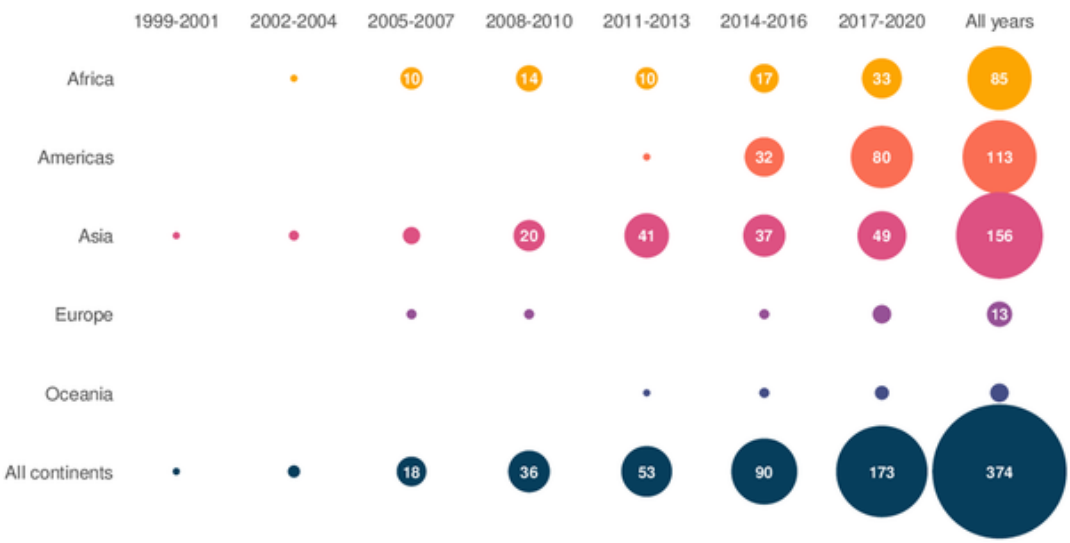

Figure 2. Global CHIKV Distribution

A. Global distribution of local transmission of CHIKV shaded in darker green as of 2022 according to the United States' Centre for Disease Control (CDC). [20]

B. CHIKV Outbreak studies from references published in 1999-2020 This figure reproduced from Bettis *et al.* (2022)[21] shows the number of CHIKV outbreak studies from 1999 to 2020 and breaks them down by region to show the growth in CHIKV studies and spread of importance of this pathogen globally [21].

1.2 CHIKV Virology

The CHIKV virion is approximately 60-70 nm in diameter, enveloped by a host derived lipid membrane with icosahedral symmetry dotted with spike glycoproteins (Figure 3) [24].

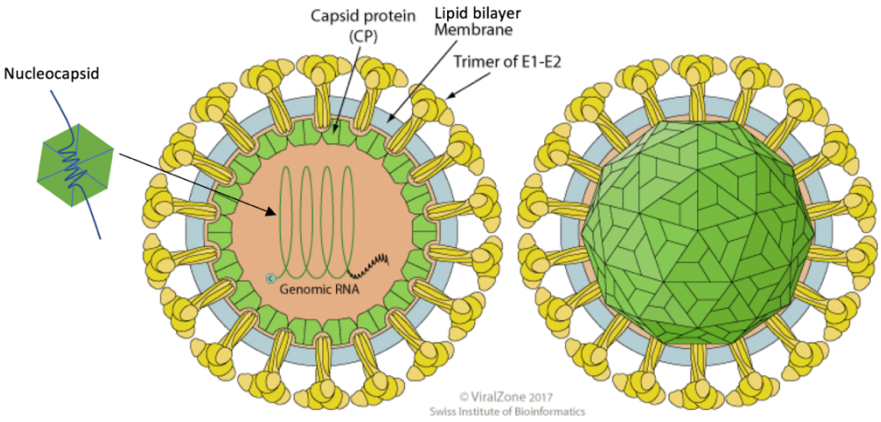

Figure 3. Alphavirus virion

The alphavirus has spherical shape which is made up of a host derived lipid bilayer, into which is embedded the viral spike proteins. The viral spike proteins are composed of 240 copied of the E1-E2 glycoproteins which form 80 trimer spikes which protrude from the surface of the virion[25]. Inside of the lipid bilayer the virion contains the nucleocapsid. This consist of 240 copies of the capsid protein forming an inner shell to further protect the positive strand genomic RNA. Adapted from Hulo et al. 2011 [26] and Mendes and Kuhn 2018[27].

The glycoprotein spikes (E1 and E2) mediate entry into the cell and facilitate fusion of the viral lipid envelope with the endosomal membrane to release the viral genome into the host cell cytoplasm[28]. The viral genome is a single stranded positive sense RNA molecule and shares features similar to eukaryotic mRNA, including a 5' type-0 N 7-methylguanosine cap structure as well as a 3' poly(A) tail [28]. The cap allows the viral genomic RNA to be protected from cellular nucleases and initiates ORF-1 translation of the viral non-structural proteins which make up the replication complex [28]. The viral

RNA (vRNA) is translated by the host ribosomes and translation machinery to produce the viral proteins necessary for its lifecycle. Elements such as a termination codon read through element (TCR) which dictates translational recoding and 5' end RNA secondary structural elements are necessary for efficient CHIKV genome replication [29],[30].

1.3 CHIKV Lifecycle

1.3.1 CHIKV Genome Organization

The CHIKV genome is organized into two distinct open reading frames (ORF) that are joined by a junctional (J) noncoding region (68 nts)[31]. The two ORFs are flanked with a 5' untranslated region (5'UTR) containing a eukaryotic-like cap structure (76 nts) and 3' untranslated region (3'UTR) with a poly(A) tail (526 nts)[31]. The CHIKV full-length positive RNA strand has a 5' type-0 N 7-methylguanosine cap structure which is synthesized and added by the viral protein nsP1[32,33]. CHIKV protein sequence and function have been mapped in relation to other closely related but better studied alphaviruses such as Semliki Forest Virus (SFV) and Sindbus virus (SINV)[34].

Kallio *et al*. 2016 found that in SFV spherule formation and negative strand synthesis was cap independent but uncapped positive transcripts are more readily degraded and poorly translated[35]. This suggested that the capping activity of nsP1 may also be important for longevity of the CHIKV transcript in the cell and possibly uncapping which can also be performed by nsP1 is involved in the switch from transcription to translation of the full length positive RNA[36].

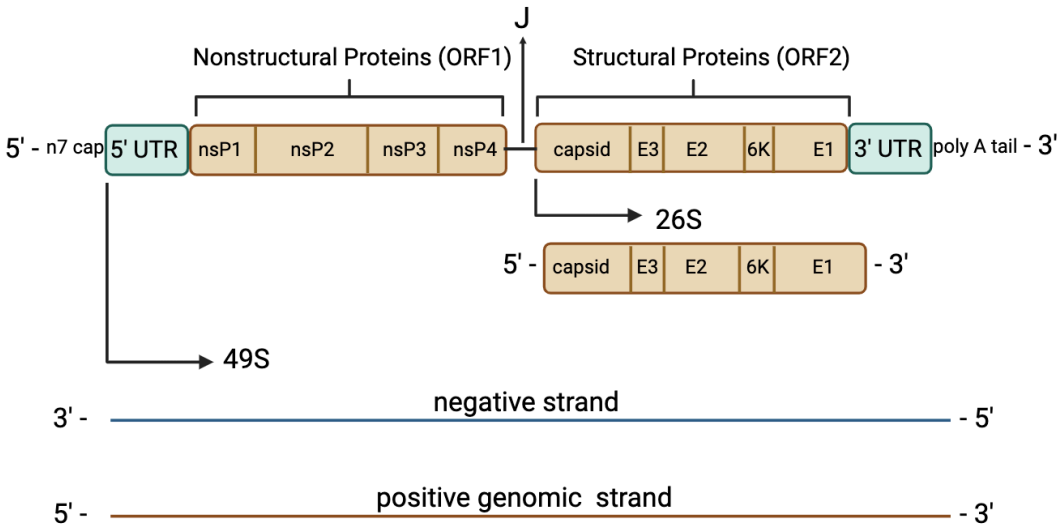

Figure 4. CHIKV Genome Organization

CHIKV genome has a positive single-strand RNA genome (RNA at the very top of the figure depicted with green and orange boxes) It has a 5' cap, a poly A tail, 5' and 3' untranslated regions (UTRs) coloured green, and two open reading frames (ORFs) coloured orange joined by a noncoding Junction region (J). ORF1 encodes for the four non-structural proteins that go on to make up the RNA replication complex. ORF2 encodes for the structural proteins that make up the viral capsid. The RdRp generates a negative strand intermediate which acts as the template for both additional full-length positive strand RNA and for a sub-genomic 26S positive strand which is translated by the ribosome to make the structural proteins. Modified from An et al. 2017 [31].

created using BioRender

CHIKV proteins are translated sequentially, with the translation of ORF1 occurring first to produce the nsP1234 polyprotein, which then goes on to be processed further through proteolytic cleavage by nsP2. nsP1234 is cleaved sequentially into single proteins nsP4 and nsP1 and two polyprotein forms nsP123 and nsP23 [28],[24]. The four non-structural proteins, along with host proteins, make up membrane bound replication complexes or spherules, type 1 cytopathic vacuoles[37]. These localize at the plasma membrane of the host cell which are the site of CHIKV genome replication[37]. This includes synthesis of the negative strand intermediate and positive stand copies of the initial genomic strand of viral RNA[37]. ORF2 is translated from a 26S mRNA, that encodes the structural polyprotein that undergoes processing to form the structural proteins of the CHIKV virion.

1.3.2 Non-structural proteins (nsPs):

nsP1 is the primary enzyme involved in capping the CHIKV RNA[28]. Using a Venezuelan Equine Encephalitis Virus (VEEV) nsP1 *in vitro*, as a model of alphavirus nsP1, Li *et al*. 2015 [38] built on work done using another alphavirus SINV[39]. Li et al. showed that nsP1 caps alphavirus RNA at the 5' end through three steps: acting as a methyltransferase (MTase), performing the guanylylation (GTase) of nsP1, and finally the transfer of the m^7GMP from nsP1 onto the viral RNA [38]. Cryo electron microscopy (Cryo-EM) structures of CHIKV nsP1 solved in the last two years showed the top of the protein contained a dual MTase GTase enzymatic domain, while the bottom of the protein was composed of two ordered hydrophobic loops believed to be involved in tethering to the membrane and oligomerization of the protein into a twelve-membered ring [32,33]. Zhang *et al*. 2022 published work showing this same sequential reaction, in which nsP1 synthesizes and adds the cap onto the 5' end of the positive strand viral RNA [36]. Their work by Cryo-EM showed snapshots of CHIKV nsP1 in complex with molecules relevant to vRNA capping, to better understand the CHIKV capping process. They determined that nsP1 engages with vRNA in a sequence specific manner and that a catalytic pocket coordinates the viral RNA capping process. It was in this pocket that the first reaction, the MTase activity using SAM as the methyl donor added a methyl group to N7 position of GTP to form m7GMP. Next the triphosphate RNA and the m7GMP are coordinated by Mg^{2+} ion. A1 and U2 of the CHIKV RNA were found to be essential to forming necessary base-specific hydrogen bonds to nsP1 within this pocket. This work was built on by Tan *et al.* 2022 who showed the multiprotein CHIKV replication complex by Cryo-electron tomography (Cryo-ET) and visualized the twelve-membered nsP1 crown-like complex at the plasma membrane as the budding spherule forms.

nsP2 is a helicase-protease, responsible for sequential proteolytic cleavage and processing of the nsP1234 polyprotein, in such a way as to provide temporal control to the production of negative, genomic and sub-genomic 26S RNA from the replication complex [24]. The C-terminal region contains the protease domain [24]. nsP2 is recruited to the membrane by interaction with

nsP1 [40]. Cryo-ET of CHIKV infected cells showed nsP2 at the base of the neck of the spherule, which formed at the plasma membrane surface [40,41]. The nsP2 helicase domain structure has been solved in complex with the 3' region of the CHIKV genome [42]. These showed specific RNA recognition sites which disrupt binding to the genomic RNA, which are be essential for synthesis of the non-genomic negative stand [42]. nsP2 also plays a proviral role in the degradation of the RPB1 subunit of RNA Polymerase II in the nucleus to halt host mRNA synthesis and interrupt innate immune signalling protein function [43, 44, 45].

The specific function of nsP3 is still unclear. However, it is known to be important in organizing interactions with host factors and mediating protein-protein interactions [46]. It is integral to the production of the negative strand vRNA and the production of the 26S vRNA, but the mechanism by which this occurs is not yet fully understood [46]. nsP3 is proposed to associate with the RNA replication complex at the budding spherule along with other host factors [41].

nsP4 is the RNA dependent RNA polymerase (RdRp). Only once nsP4 is cleaved from the nsP1234 polyprotein by nsP2 can it engage in its function. nsP4's function is to synthesize the negative strand RNA intermediates and positive strand RNA copies of the viral genome [37]. nsP4 protein is essential to RNA recognition and replication efficiency [47].

1.3.3 Structural proteins

The capsid protein (C) makes up the inner shell of the virion and associates with viral genomic RNA to form the nucleocapsid, which ultimately gets packaged into the final virion [24]. In SINV the n-terminal region of the capsid protein is integral to RNA biding and packaging [28].

E3 is a short peptide cleaved from PE23. It is thought to not to be associated with the virion but is instead released from infected cells [28]. In SFV and SINV this protein has been suggested to assist the folding of the mature spike protein through a furin-like protease mediated cleavage [28,48].

E2 and E1 are the two protein components of the trimer of heterodimers that make up the spike glycoprotein of CHIKV [24]. Like host membrane-bound

proteins, the CHIKV envelope proteins are folded and post-translationally modified, which includes glycosylation, in the endoplasmic reticulum and Golgi apparatus[49,50]. They are then incorporated into the plasma membrane of the cell, where the nucleocapsid will bud off wrapped in the protective coat of a host derived lipid bilayer and the viral glycoproteins [24].

6K is a Class II.A viroporin, which has a helix turn helix hairpin motif to span lipid bilayer membranes [51,52]. In approximately 10-15% of instances during translation of 6K from the transcript there is a -ORF frameshift when the ribosome encounters an alphavirus conserved slippery sequence UUUUUUA to generate TF (transframe protein) [53]. TF shares 6K's N-terminal region which includes an initial transmembrane domain which underlies ion channel activity[53]. Both 6K and TF have been detected by mass-spectrometry to be incorporated into CHIKV released virions [54,55]. These ion channel proteins are thought to play a proviral role in virus assembly [56,57, 58,55].

1.3.4 CHIKV Lifecycle

The CHIKV lifecycle takes place in a sequential manner that amplifies the virus over time using host and virally encoded proteins (Figure 5). The CHIKV virion attaches to the cell surface through interaction between the E1/E2 viral glycoproteins and the glycosaminoglycans expressed at the cell membrane: mainly T-cell immunoglobulin and mucin 1 (TIM-1), DC-specific intercellular adhesion molecule-3-grabbing non-integrin (DC-SIGN), [59]. Then, though clathrin-mediated endocytosis in conjunction with the cell adhesion molecule: Matrix Remodelling Associated 8 (Mxra8), which is a CHIKV receptor, the virus is taken up into the endosome [59]. In the endosome the pH drops and triggers the fusion of the viral membrane and that of the endosome, releasing the capped positive-strand genomic viral RNA into the cell's cytoplasm [31]. The virus genomic RNA acts as a direct template for the translation of the nsP1234 polyprotein that forms the replication complex and undergoes proteolytic cleavage to generate the sub-genomic RNA that goes on to encode for the structural proteins and copies of the genomic viral RNA (gvRNA)[31]. The CHIKV capsid protein auto proteolytically cleaves itself from

the polyprotein through its serine protease domain [28]. Capsid then combines with the positive gvRNA to form nucleocapsid which buds off from the cell wrapped in a host derived lipid bilayer in which the E1/E2 glycoproteins are anchored [31].

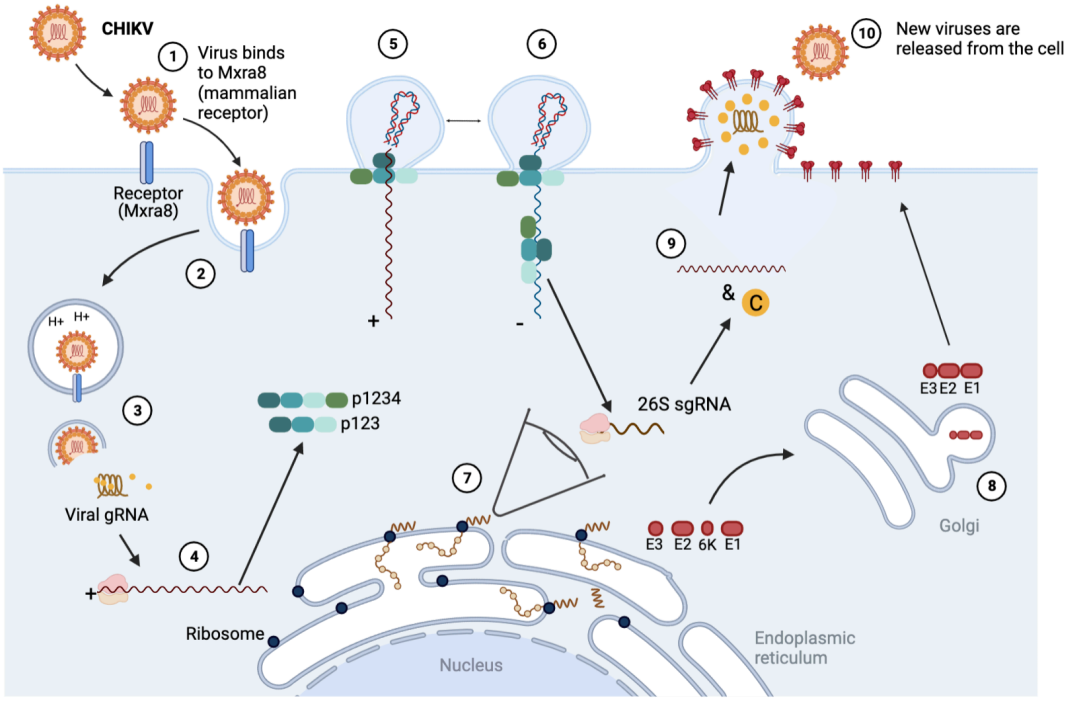

Figure 5. CHIKV Lifecycle

1.Virion binds Mxra8 and **2.** is taken into the cell by endocytosis. **3.** The pH drops in the vesicle which leads to uncoating of the virion and release of the viral genomic RNA. **4.** This +ve single stranded RNA is directly translated by host cell machinery to produce the polyprotein nsP1234. **5.** The nsPs localize to the plasma membrane where they replicate the +veRNA producing the -veRNA replication intermediate. **6.** The -veRNA is used as a template for replication of both full length and the sub-genomic 26S +veRNA. **7.** The 26S RNA is used as a template in the endoplasmic reticulum to encode the structural proteins, including Capsid and the envelope proteins. **8.** The envelope proteins are glycosylated in the Golgi Body and transported to the plasma membrane of the cell. **9.** The full-length genomic RNA is encapsulated by the Capsid protein and localized to the membrane. **10.** The capsid, gvRNA buds from the membrane to form a lipid bilayer bound virion containing the envelope proteins on its surface. Modified from An et al. 2017 [31].

Created using BioRender

1.4 Genome Replication

1.4.1 CHIKV genome is replicated by a replication complex

The CHIKV genomic RNA is replicated by the multiprotein complex made up of the nsPs which form a replication complex to replicate CHIKV RNA. Both positive and negative strands are replicated within membrane bound

spherules at the host cell's plasma membrane[37]. The negative strand is synthesized by the RdRp and serves as the template for both the full length positive and sub-genomic positive RNAs (Figure 6).

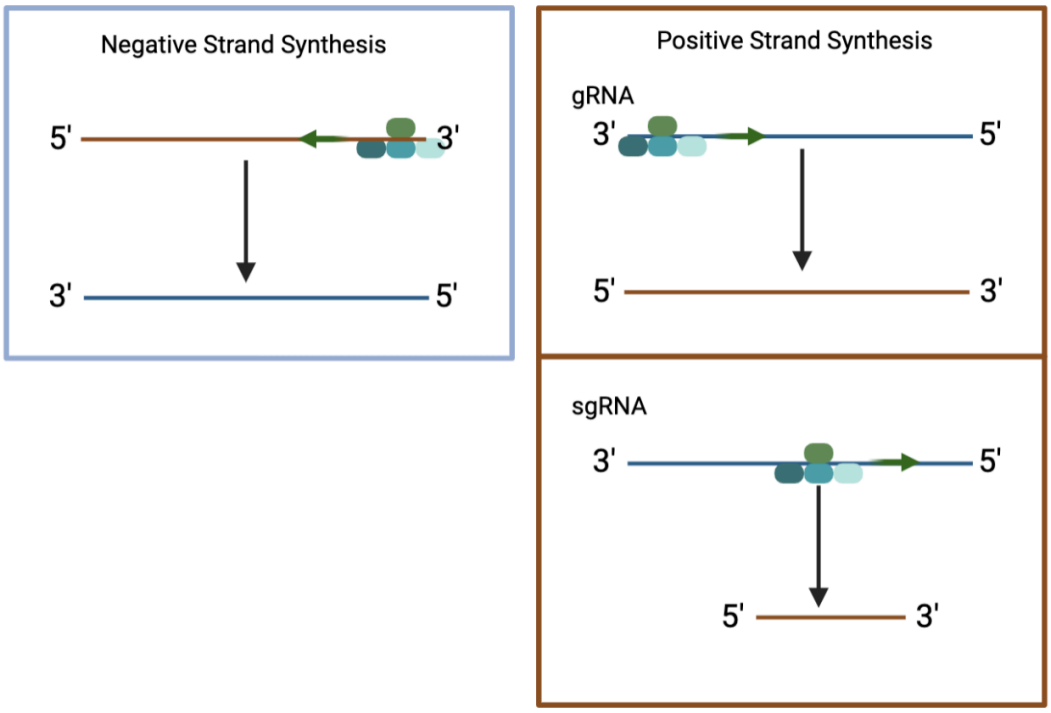

Figure 6. CHIKV RNA synthesis

The viral RNA-dependent RNA polymerase synthesizes both the full length positive (orange) and negative strand (blue) RNA from the corresponding template. This includes the sub-genomic positive strand RNA from the negative full-length RNA template from an internal start site on the transcript. 4 coloured ovals indicate the 4 nsPs involved in the replication complex. Modified from Thal et al. 2007 [60].

Created using BioRender

Genome replication initiates with the production of a double stranded intermediate containing the negative anti-sense copy of the genomic strand. nsP1 tethers to the plasma membrane and recruits the other three non-structural proteins to the neck of the forming spherule. Research on other alphaviruses showed that there was a switch from primary transcription of the negative strand (which is detected earlier on in the replication of the virus) to positive strand transcription, involving specific proteolytic cleavage by nsP2 and suggested rearrangement of the nsPs complex [24]. When fully processed, the CHIKV replicase complex, which also contains essential host

factors shifts to producing the 26S vRNA from the negative stand vRNA[28],[41]. During this stage there is a dramatic shift from translation of host to viral proteins[61].

Recent work by both Laurent *et al.* 2022 and Tan [et al.] 2022 independently published work visualizing the formation of CHIKV replication complexes at the plasma membrane by Cryo-ET [40,41] (Figure 7). Both of their studies showed that multiple units of nsP1 form a ring at the neck of the budding spherule, which then associate with nsP2 and nsP4, with single stranded viral RNA fed through the neck to form the double stranded vRNA isolated from immune sensors within the membrane bound complex. Tan *et al.* 2022 also showed that the likely stoichiometry of the well-ordered replication complex was nsP1+2+4 in a 12:1:1 ratio. nsP3 and other spherule associated proteins (perhaps RNAs as well) are also predicted to localize the area to facilitate the formation of the vRNAs.

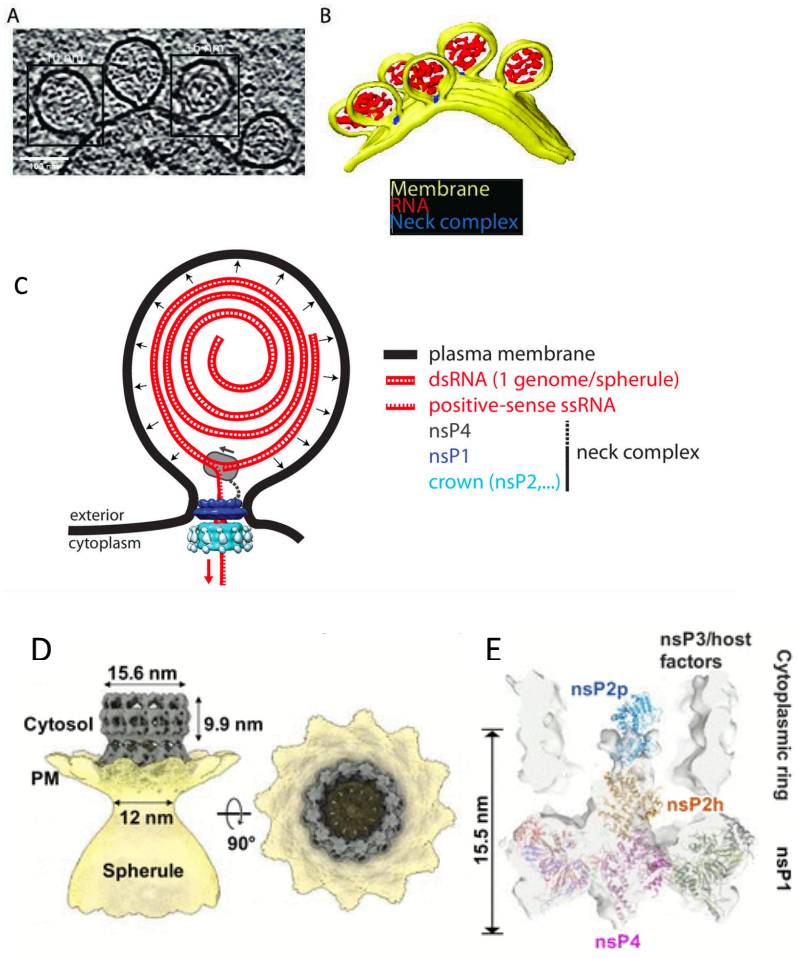

Figure 7. Cryo-electron tomography reconstruction and two published models of chikungunya virus replication complex

Figures taken from Laurent et al. 2022 [40].

A. Cryo-ET of a section from CHIKV replicon transfected BHK cells showing spherule forming at the plasma membrane.
B. 3D segment through the slice showing membrane in yellow, viral RNA in red, and neck complex proteins in blue.
C. A model of the spherule showing the position of viral components and growth through generation of dsRNA.

Figures taken from Tan et al. 2022 [41]

D. Cryo-ET 3D rendition of the spherule showing a cytoplasmic ring made up primarily of nsP1, nsP2, and nsP4.
E. nsP1+2+4 fitted into 3D rendition of the neck region. They propose space also filled by nsP3 and host factors not yet identified.

During transcription the RNA feeds through the RdRp to form the positive and negative viral RNAs, with the double-stranded RNA (dsRNA) protected from the cell's innate immune sensing within the replication complex [40]. Further work published in 2023 by Laurent *et al.* which built on their initial Cryo-ET of the CHIKV spherule suggests that the CHIKV dsRNA occupies the lumen of the spherule uniformly and orthogonally to the RdRp at the neck of the spherule [62]. Self dsRNA, such was siRNAs, and non-self dsRNA, such as the CHIKV viral RNA, elicit different cellular responses. Cellular proteins RIG-1 (retinoic acid inducible gene I) an RNA helicase and MDA-5 (melanoma differentiation associated gene-5) have been identified as the major sensors of viral dsRNA which go on to induce innate immune proteins called Interferons [63]. Interferon stimulated genes (ISGs) are a suite of genes that are triggered by the production of these signalling proteins to induce a strong immune response in the cell, including antiviral proteins which regulate infection [64,65].

1.4.2 CHIKV 5' UTR and nsP1 coding region RNA structures

RNA can form dynamic, complex, and biologically relevant secondary structure. Work published by Kendall *et al.* 2019 and Madden *et al.* 2020 both showed secondary structure mapping of the 5' UTR and nsP1 coding region of the CHIKV genome [66,67]. They used combinations of RNA SHAPE mapping, free energy minimisation and reverse genetic approaches (Figure 8) [66,67]. SHAPE analysis provides information on RNA dynamics by using an electrophilic small molecule, such as the SHAPE reagent NMIA, to probe for available 2'-hyroxyl groups of flexible nucleotides in RNA [68,69,70]. These regions of reactivity can then be detected by primer extension, exonuclease digestion, or next generation sequencing approaches [68,69,70]. In the study by Kendall *et al.* 2019 they identified two stem loops in the 5'UTR region (SL3 and SL47) and five stem loops in the adjacent nsP1 coding region (SL85, SL102, SL105, SL194, and SL246) (Figure 8 A) [66]. They characterised the importance of these structures by disrupting their formation and then restoring their formation by mutagenesis [66]. This allowed them to assess the stemloops' relative function in both mosquito and human cell lines [66]. They

found that SL3 was important for viral replication in both human and mosquito cell lines [66]. SL47, SL85, SL102, SL105, and SL194 were each required for viral replication in only human cell lines [66]. While SL246 was required for viral replication in only mosquito cell lines [66]. In a later study by Prosser *et al.* (2023) the essential 5' CHIKV RNA secondary structures were targeted with antisense locked nucleic acids oligonucleotides (LNAs) and shown to significantly inhibit viral replication [71]. The study by Madden *et al.* (2020) mapped this same region and identified a single stemloop, SL3, and the 5'CSE. Madden's single SL3 corresponded to Kendall's two SL85 and SL102, while Madden's 5'CSE corresponded to Kendall's SL165 and SL194 (Figure 8). The 5'CSE was a conserved structure important for viral replication across CHIKV, SINV, and VEEV [72]. Both of these models indicated important secondary structure in the CHIKV genomic RNA that played a role in viral RNA replication in both their mammalian and insect host cells.

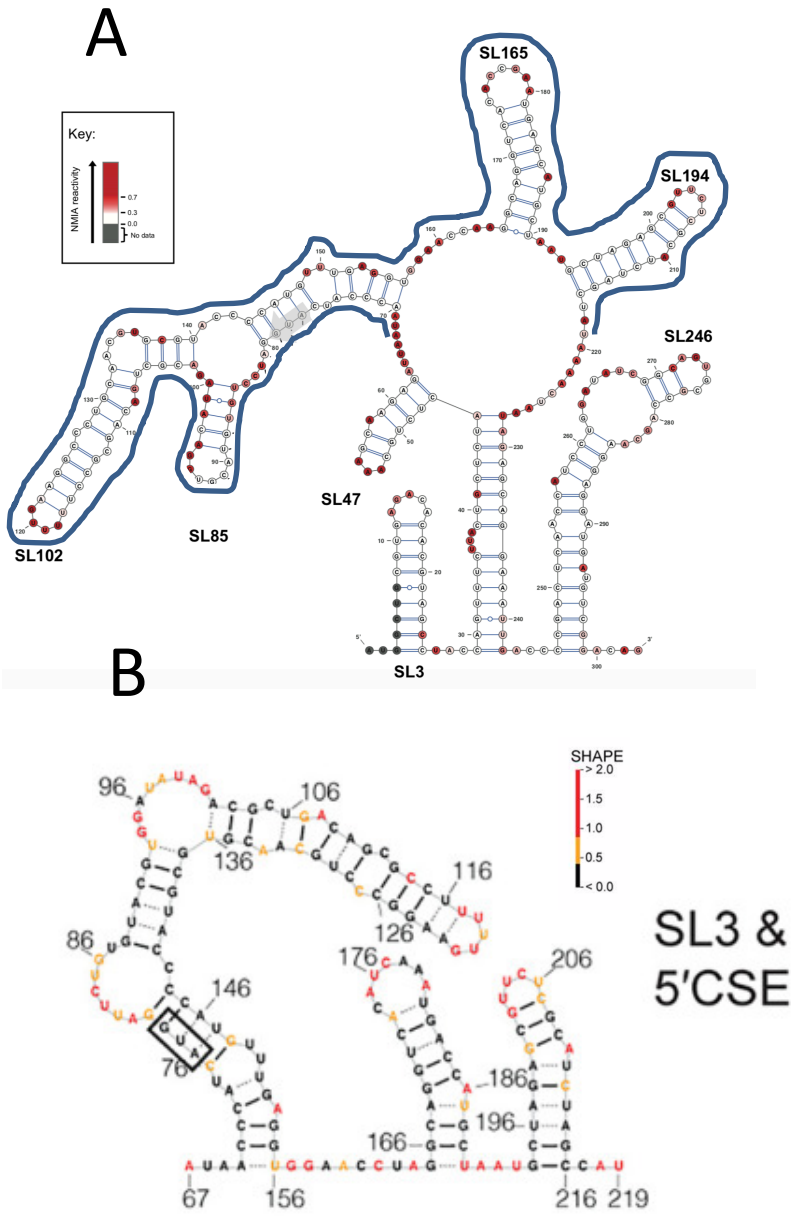

Figure 8. Two models of CHIKV RNA secondary structure in 5' region

A. Proposed structure of the first 303 nucleotides of the CHIKV genome SHAPE mapped by Kendall *et al.* 2019, the start codon was indicated in grey arrow, and the region of the Madden *et al.* 2020 structure shown below indicated by the blue outline to show the same mapped regions on the two alternative models [66]. The analysis performed on this structure shows increasing nucleotide reactivity (which suggests that nucleotide is not base paired) from white, pink, to red.

B. Proposed structure of nucleotide 67 to 219 of the CHIKV genome by SHAPE-Map by Madden *et al.* 2020, start codon outlined by a black box, SL3 and a 5'CSE shown[67]. The analysis done on this structure shows increasing nucleotide reactivity (which suggests that nucleotide is not base paired) from yellow, orange, to red.

1.5 RNA Modification

In the eukaryotic cell DNA is protected in the nucleus, tightly wound, wrapped around histones, and contains all of the information to encode the proteins and molecules that compose the cell. RNAs include the intermediate coding molecule, mRNA, that links DNA to the resultant protein products. Non-coding RNAs (ncRNAs) serve biological functions within the cell acting for example as scaffold or enhancers to biological processes [73]. Pre-mRNA is transcribed by muti-subunit complexes called RNA polymerases (RNAP) I, II, and III [74]. RNAP I and III are responsible for transcribing non-coding RNAs, transfer RNAs and the most highly abundant ribosomal RNAs. RNAP II transcribes pre-mRNAs which are precursors to the protein coding mRNAs [74]. Pre-mRNA contains regions called introns and exons. In the mature mRNA the introns are removed from the transcript, leaving only the exons in a highly conserved process called splicing [75]. Transcription of mRNA, from DNA allows for a level of spatial and temporal control, enabling the cell to rapidly adjust to environmental changes and needs. Chemical modifications to all forms of RNA further allow the cell to control of the fate of the transcript, and make up part of the epitranscriptome [76]. Eukaryotic mRNAs are capped at the 5' end to induce splicing, nuclear export, recruitment of translation initiation factors and self-recognition to protect against innate immune activation [77]. RNA viruses exploit RNA modifications, such as capping and chemical modification, to promote their lifecycle within the cell and evade immune recognition [77,78]. For CHIKV, after the synthesis of the positive strand full-length RNA, the viral protein nsP1 caps the transcript to protect it from degradation and promote translation of the viral proteins. Over 170 chemical RNA modifications have been discovered and occur mostly on the RNA base many with implications on human disease [79]. One of these modifications is N^6-methyl-adenosine RNA modification (m^6A).

1.6 N^6-methyl-adenosine RNA modification (m^6A)

1.6.1 m6A added and removed in a reversible catalytic reaction

m^6A is a reversible and ubiquitous RNA modification, which involves the addition of a methyl group to the N^6 position on the adenosine [80] (Figure 9.A). m^6A modification to RNA was initially described in the 1970s [81,82] and has been under investigation since to determine its role in cell biology, including virology, cancer, and metabolism.

A.

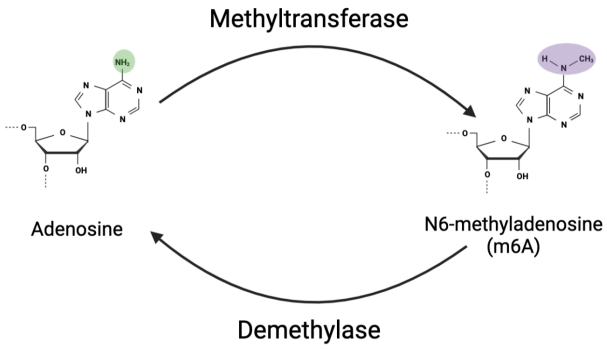

B

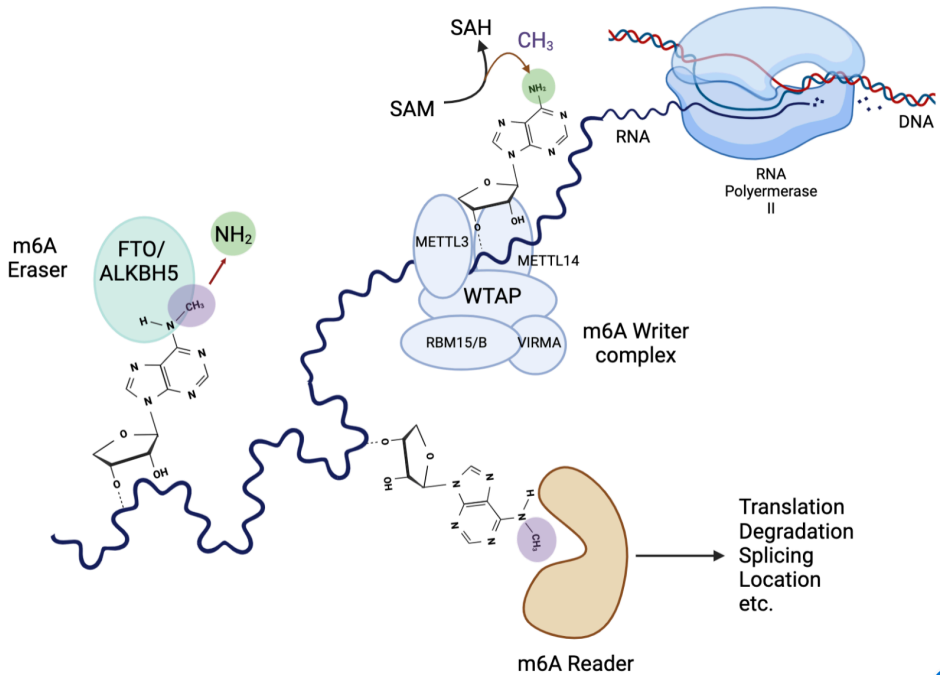

Figure 9. m^{6}A addition, removal, and recognition by cellular proteins

A. Methylation of an adenosine at the N6 position on the molecule is catalysed by a methyltransferase and removed by a demethylase. The chemical structure of adenosine and m^{6}A are shown with the unmethylated N6 position in green and the methylated N6 position in purple.

B. RNA is transcribed from DNA by RNA polymerase II. Methylation of the N6 position of an adenosine takes place by the multiprotein m^{6}A writer complex with SAM acting as the methyl donor. The m^{6}A mark is read by a variety of m6A reader proteins directing the transcript to a multitude of fates. The methylation can be removed by an m^{6}A eraser protein, restoring the adenosine to its initial state.

Figure created using BioRender. Information adapted from Manners *et al.* 2019 [83].

The m^{6}A reaction is catalysed by a large multiprotein complex of ~1100kDa in size[84]. The catalytic protein METTL3 acts as the methyltransferase and forms a strong dimer with METTL14 [85,86] (Figure 9.B). S-adenosyl methionine (SAM) acts as the methyl donor molecule in the reaction catalysed by METTL3 [80]. The methyl group is mostly added at a highly conserved sequence termed the DRACH site (D = A, G, or U; R = G or A; H = A, C or U)[87]. m^{6}A sites are often clustered on the transcript but approximately 20% of m^{6}A modified residues are outside of the DRACH sequence [88,89]. In mammalian transcripts 70% of the m^{6}A modifications are present in the last exons with >40% in the 3'UTR [90]. m^{6}A modifications generally appear around stop codons and in long internal exons. Recent work by Schwartz *et al*. 2023 propose a model that all m^{6}A consensus sequences are modified unless they are within 100 nucleotides of a splice junction and that exclusion from these sites are dictated by a likely physical exclusion from these zones by proteins that make up the Exon Junction Complex (EJC) [91].

METTL3, was first reported by Bokar *et al.* in 1997 [92]. This approximately 65 kDa protein was shown to have similar methylation motifs to prokaryotic DNA m^{6}A methyltransferases and to bind SAM [84]. METTL14 stabilizes the structure and increases the methylation activity of METTL3 [93]. Warda *et al.* (2016) also identify METTL16 as an alternative m^{6}A methyltransferase protein, primarily acting on non-coding RNAs (ncRNA), long non-coding RNAs (lncRNA), and intron regions of pre-mRNAs [94].

Other proteins make up the m^{6}A writer multiprotein complex and act as scaffold, including Wilms' tumour 1-associating protein (WTAP)[95]. WTAP makes up the core of the methyltransferase complex with METTL3 and METTL14. WTAP acts as an adaptor protein and interacts with RNA polymerase II [96]. WTAP has been shown to be required for m^{6}A methylation[97]. WTAP dependent m^{6}A sites are reduced in highly expressed housekeeping genes, likely to protect them from m^{6}A induced degradation[97].

Another essential component of the complex is KIAA1429 encoded by the VIRMA gene. It is the largest protein in the methyltransferase complex (200

kDa); it has been shown in immunoprecipitation assays to associate with WTAP and its depletion leads to lengthening of transcript 3'UTRs and reduced levels of m^{6}A methylation [97,98]. RNA-binding motif protein 15 (RBM15B) recruits the methyltransferase complex to RNAs [99]. It has been shown to localize primarily to the nucleus, residing in nuclear speckles [100] but has also been detected in the cytoplasm. Due to its role in the m^{6}A methyltransferase reaction KIAA1429 also has been proposed as a target in the treatment of SARS-CoV-2, for disruption to essential m^{6}A methylation [101].

The methyl group can be removed from m^{6}A methylated transcripts by oxidative demethylases: fat mass and obesity-associated protein (FTO) and ALKBH5, making this methylation a dynamic mark on the transcript [102,103,104]. Both FTO and ALKBH5 are in the same family of AlkB protein dioxygenases. Experimental reduction of FTO in mammalian cells increased detectable m^{6}A and overexpression of FTO resulted in the reverse [104]. Experimental reduction of ALKBH5 increased levels of m^{6}A modifications across mammalian transcripts [103]. FTO and ALKBH5 knockdowns or chemical inhibition are regularly used in the study of m^{6}A as the default way to increase m^{6}A methylation in the cell and investigate the role of m^{6}A in other processes or pathways.

m^{6}A marks have also been linked to translational control when located in the 5' UTR [105]. Coots *et al*. found that depleted METT3 led to reduced translation of RNAs, due to interaction with the translation complex through Eukaryotic initiation factor 4F (EIF4F) [106]. Mauer *et al.* (2017) showed that the mRNA 5'cap is stabilized by a particular methylation at an Adenosine directly after the cap when Adenosine is the first transcribed nucleotide [107]. This is called N^6,2'-O-dimethyladenosine (m^{6}Am) [107]. The m^{6}Am neuronal signature can be influenced by stress, influencing gene expression of stress induced transcripts, this cap adjacent m^{6}A methylation is added by the specific methyltransferase CAPAM and also can be removed by FTO [108], [109,110].

m^{6}A is thought to be a modification primarily added to transcripts in the nucleus but early work from Harper *et al.* 1990 demonstrated m^{6}A

methyltransferase activity in cytoplasmic extracts, suggesting the presence of m^{6}A methyltransferase proteins in the cytoplasm [111,112]. Subsequent work went on to identify METTL3, METTL4, and FTO in the cytoplasm; identifying the specific protein components of the machinery allowed m^{6}A methyltransferase activity to be further characterised and understood [113,114,115]. This included work on m^{6}A and a category of viruses that solely replicate in the cytoplasm[116,117]. This pointed to distribution of the m^{6}A proteins actively marking RNAs in the cytoplasm. For instance METTL3, METTL14, and FTO were all identified in cytoplasmic fractions of both Huh7 cells (hepatocyte-derived carcinoma) infected with hepatitis C virus (HCV) and mock infected cells[116]. This suggested that m^{6}A proteins existed in the cytoplasm regardless of infection and pointed to the possibility of m^{6}A addition to and removal from host transcripts after export from the nucleus to the cytoplasm [116].

1.6.2 m^{6}A Recognized by Reader Proteins

m^{6}A essentially acts as a mark on regions of the RNA, the function of the modification is then dictated by the m^{6}A reader protein it recruits. m^{6}A is implicated in RNA structure[118], RNA stability, splicing[119,120], translation[121], and decay[122]. m^{6}A is also recognized and bound by a number of proteins in the cytoplasm. This includes the previously discussed protein METTL3, which can change its function from writer to reader, to regulate translation of the mRNA when exported to the cytoplasm[114]. Proteins which contain a YT521-B homology (YTH) domain also make up a class of well-studied m^{6}A reader proteins[85]. The YTH domain is composed of an aromatic cage pocket, which facilitates m^{6}A specific binding[123]. Proteins in this family also rely on electrostatic hydrogen bonds with the recognized RNA molecule to retain it in the aromatic pocket[123]. Recent work by Röder *et al.* 2022 used computational techniques to show the opened up structure of a stem loop of Kaposi Sarcoma Virus (KSHV) RNA when it is m^{6}A methylated [124]. This illustrates the way in which the chemical modification itself can modify RNA structure locally and influence protein binding and recognition by reader proteins.

YTHDF1 promoted translation of m^{6}A methylated transcripts and was shown to interact with translation initiation factor e1F3 [125]. YTHDF1 has been shown to direct translation of an immune response regulator through an m^{6}A site identified near the stop codon, supporting intestinal immune response to bacteria in micev [126]. Conversely, YTHDF2 decreased stability and promoted degradation of m^{6}A methylated transcripts [121].

Other proteins have also been shown to recognize m^{6}A modification on RNA to influence the fate of the transcript. Seven proteins in what has been named the Royal family of proteins contain the Tudor domain and were identified to recognize m^{6}A-modified RNA, likely dependent on the specific sequence and structure of the RNA [127]. This family of proteins included, SND1, which was identified as important for KSHV early gene expression [127].

Another protein family which includes three known m^{6}A reader proteins is the heterogeneous nuclear ribonuclear protein family (HNRNPs) [118],[128]. They are able to recognize m^{6}A modification by the change in secondary structure induced by m^{6}A modification, this is called an m^{6}A switch function[129]. These proteins go on to impact microRNA processing and RNA splicing of the detected RNA [118],[128]. The RNA secondary structure change that the HNRNPs recognize is due to the m^{6}A-U pairing being less thermodynamically stable than an unmodified A-U pairing as well as increased stabilization of a single stranded form with the m^{6}A modification [130]. Another m^{6}A binding reader protein family are the generally cytoplasmic insulin-like growth factor 2 mRNA binding proteins (IGF2BPs) which increase stability and translation of mRNAs important in processes such as tumorgenicity due to MYC [131],[132,133],[134].

The prevailing theory is that a specific m^{6}A reader binds the m^{6}A methylated mRNA to dictate its fate, whereas an alternative model suggested by Zaccara *et al.* 2020 claims that multiple readers bind the same m^{6}A methylated mRNAs and act redundantly to mediate mRNA fate [135]. They look at the YTHDF proteins and suggest that there is no intrinsic difference of their binding to the m^{6}A signature on an RNA [135]. Rather the difference in the binding ability of the different YTHDF proteins would be explained by

local RNA secondary structure changes and stoichiometry of these proteins which vary due to expression levels and post-translational modification [136,137].

This already dynamic epigenetic interaction of m^{6}A-modified RNAs with proteins can be re-choreographed in the face of infection with an RNA virus [138] or with other stress such as hypoxia [139]. Both YTHDF1 and YTHDF3 proteins have recently been identified as impacting the replication of CHIKV through recognition of the viral transcript [140]. Previously, work on ZIKV and m^{6}A showed that YTHDF2 directly bound to and reduced levels of ZIKV genomic RNA [117].

The proteins involved throughout the m^{6}A methylation process are of interest for potential knockdown experiments to disrupt and discern the role of m^{6}A in CHIKV replication.

1.6.3 Experimental methods for m^{6}A detection

To investigate the importance of m^{6}A within a system, experimental reduction of cellular m^{6}A related proteins is a widely performed approach. This can be done using knockdown of m^{6}A proteins through transfection of single stranded complementary sequence (siRNA) or a lentiviral delivery system of short hairpin sequence (shRNA) for the relevant protein, like METTL3, FTO, or WTAP. To knockdown at the RNA level, the shRNA's DNA sequence is integrated into the cell's genome. The region is transcribed and the shRNA is exported from the nucleus, processed by DICER to produce the siRNA for knockdown of the gene of interest. The siRNA is loaded by the RNA induced silencing complex (RISC), using host pathways to experimentally reduce gene expression at the RNA level [141].

Methylated RNA Immunoprecipitation Sequencing (MeRIP-seq or m^{6}A-seq) has been widely used in the study of m^{6}A; most studies utilize this method as the blueprint to check the efficacy of new methods. MeRIP-seq identifies regions of m^{6}A modification using a m^{6}A specific immunoprecipitation. RNA is fragmented into sizes of 1000 - 100 nts, depending on the desired window of interest in the transcript. These specifically precipitated fragments are then reverse transcribed into a cDNA library and aligned back onto the whole sequence of the known transcript. As a majority of m^{6}A happens at a

DRACH site, the m^{6}A site can then be discerned through identifying likely Adenosine bases within the mapped fragment's deep sequencing peak that corresponds to DRACH sequences. m^{6}A sites tend to cluster, which can complicate identification of specific functional m^{6}A sites if the fragmentation size is larger.

The difficulty to definitively pinpoint m^{6}A sites by MeRIP-seq led to a desire to map m^{6}A sites with single nucleotide resolution. These methods which can identify m^{6}A sites within 3 nucleotides of one another include DART-seq[142], eTAM-seq [143], and GLORI[139].

Both DART-seq and eTAM-seq apply an enzyme to induce changes to the m^{6}A-methylated RNA which can then be mapped using sequencing tools. The DART-seq technology exploits the YTH domain found in the YTHDF reader proteins. The YTH domain guides a fused deaminase to a methylated DRACH site where the C directly adjacent to the A is mutated to a U. This deamination and downstream analysis fits into existing RNA-seq workflows and can be detected by next generation sequencing (NGS) [142]. This method can be used through expression of the enzyme into cell lines or performed on RNA extracted from cells. Both *in-cell* and *in-vitro* methods show strong overlap in results. This method has been expanded on to perform individual cell DART-seq, which has been used to reveal cell to cell variation in m^{6}A signatures [144]. The Meyer group, which developed this technology and published it in 2019, presented their unpublished work at the Epitranscriptomics: Methods, Technologies, and Innovation Virtual Symposium July 24, 2023. They showed that by using transgenic mice which express the DART enzyme they could distinguish cell type variation in m^{6}A signatures even within tissues and cell types. This allowed them to show that microglia, the specialized immune cell of the brain, had fewer m^{6}A methylated sites on their RNAs than other RNAs of other cell types in the brain. They also suggest neuron specific changes to methylation of the amyloid precursor protein (APP) transcript with aging in the mice. This type of study may shed light on the development of amyloid plaques in the aging brain.

Whereas DART-seq seeks out the m^{6}A methylated DRACH sites eTAM-seq instead utilises a hyperactive transfer RNA adenosine deaminase (TadA) which modifies >99% of Adenosine present to inosine, except in the case of where the site has been m^{6}A methylated [143]. So rather than looking for the presence of m^{6}A as is the case with DART-seq, eTAM-seq looks for its absence. Using NGS, whole transcriptome m^{6}A methylations were mapped in both human HeLa cells and mouse embryonic stem cells (mESCs) [143]. However, while the authors concede that this method may not be able to access As in highly structured RNA secondary structures, they were able to detect two known m^{6}A sites in highly structured rRNAs [143]. Some of the limitations of this method include generating the enzyme deaminase and that there is no enrichment step, which then requires a lot of sequencing depth of the whole transcriptome to draw conclusions. However, a drawback of the classic antibody-based method was that the enrichment can precipitate very low stoichiometry transcripts. Detecting these low stoichiometry transcripts may not be as meaningful if the main consideration of the experiment is to determine m^{6}A load in the system rather than m^{6}A methylation of particular transcripts of interest.

Glyoxal and nitrite-mediated deamination of unmethylated adenosines (GLORI) is another method for mapping m^{6}A sites [139]. Like eTAM-seq it generates an inosine in place of the Adenosine RNA base but it does so through a chemical rather than enzymatic reaction.

Nanopore direct RNA sequencing has been shown to have the capacity to directly detect epigenetic modifications to RNA bases, including m^{6}A [145,146,147]. Nanopore uses changes in electrical current as nucleic acid passes through a protein nanopore to determine sequence [148,149]. Liu *et al.* 2019 and Lorenz *et al.* 2020 showed that they independently could detect m^{6}A within RNA using the nanopore technology in conjunction with machine learning to align a set of features to m^{6}A on transcripts which were also sensitive to METTL3 (or *ime4* knockout in yeast) and FTO[146,150]. Work by Huang *et al.* 2022 also show that using their MsPA nanopore they are able to not only recognize specific saccharides but also other epigenetic modifications to monophosphates including m^{6}A[151]. So, while this technology is not yet

paired with sequencing capacity, it allows for quantitative detection of a range of epigenetic modifications, including currently unknown modifications, within samples.

1.7.4 m^{6}A in mosquitoes

m^{6}A is a ubiquitous conserved RNA modification that has been identified in human cell lines [88], mouse [97], fly [152], and a variety of mosquito species [153],[154]. This discovery was supported by the identification of homologues m^{6}A machinery through the use of basic local alignment search tool (BLAST) across organisms, importantly aligning sequences of the writer, eraser, and reader proteins in human and mosquito *Anopheles* species (Figure 10). They found that in *Anopheles* species of mosquito there was sex-dependent variability in m^{6}A signatures as well as reduced mRNA expression levels of VIRMA and the YTHDCs in males in comparison females [153]. In the study of arboviruses these sex differences could be an interesting area of study as female mosquitoes are the vectors of CHIKV through their blood meal and may inform exploitable vulnerabilities to target therapeutics through. Although CHIKV is transmitted primarily by *Aedes* spp. mosquitos, this work offered insight into presence and variation of m^{6}A proteins in mosquitoes, rather than relying solely on homologies studies in Drosophila.

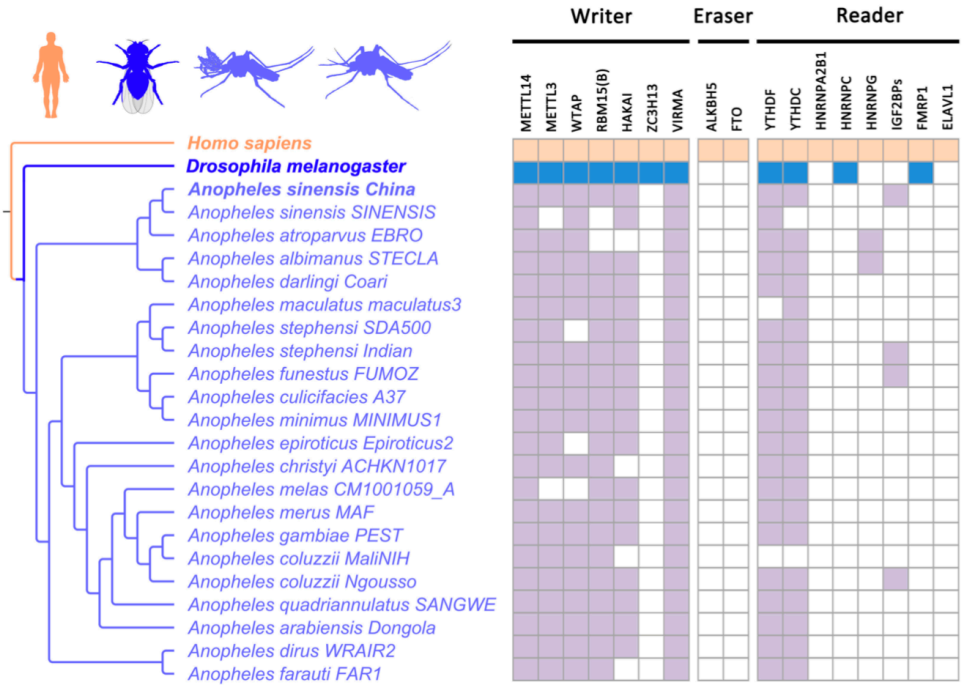

Figure 10. m^{6}A Writer, Eraser, and Reader Proteins identified across multiple species

m^{6}A relevant proteins presence identified by BLAST assisted homology mapping in *Homo sapiens*, *Drosophila melanogaster*, and a variety of *Anopheles* species of mosquito. m^{6}A writers, erasers, a few families of known m^{6}A readers proteins present indicated in purple for *Anopheles* species while presence in *Drosophila melanogaster* indicated in blue, and presence in *Homo sapiens* indicated in orange.

Figure reproduced from Liu *et al.* (2022)[153]

1.7 m^{6}A and Viruses

m^{6}A is known to impact the viral lifecycle of 14 RNA viruses and 18 DNA viruses to date, impacting their RNA longevity, transcription, and translation[155]. This includes DENV which is an RNA arbovirus transmitted by the same mosquito vectors as CHIKV. DENV also presents with such similar symptoms in human patients that CHIKV infection has been historically misidentified as DENV[19,11]. Recent work looking at m^{6}A signatures in *Aedes aegypti* cells show changes in m^{6}A methylation of mosquito transcripts following infection with DENV as well as confirmation of 5 m^{6}A sites in the DENV genome by MeRIP[154].

As addressed above it is currently known that m^{6}A methyltransferases and demethylases generally localize to the nucleus, and that a majority of m^{6}A methylation of mRNAs happens within the nucleus and recognition by reader proteins occurs when the mRNA has been exported to the cytoplasm. RNA viruses that have a portion of the lifecycle in the nucleus, such as HIV-1 and KSHV, have been shown to be influenced by m^{6}A methylation. However, recently positive RNA viruses that solely replicate in the cytoplasm such as, Hepatitis C virus (HCV), DENV, Zika virus (ZIKV), and CHIKV, have been shown to either have methylated transcripts and/or be influenced by m^{6}A methylation through recognition by reader proteins [116,117,156]. Work in flaviviruses has also experimentally shown that METTL3, METTL14, and FTO can be found in both nuclear and cytoplasmic fractions[115]. Another cytoplasmic replicating virus, SARS-CoV-2, was also shown to have m^{6}A cites in its RNA genome. This work used experiments involving knockdown of m^{6}A writer and eraser proteins as well as miCLIP and m^{6}A-seq[157]. While many of the cytoplasmic replicating virus studies used antibody-dependent methods to detect m^{6}A methylation recent work on the genome of SARS-CoV-2 also show 15 putative m^{6}A sites by Oxford Nanopore direct RNA sequencing[158]. This group performed downstream processing of their data of RNA extracted from the supernatant of SARS-CoV-2 infected Vero cells using the m6Anet analysis tool which according to Zhong *et al.* 2023 provides some of the highest precision analysis of available tools for m^{6}A ONT data.

This project was specifically focused on investigating the interplay between N^6-methyl-adenosine RNA modification (m^{6}A) and CHIKV replication. Interestingly, recent work published during this project by Kim *et al.* 2020 experimentally show that the packaged CHIKV RNA genome is m^{6}A methylated in the first 5000 nts. Using a new method termed viral-crosslinking and solid-phase purification (VIR-CLASP), a form of liquid chromatography-tandem mass spectrometry (LC/MS/MS) which identified pre-replicated viral genomic RNA and protein interactions, they were able to show that m^{6}A reader proteins YTHDF1, YTFDF 2, and YTHF3 interact with the CHIKV genome[156]. They also identify that the DNA-sensor Interferon inducible protein 16 (IFI16) also binds and reduces replication of the CHIKV

genome. m^{6}A has been implicated as an important regulatory signal for replication of other RNA viruses [156].

For instance, shRNA-mediated depletion of METTL3 leads to an increase in productive ZIKV replication. Reduced levels of FTO by shRNA results in a decrease in replication of ZIKV RNA[117], suggesting that m^{6}A may be acting in an anti-viral capacity, either through regulation of the ZIKV genome or host transcript interactions with the viral genome or necessary proteins. They also saw dysregulation of cellular m^{6}A modified transcripts with ZIKV infection with an increase in deposition of m^{6}A in the 5' UTRs of host transcripts and a concurrent depletion in the 3'UTRs [117]. Conversely, mutating two m^{6}A sites within the enterovirus 71 (EV71) genome resulted in a significant decrease in virus replication and an interaction between METTL3 and EV71 genome was characterised [159].

Virus	Detection	Phenotype	Main Function for m^{6}A	Reference
RNA viruses				
HIV-1	m^{6}A-seq	Proviral	vRNA nuclear export	[160]
	PA-m^{6}A-seq	Proviral	vRNA abundance and protein expression	[161]
	m^{6}A-seq	Antiviral	YTHDF1-3 proteins inhibit HIV-1 infection by decreasing HIV-1 reverse transcription	[162,163]
	-	Antiviral	YTHDF3 inhibits HIV-1 infection at the step of reverse transcription	[164]
HCV	m^{6}A-seq	Antiviral	m^{6}A modifications in E1 are bound by YTHDF proteins to negatively regulate HCV packaging	[116]
ZIKV	m^{6}A-seq	Antiviral	vRNA abundance and protein expression	[117]
DENV /WNV	m^{6}A-seq	X	m^{6}A present in the genome	[116]
DENV	m^{6}A-seq	Proviral	In Aedes. aegypti cells: m^{6}A present in genome. YTHF3 promotes DENV replication	[154]
PEDV	m^{6}A-seq	Antiviral	m^{6}A modifications reduce viral RNA production and viral titres	[165]
IAV	PA-m^{6}A-seq	Proviral	m^{6}A modifications increase vRNA expression	[166]
RSV	m^{6}A-seq	Proviral	m^{6}A modifications enhance RSV replication and gene expression	[167]
SARS-CoV2	m^{6}A-seq and miCLIP ONT Direct RNA sequencing	Antiviral	m^{6}A inhibits SARS-CoV2 replication 15 putative m^{6}A sites detected in the viral genome	[157, 158]
CHIKV	m^{6}A-IP	Both	YTHF1 and YTHDF3 restrict CHIKV replication, while YTHF2 promotes it	[140]
EV71	m^{6}A-seq	Proviral	METTL3 induces enhanced sumoylation and ubiquitination of the viral RNA polymerase to facilitate viral replication	[159]
HMPV	m^{6}A-seq	Proviral	m^{6}A modifications enable vRNA to escape recognition by RIG-I	[168]
VSV	miCLIP	Proviral	m^{6}A modifications reduce viral dsRNA formation leading to reduced virus-sensing by innate receptors	[169]
B77 Avian Sarcoma Virus	DEAE-cellulose chromatography	Not reported	Internal m^{6}A modification detected in viral RNA	[170]
DNA viruses				
SV40	PA- m^{6}A-seq	Proviral	m^{6}A enhances the translation of viral late transcripts	[171]
KSHV	m^{6}A-IP	Proviral	Splicing of *ORF50* pre-mRNA	[172]
	m^{6}A-seq	Antiviral	vRNA stability of latent and lytic transcripts	[173]
	m^{6}A-seq	Both	vRNA abundance and protein expression	[174]
	m^{6}A-seq	Proviral	vRNA abundance and protein expression	[127]
EBV	m^{6}A-seq	Both	vRNA stability of latent and lytic transcripts	[175]
	m^{6}A-seq and PA- m^{6}A-seq	Antiviral	YTHDF1 promotes EBV RNA decay	[176]
Ad5	m^{6}A-seq and nanopore	Proviral	m^{6}A is required for splicing of adenoviral late transcripts	[147]
HBV	m^{6}A-seq	Both	vRNA stability and viral reverse-transcription	[177]

Table 1. Table of role of m^{6}A on viruses

Table summarizes the method of m^{6}A detection, a summary of the role of m^{6}A on the virus listed, and the corresponding literature. This table was originally published in and adapted from Baquero-Perez et al. 2021 [155], with information included from Dai et al. (2022) [154]

m^{6}A has been linked to innate immune signalling through the stimulation of ISGs and specifically Interferon Beta, which was found to be m^{6}A methylated within the coding and 3' UTR region of the transcript [178],[179]. In the context of human cytomegalovirus infection Rubio *et al.* 2018 linked experimental ALKBH5 reduction to an increase in viral replication with the reduction of METTL14 showing the inverse[178]. Winkler *et al.* 2019 show that a reduction in METTL3 and YTHDF2 led to an increase in expression of ISGs [179].

This data suggests that, m^{6}A RNA modification of host cell transcripts, as well as the virus genome itself, can influence virus replication. Different viruses exploit or are affected by m^{6}A in different ways, in some cases pro-viral and in others antiviral. The cellular methylome has also be proposed to be reprogrammed during flavivirus infection, which suggests the importance of investigating both cellular and viral transcripts [115].

1.8 Aims and Objectives

The aim of this study was to investigate the impact of m6A methylation on CHIKV replication in human and mosquito cells following four defined objectives.

Objectives:

1. Determine the effect on CHIKV replication of m^{6}A inhibition with a small molecule inhibitor.
2. Map potential m^{6}A sites on the CHIKV genome using an *in silico* approach and MeRIP followed by validation by reverse genetic approaches.
3. Investigate the functional consequences of m^{6}A on CHIKV infected cells, using shRNA knockdown of essential m^{6}A machinery proteins.
4. Analysis of the stage at which m^{6}A is important in the virus lifecycle using a trans-complementation assay system.

2 Chapter 2- Methods and Materials

2.1 Cell culture

2.1.1 Mammalian cell Culture

Huh7, Human Rhabdomyosarcoma (RD), BHK-21 (baby hamster kidney), and 293T (human embryonic kidney) cells were maintained at 37 °C in 5% CO_2 in Dulbecco's Modified Eagle Medium Serum (Sigma-Aldrich) (DMEM) with 10% Foetal Bovine Serum (Sigma-Aldrich) (CDMEM) and 1% penicillin-streptomycin (P/S) (Sigma-Aldrich). Cells were split before they reached a confluency of 90%. To passage, cells were washed twice with 1x PBS, harvested using Trypsin, and diluted 1:10 to be passaged again approximately two days later.

RD cells were procured from the European Collection of Authenticated Cell Cultures (ECACC)- Ac no: 85111502, Lot: 16J014, REP 7638, Order: 448300, Delivered October 18, 2019. Initially the cells were frozen down (In 10% DMSO 90% FBS) in three aliquots of one million cells at passage 13 and kept in liquid nitrogen. An additional 20 vials were frozen down under same conditions at the earliest possible passage.

2.1.2 Mosquito Cell Culture

C636 cells were gifted by Professor Alain Kohl (University of Glasgow) and were maintained at 28 °C with no supplemental CO_2. They were grown in Leibowitz's L-15 medium (ThermoFisher Scientific) supplemented with 10% FBS (Sigma-Aldrich) 10% TPB (Sigma- Aldrich) and 1% penicillin-streptomycin (Sigma-Aldrich). When they reached about 90% confluency, they were harvested by mechanical scraping and split 1:10, approximately every two days.

2.2 DNA Plasmid Amplification

Mix and Go! (Zymo Research) *Escherichia coli* (*E. coli*) were used for plasmid transformation[180]. 1 µL of plasmid DNA was mixed with 50 µL of the thawed competent *E. coli*. For ampicillin selection the bacteria were then

plated directly onto a warm selection LB-Agar ampicillin (100 µg/mL) plates and incubated at 37 °C overnight until individual raised colonies were visible. For Kanamycin selection the bacteria and plasmid mix was kept on ice for 15 minutes and then 4 volumes of SOC outgrowth media was added to the Eppendorf, set shaken at 200 rpm for 1 hour, then 50-100 µL of the total mixture was plated onto a prewarmed LB-Agar selection plate and incubated at 37 °C overnight. The next day single colonies were picked and inoculated into 7-10 mL of LB + selection antibiotic (at a concentration of 100 µg/mL) to shake at 37 °C overnight. The culture was then pelleted at 4000 RPM for 10 minutes and the pellet harvested for DNA plasmid purification by GeneJET Plasmid Miniprep kit (Thermo Scientific)[181].

2.3 Restriction Enzyme Digestion

Restriction enzyme digestion was used to either linearize circular plasmid DNA with a single enzyme or to double digest a plasmid for use in a cloning reaction with two enzymes. 1-10 µg of DNA was digested with 2µL of restriction enzyme in a 50-100 µL total reaction with CutSmart Buffer at 1x at 37 °C for 2 hours. Ethanol precipitation or Qiagen RNAeasy Spin Column was used to purify linearized plasmid. To purify double digested plasmid, the complete reaction was analysed on a native TAE agarose gel to separate DNA sections by size, the relevant bands were excised from the gel, and purified using the NEB Monarch DNA gel extraction kit according to the manufactures protocol.

2.4 Primers

All oligonucleotide primers were specifically designed for sequencing, polymerase chain reaction (PCR) and mutagenesis (**Table 2**). They were synthesized by Integrated DNA Technologies, resuspended in nuclease-free water to a concentration of 100 nM and stored at -20 °C.

Primer Name	Sequence
Sequencing Primers	
CHIKV qRTPCRFwd	CCGACTCAACCATCCTGGAT
CHIKV qRTPCRRev	GGCAGACGCAGTGGTACTTCCT
CHIKV_1_T7	ATG GCT GCG TGA GAC ACA CG
CHIKV 3'UTR seq	TGG CAA ACG GAA GAG ATG T
PUC57 CHIKV 3'UTR primer	AGC AAG ATC CAG GGC
Firefly Luc forward	ATG GAA GAT GCC AAA AAC AT
Firefly Luc reverse	CGG CGA TCT TGC C
CHIKV E1 qRT-PCR Forward	GCA TCA GCT AAG CTC CGC GTC
CHIKV E1 qRT-PCR Reverse	GGT GTC CAG GCT GAA GAC ATT G
MERIP primers	
m6A (96) forward	AAA GCA AGA GAT TAA TAA CCC
m6A (96) reverse	CAC GTT GCA GGG CCT TCA
m6A (11749) forward	GCA GCC GAA CTC ACT TTG AG
m6A (11749) reverse	AAC ATC TCC TAC GTC CCT GT
SLC39A14 -ve forward	GCA GGA TCT AAT ACA TCG GTA TGG
SLC39A14 -ve reverse	TGG TTG AGT AGG GCC TTC AG
GAPDH 1 neg m6A forward	GCA TCT TCT TTT GCG TCG CC
GAPDH 1 neg m6A reverse	TTG ACT CCG ACC TTC ACC TTC C
GAPDH 2 neg m6A forward	TGC ACC ACC AAC TGC TTA

GAPDH 2 neg m6A reverse	ATG AGT CCT TCC ACG ATA CC
1. CHIKV m6A neg ctrl forward	GCT TTG GCG GAG CAA G
1. CHIKV m6A neg ctrl reverse	ATA GCC TGA GGG CAC TAG
2. CHIKV m6A neg ctrl forward	AGT GCG GCT TCT TCA AT
2. CHIKV m6A neg ctrl reverse	TAC ACC GCC TGG AGA TAC
3. CHIKV m6A neg ctrl forward	CGA AAG GAA ACT TCA AAG
3. CHIKV m6A neg ctrl reverse	GGT GAC TGC AGA TGC CC
Q5 mutagenesis primers	
Q5 96 m6A A to G mut forward	GTG TAC GTG GGC ATA GAC GCT
Q5 96 m6A A to G mut reverse	AGG ATC CAT GAT GGG TTA TTA ATC
Q5 96 m6A A to G mut forward	AGC ATA CCG AGC TCT TCC ACG
Q5 96 m6A A to G mut reverse	ATG CCT ACT TCT CAA AGT GAG

Table 2. Primer Names and Sequences

2.5 Western Blots

Protein material was incubated with 2X sample loading buffer for 5 min at 95°C. Samples were loaded onto sodium dodecyl sulphate–polyacrylamide (SDS-Page) resolving gels comprised of 10% resolving gel atop a 6% separating gel and run at 80 Volts (V) for 1.5 hours.

10% resolving gel	
30% acrylamide	3.3 mL
1.5M Tris-HCl (pH 8.8)	2.5 ml
double distilled water (ddH_2O)	4.0 ml
10% SDS	100 µL
APS	100 µL
TEMED	10 µL
6% stacking gel	
30% acrylamide	0.97 mL
0.5M Tris-HCl (pH 6.8)	0.63 ml
double distilled water (ddH_2O)	3.4 ml
10% SDS	50 µL
APS	50 µL
TEMED	5 µl

Table 3. SDS-PAGE Ingredients for Stacking and Resolving Gels

SDS refers to sodium dodecyl sulphate, APS refers to ammonium persulfate, TEMED refers to tetramethyl ethylenediamine. All ingredients were added in the order listed here.

The gel was transferred onto a PVDF (Immobilon) membrane at 240 mA (milliamps) for 2 hours, the membrane was blocked in 1:1 LICOR blocking buffer: 1x Tris Buffered Saline (TBS) for one hour at room temperature, then it was incubated at 4°C overnight in 5mL of diluted primary antibodies. The next day membranes were incubated in anti-mouse secondary antibody in

the dark at room temperature for 2 hours. The membrane was imaged using the LICOR Odyssey Imaging System. The protein expression was quantified using the ImageJ analyse gel tool, taking the area corresponding to the protein band from the plots generated in the programme.

2.6 Denaturing Agarose Gels

2.6.1 Agarose TAE Gel Electrophoresis

DNA quality and size were analysed by agarose TAE gel electrophoresis. DNA of expected size >500 bp was analysed on a 1% agarose gel. To resolve smaller fragments a 2% agarose gel was used. Agarose was dissolved in 1x TAE (40 mM Tris, 20 mM Acetate, and 1mM EDTA) by heating. Once cooled, SYBRsafe® DNA gel stain (1:10,000, Invitrogen) was added to the liquid mix and was poured into a cast. DNA samples (including 1 kb Plus NEB DNA ladder) were mixed with Gel loading DNA dye (6x, NEB), loaded into the wells of the agarose gel, and electrophoresed at 90V for 1 hour. The separated DNA samples were visualized by blue light (470 nm).

2.6.2 Agarose MOPS Gel Electrophoresis

RNA quality and size were analysed by agarose MOPS gel electrophoresis. RNA of expected size >500 nt was analysed on a 1% agarose gel. To resolve smaller fragments a 2% agarose gel was used. Agarose was dissolved in 1x MOPS (10x MOPS: 0. 0.4 M MOPS pH 7.0, 0.1 M Sodium Acetate, 0.01 M EDTA pH 8.0) with formaldehyde by heating. Once cooled, SYBRsafe® DNA gel stain (1:10,000, Invitrogen) was added. RNA samples were mixed with 2x Gel loading RNA dye (RNA), loaded into the wells of the agarose gel, and electrophoresed at 90V for 1 hour. The samples were analysed alongside a Millennium RNA ladder (NEB). The separated RNA samples were visualized in the matrix of the gel by blue light (470 nm).

2.7 *In vitro* Transcription

In vitro transcription of 2ug plasmid DNA was performed by incubating the template plasmid DNA with the AmpliCap SP6 High Yield Message Maker kit (Cat. No. C-AC0706) at 37 °C for 2 hours to produce 5' capped CHIKV RNA as per the manufacturer's instructions. The DNA template was digested by incubation with Turbo DNase for 15 minutes. The 5' capped CHIKV RNA was then purified using phenol-chloroform extraction.

2.8 Phenol-Chloroform Extraction with Ethanol Precipitation

The sample of interest was resuspended in 500 µL of phenol:chloroform:isoamyl alcohol (pH 6.7; Ambion AM9730) and vortexed. 200 µL of Chloroform was added to the tube. The upper aqueous phase was transferred to a fresh tube. 0.1 volumes of 3M sodium acetate (pH 5.2) and 2.5 volumes of ice cold 95% ethanol were then added and mixed well and incubated at -80°C overnight. The next day the samples were centrifuged at 17,000 RPM at 4°C for 10 minutes. The supernatant was aspirated and the RNA pellet was washed with 1 ml of 70% ethanol. The RNA:ethanol was centrifuged at top speed at 4°C for 15 min. The ethanol was removed and the RNA was allowed to dry at room temperature, before being resuspended in 20 µl of nuclease free H_2O. Concentration and purity were determined using Nanodrop spectroscopy. RNA size and integrity were analysed by loading 1-2 µL of the RNA on a denaturing MOPS agarose gel. RNA was stored at -80°C until further use.

2.8.1 Ethanol Precipitation

When purifying or concentrating DNA or RNA the sample solution was made up to 500 µL with nuclease free H_2O. 50 µL of 3M Sodium Acetate (pH 5.2-5.5) and 500 µL of 100% cold Isopropanol were added, mixed well and incubated at -80°C overnight. The next day the sample was centrifuged at top speed at 4°C for 10 minutes. The supernatant was removed and the DNA or RNA pellet was washed with 1 mL of 70% ethanol. The RNA:ethanol or DNA:ethanol was centrifuged at top speed at 4°C for 15 min. The ethanol was removed and the DNA or RNA was allowed to dry at room temperature,

before being resuspended in 30-50 µl of nuclease free H_2O. Concentration and purity were determined using Nanodrop spectroscopy. RNA size and integrity were determined by analysing 1-2 µL (approximately 2000 µg) of the RNA on a denaturing MOPS agarose gel. RNA was stored at -80°C until further use. DNA size and integrity were determined by running approximately 500 ng of the DNA on a denaturing TAE agarose gel. DNA was stored at -20°C for long term storage or 4°C if it was being used in the next few weeks.

2.9 Generating Infectious Chikungunya Virus

2.9.1 Transfection by Electroporation

1 µg of WT CHIKV RNA was transfected by electroporation into BHK-21 cells. The flask of cells was immediately take to the Biosafety Level 3 facility for incubation at 37 °C in 5% CO_2 for 48 hours. The supernatant was collected and frozen into aliquots and stored at -80°C. The titre of the infectious virus was determined by plaque assay.

2.9.2 Chemical Transfection

$1.4x10^6$ C636 cells were seeded into a T75 the day prior. They were incubated overnight until they reached 70% confluency. 10 µg of *in vitro* transcribed and capped viral RNA was added to 500 µL of Opti-MEM™. 10 µL of Lipofectamine-2000 (ThermoFisher) was added to 500 µL of Opti-MEM™. They were independently incubated at room temperature for 5 minutes. Then the RNA mixture was gentled added to the Lipofectamine-2000 mix and incubated at room temperature for 20 minutes. The cells were washed with 1x PBS and 4 mL of Opti-MEM™ was added to each well. After the 20 minute incubation, the DNA and Lipofectamine-2000 mixture (transfection mixture) was added dropwise into the flask. The cells were incubated with the transfection mixture for 4- 6 hours. Then the mixture was removed, the cells were washed with 1x PBS, and replaced with media. After 24 hours the supernatant was removed, centrifuged to pellet dead cells, and aliquoted to be frozen at -80 °C for analysis by plaque assay

2.10 Plaque Assay

BHK-21 cells were plated at 100,000 cells per well in a 12-well plate. The next day in a 96-well plate 10-fold dilutions were made of the sample being assessed, (20 µL was diluted initially diluted into 180 µL of CDMEM). Each dilution was prepared in duplicate. 150uL diluted virus was added to each well. The samples were incubated on the gentle shaker to ensure virus coated the well and incubated at 37 °C. After one hour the virus was aspirated, washed with 1x PBS, and the cells were overlaid with a 1:1 dilution of DMEM and 1.6% methylcellulose (DMEM:MC). After two days the overlay was removed, washed with 1xPBS, fixed in 4% Paraformaldehyde, and stained with Crystal violet solution (0.25% crystal violet, 10% Ethanol, 5mM $CaCl_2$, 25 m< Tris in water) to visualize and count plaques. Virus titre was determined using the equation:

$$\frac{PFU}{mL} = \frac{number\ of\ plaques}{dilution\ factor\ 10^{-x}\ \times\ volume\ added\ per\ well\ in\ mL}$$

To determine the multiplicity of infection to use in experiments this equation was used:

$$MOI = \frac{PFU\ per\ mL\ \times\ mL\ used\ per\ well}{number\ of\ cells\ per\ well}$$

2.11 3- Deazaadenosine (c3Ado) Inhibition Assay

A 12-well plate was plated with 100,000 cells per well the day prior to the experiment. Mammalian cells were pre-treated with media containing 50µM c3Ado or untreated complete DMEM as a negative control for one hour prior to infection. C636 cells were incubated with 500 µM c3Ado. Cells were infected with WT CHIKV in the appropriate media. After one hour the supernatant was removed, washed with 1xPBS, and replaced with the appropriate media for the condition. The cells were left to incubate at 37 °C for 24 hours after which the supernatant was removed and frozen down at -

80°C before plaque assay to assess released viral titre. The remaining monolayer of cells were also lysed in TriReagent (Sigma Aldrich: **93289**) for RNA extraction and qRT-PCR of CHIKV genome. This experiment was designed in the style of the experiment described in Muller et al. 2019 which involved the treatment of human and mosquito cells with compounds and subsequent infection with CHIKV[182].

2.12 MTT Cytotoxicity Assay

One day before experiment 10,000 cells/well were seeded in a 96 well plate in 100 µL of media containing a range of c3Ado drug dilutions. On the day of the MTT assay, MTT Mw414 (Sigma) was dissolved in serum free media at 1mg/mL. Sterile filtered media with MTT. The assay was performed 27 hours after treatment with c3Ado. To perform the assay, media was removed from the wells, 100 µL MTT solution was added to each well and incubated at 37 °C for 30 minutes covered in aluminium foil in the dark. The MTT solution was discarded, replaced with 100 µL DMSO and shaken for 5 minutes at 60 rpm to dissolve purple precipitate. Dissolving of the purple precipitate in the DMSO was checked and any bubbles were removed with a pipette. The results of the assay were analysed on a plate reader at 570 nm on the Infinite F50 microplate reader (Tecan)[182].

2.13 ATP-lite Cytotoxicity Kit

The ATP-lite Cytotoxicity™ kit (Perkin-Elmer) was used to assess cytotoxicity of c3Ado in C636 cells[183]. The kit was used according to the manufacturers protocol. 30,000 C636 cells/well were seeded into a 96 well plate. The cells were incubated in media containing varying concentrations of c3Ado and DMSO. After 27 hours the media was removed, the cells were washed with 1x PBS, 50 µL of mammalian lysis solution was added to each well, shaken on an orbital shaker at 200 rpm to lyse the cells, 50 µL of the reconstituted lyophilized substrate was added to each well and shaken for an additional 5 minutes. The plate was then dark adapted for 10 minutes and the signal was assessed using the FLUOstar Plate Reader (BMG LABTECH).

2.14 Methylated RNA Immunoprecipitation (MeRIP)

2.14.1 Preliminary MeRIP

Preliminary MeRIP began with washing a 25 µL of slurry of Magna ChIP Protein A+G magnetic beads (Merck Millipore) with IP/wash buffer [20 mM Tris HCl pH 7.4, 150 mM NaCl, and 0.1% NP40 (v/v)]. After the final wash, 5 µg of rabbit anti-N6-methyladenosine (m^6A) antibody (ABE572) (Merck Millipore) was added to 100 µl of IP/wash buffer. This was used to coat the beads for 45 min at room temperature with rotation. The beads were washed three times with the 1x IP/wash buffer. The antibody-coated beads were then mixed with 900 µL of IP/wash buffer, 35 µl of 0.5 M EDTA pH 8.0, 4 µl of *RNasin Plus* (Promega), 26.37 µg of CHIKV replicon transfected RD cell RNA and 22.82 µg of non-transfected sample RD cell RNA. Samples were then incubated overnight at 4°C with rotation. The next day, the beads were washed six times with IP/wash buffer. Then the samples were further incubated with 126 µL of IP/wash buffer, 15 µl of 10% SDS (v/v) and 9 µL of PCR-grade proteinase K (20 mg/mL) (Thermo Scientific) for 30 min at 55 °C. This released the captured RNA from the beads. The elutant was mixed with 250 µl of IP/wash buffer. To purify the RNA a phenol:chloroform:isoamyl alcohol (Sigma-Aldrich) purification was performed followed by a sodium acetate/ethanol-precipitation (both outlined above). The RNA was resuspended in 15 µL of nuclease-free water and the concentration was measured by nanodrop spectroscopy (RD-15.5ng/ µL and 11.5ng/ µL). 9uL of each IP extracted RNA sample was used to create a cDNA library with the Applied Biosystems High-Capacity RNA-to-cDNA kit in a total reaction volume of 20 µL according to published protocol.

Using the 2x qrtPCRBIO SyGreen Blue Mix Lo-Rox, CHIKV replicon RNA was measured by RT-qPCR using both 23 ng or 96 ng of each eluted RNA sample. The primers used were “CHIKV qRTPCRFwd” and “CHIKV qRTPCRRev” (Table 2). The samples were assessed by RT-qPCR alongside a CHIKV standard curve which allowed us to determine the genome copy present in each sample.

2.14.2 Optimised MeRIP

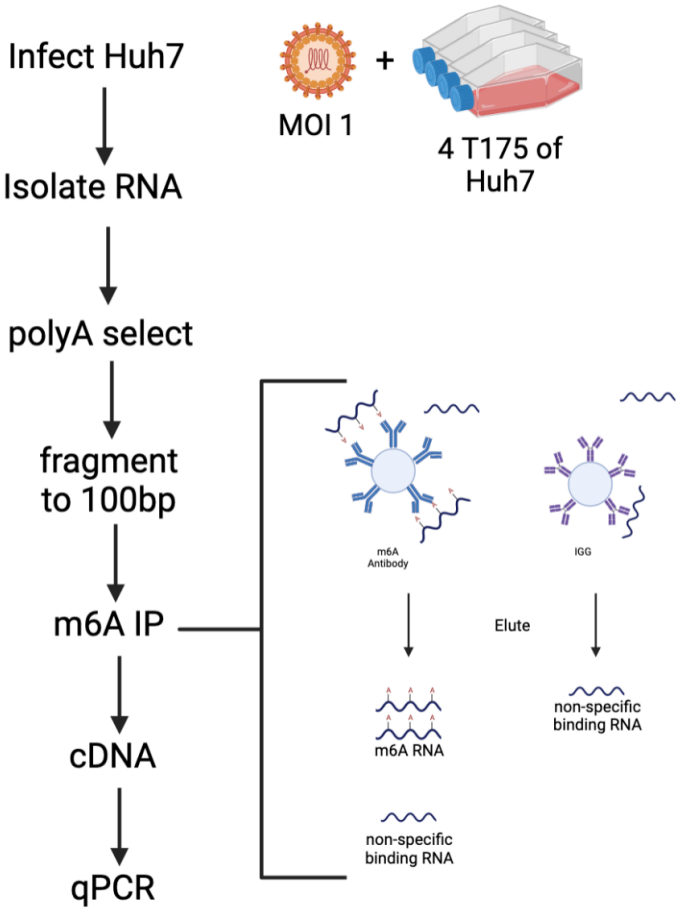

Figure 11. Flow Diagram of Optimized CHIKV infected Huh7 cell for a MeRIP

4 T175 flasks of Huh7 cells were infected at an MOI of 1 with CHIKV. After 24 hours the cells were lysed and the total RNA was isolated. That total RNA was then Poly(A) selected, fragmented to 100bp, then the MeRIP was performed using either the anti-m6A antibody or negative control IgG antibody coated beads. The RNA that was eluted from the beads was reverse transcribed into a cDNA library and then probed by qrt-PCR for transcripts.

Figure created using BioRender.

Four flasks of 70% confluent Huh7 cells were infected for 24 hours with MOI 1 CHIKV. The monolayer of cells was lysed in TriReagent and frozen at -80°C overnight. This was then phenol-chloroform extracted (, DNase I treated at 37 °C for 30 minutes, and then Phenol-Chloroform extracted

again. Resultant RNA was then fragmented to approximately 100 nucleotides in length using the Ambion/ Invitrogen™ RNA Fragmentation Reagents (the company changed during the time of using the reagent but reagent was used as advised). The fragmented RNA was ethanol precipitated overnight at -80C for use in the IP.

IP was performed according to the instructions provided by m^{6}A Magna MeRIP™ m^{6}A Kit- Transcriptome-wide Profiling of N6-Methyladenosine (Sigma-Aldrich). Approximately 3-4 µg of PolyA selected fragmented RNA was used. 10% of the input was removed and stored immediately at -80°C for cDNA library generation later. One substitution used for a majority of experiments reported in this thesis was to use double the magnetic beads and double the antibody (10 µg of antibody and 200 µL of beads) recommended.

Two methods were trialled and yielded similar RT-qPCR results regardless. The eluted precipitated RNA was purified using Phenol/Chloroform Ethanol precipitation. Alternatively, the eluted precipitated RNA was collected using the RNeasy MinElute Cleanup Kit (Qiagen) [184] according to manufacturer's instructions which was specifically recommended in the m^{6}A Magna MeRIP™ m^{6}A Kit protocol.

A cDNA library was generated (using ProtoScript® II Reverse Transcriptase) from the eluted RNA as well as the 10% of input RNA that was set aside prior to immunoprecipitation.

Then using qPCRBio SyGreen Mix with the primers detailed in (Table 2) the samples were assessed for genes of interest including CHIKV RNA and m^{6}A positive control genes.

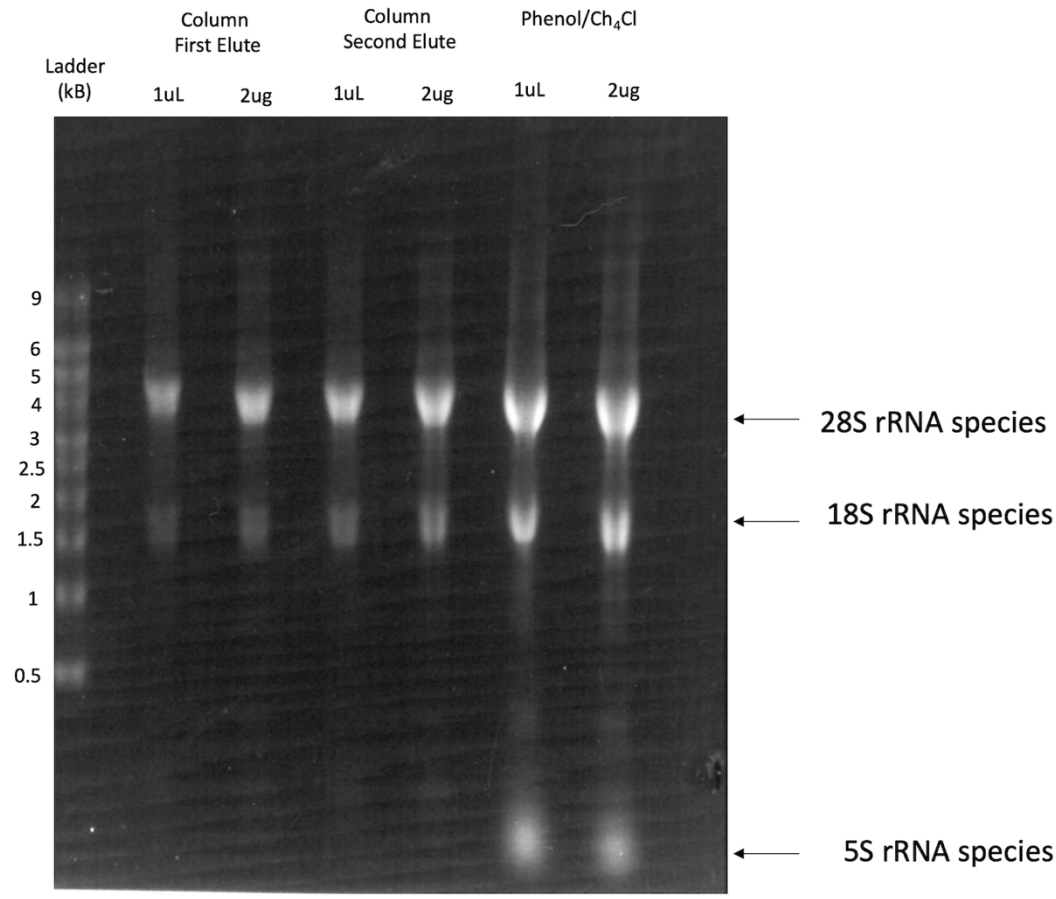

Figure 12. Purification of RNA for MeRIP

The RNA isolated using the Qiagen RNAeasy spin column showing both the first and second elute show that the ribosomal rRNA bands are strong but Phenol/Chloroform followed by an Ethanol Precipitation retained even smaller RNA bands as well.

Denaturing 1% agarose MOPS gel electrophoresis, ThermoFisher Millennium™ RNA Marker.

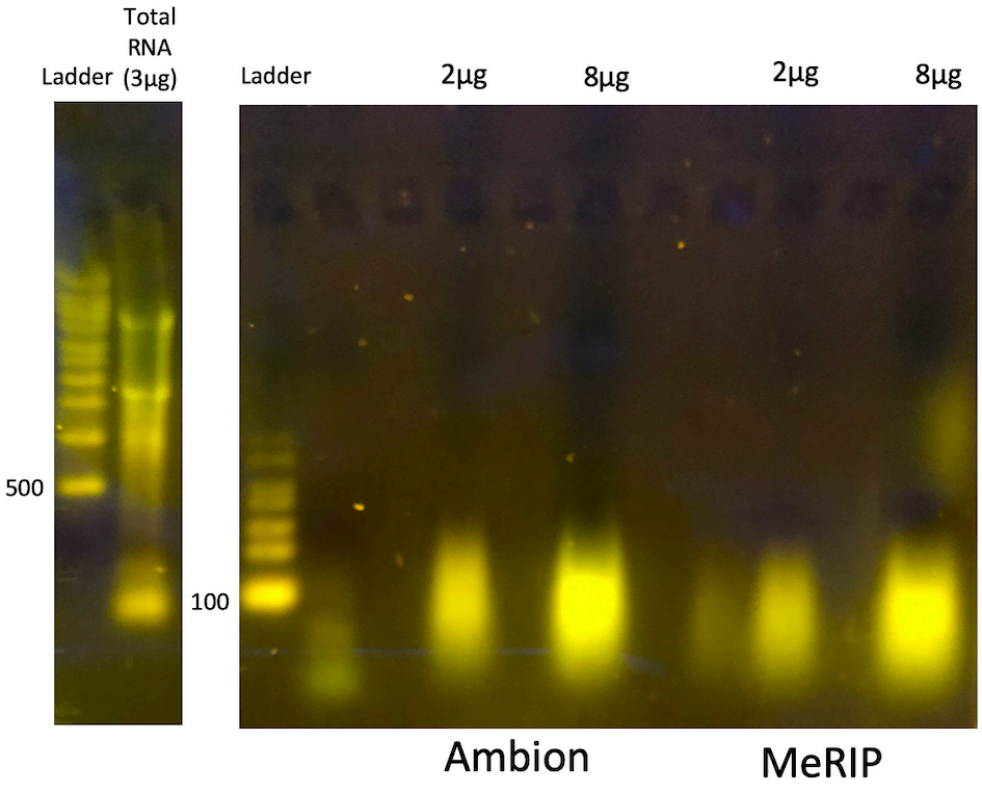

Figure 13. RNA fragmentation by comparing two chemical approaches show the desired 100nt fragments

Total RNA from CHIKV 1 infected RD cells (MOI) (this material has not undergone the PolyA selection) using two fragmentation methods showing that under the conditions both result in a mixture of RNA length species but the ideal desired 100nt length species is present.

Analysed by denaturing 2% agarose MOPS gel electrophoresis.

ThermoFisher Millennium™ RNA Marker (left most ladder)

ThermoFisher Century™ RNA Mark (right most ladder)

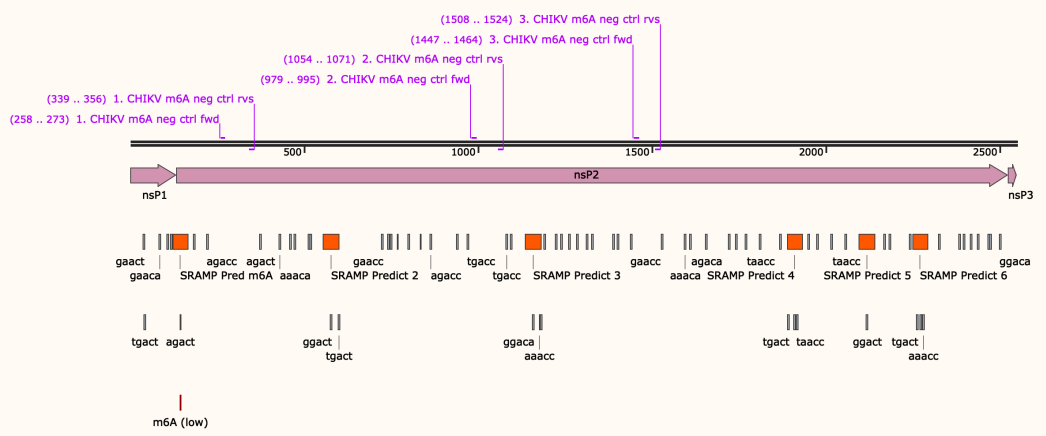

Figure 14. Identification of m^{6}A negative region in CHIKV nsP2 coding sequence

Region of NSP2, orange boxes indicate 100 nts length regions containing the SRAMP predicted m^{6}A site, all DRACH permutations are shown, three pairs of negative control m^{6}A primers forward and reverse primers shown in purple.

First mixture was composed of	
RNA	7µL
Random Primer mix (60µM)	2 µL
10 mM dNTPs	1 µL
First mixture of 10 µL was denatured at 65 °C for 5 minutes then placed on ice until the next components were added:	
5x Protoscript II Buffer	4 µL
0.1 M DTT	2 µL
Nuclease-Free Water	2.8 µL
Protoscript II Reverse transcriptase (200U/µL)	1 µL
RNase Inhibitor (40U/µL)	0.2 µL
The 20 µL total cDNA synthesis reaction mixture was placed in the thermocycler to heat at 25 °C for 5 minutes, 42 °C for one hour, and then an activation step of 65 for 20 minutes. The cDNA product was then stored at 4C to -20 °C depending on if it was used that day.	

Table 4. ProtoScript II RT (NEB) conditions

A range of primers were used to detect potential m^6A sites within the CHIKV genome, known m^6A methylated sites on human host transcripts Slc6a19 (SLC), and the human host EEAF1 primers that came with the kit (Table 2).

Each qPCR reaction was done in duplicate and was composed of:

Reagent	Volume
2x qPCRBio SyGreen Mix [185]	10 µL
Forward Primer (10 µM)	0.8 µL
Reverse Primer (10 µM)	0.8 µL
Template cDNA	2 µL
Nuclease Free Water	6.4 µL
Total	20 µL

Table 5. qPCRBio SyGreen Mix [185] Reaction Mix

Thermocycler Conditions for the qPCR:

Cycle Number	Temperature	Time	Step
1 cycle	95 °C	2 min	Polymerase Activation
40 cycles	95 °C	5 sec	Denaturation
	60 °C	30 sec	Anneal/Extension
1 cycle	95 °C	1 min	Melt Analysis
	55 °C	30 sec	
	95 °C	30 sec	

Table 6. qPCR Thermocycler Condition for qPCRBio SyGreen

2.15 shRNA Lentiviral Knockdown

2.15.1 Plasmids Used

ShRNA	Mission shRNA glycerol stocks
METTL3	TRCN0000034**714** TRCN0000289**742** TRCN0000289**812** TRCN0000289**814**
FTO	TRCN0000246**247** TRCN0000246**248** TRCN0000246**249** TRCN0000246**250** TRCN0000255**403**
WTAP	*TRCN0000231423* (labeled as **425**) TRCN0000231**424**

Table 7. shRNA plasmid glycerol stock numbers

2.15.2 Grow Up Lentiviral Plasmids

To generate the psPAX.2 (also labelled pSPAG) and pVSV.G envelope helper plasmids, Mix&Go Competent *E. coli* cells were transformed. 50µL of cells were mixed with 2.5 µL of plasmid of interest (The Zymo Research Corp official Mix&Go Transformation protocol uses µL not µg amount, so this varied between constructs). The cells and plasmid were incubated on ice for 5 minutes. Under antiseptic conditions the transformed cells were plated on LB+ampicillin (100 µg/mL) agar plates. The plates were incubated overnight at 37 °C. A single colony was picked and used to inoculate 6 mL of LB+ampicillin broth for 6.5 hours shaking at 37 °C, that initial culture was then transferred to 250 mL of LB+ ampicillin and incubated overnight at 37 °C. The cultures were centrifuged at 6800g and the plasmid was isolated from lysed cells using the Thermo Scientific GeneJET Maxiprep Kit Protocol.

To generate the shRNA plasmids, Aldrich MISSION shRNA (Sigma Aldrich) bacterial glycerol stocks were streaked on warm LB+ampicillin agar plates under antiseptic conditions (from Dr Belinda Belmarez, Table 7). Five constructs targeting FTO and four constructs targeting METTL3 and WTAP. They were grown overnight at 37°C. Single colonies from each plate were inoculated into 6 mL of LB+amp broth to grow overnight at 37°C. Plasmid DNA was extracted from cultures using Thermo Scientific GeneJET Miniprep Kit Protocol. Uncut plasmid preparations were analysed on a 1% TAE Agarose gel for 43 minutes at 100V in 1xTAE Buffer.

2.15.3 Lentivirus particle production and transduction

293T cells were plated in fresh media in a 6-well plate (one well per shRNA to be tested, including scrambled), 500,000 cells/well. Cells were incubated at 37 °C in a humidified incubator in an atmosphere of 5% CO2. The next morning the cells were >80% confluent. Cells were transfected with the following 0.65 µg psPAX2 vector, 0.65 µg pVSV.G vector, 1.2 µg lentiviral vector containing target gene of interest, 4 µL Lipofectamine2000 and 200 µL OPTI-MEM. The cells were incubated in this transfection media for 5 hours and then replaced with 1.5 ml fresh DMEM medium without P/S. Incubated the cells for an additional 48 hours to allow for lentivirus production into the supernatant. After 48 hours, the cell line of interest was collected at a concentration of 300,000 in 0.5ml DMEM NO P/S, added 1 mL of filtered virus supernatant from each well of 293T cells directly into tubes of RD cells (0.45um filters). The cell line of interest was then spin inoculated for one hour at 1200 rpm. After one hour 1.5 ml medium/cells was transferred into 6-well plates, including control cell line of interest. The cells were incubated until the end of the day and changed the media to fresh total DMEM without Pen/Strep. After another 48-hour incubation period the medium was removed ,the cells were washed with PBS, and selection medium containing DMEM with puromycin- at a 2µg/ml final concentration was added. The selection medium was changed with fresh antibiotic every 2-3 days. Once they reached 80% confluency in the 6 well plates they were transferred to a T25 flask. Once they reached 80% confluency in the T25, three-fourths were frozen down in 10% DMSO FBS and stored at -80°C. The

remaining cells were continuously passaged. Cells were always kept under antibiotic selection and were assessed for knockdown after 7 days post-transduction. In Huh7 cells, the knockdown was optimized for experiments, assessing cells each day post-transduction.

2.15.3 Analysis of Knockdown Efficiency

Western blot analysis of protein knock-down efficiency was performed for each shRNA cell line. 25 µg (as determined by Thermo Scientific Pierce BCA Protein Assay Kit) of each sample was loaded on an SDS-Page resolving gel (10% stacking and 6% separating) and was run them 120V for 1.5 hours. The protein was transferred from the gel onto a PVDF (Immobilon) membrane at 240 mA for 2 hours, blocked membrane in LICOR blocking buffer for 1 hour at room temperature, then set to rock at 4°C overnight in 5mL of diluted primary antibodies (anti-actin (mouse) Ab (1:10000) with either Anti-WTAP (Abcam Ab195380) Anti-METTL3 (Rabbit) Bethyl A301-567A (1:250), or Anti-FTO (Rabbit) Abcam EPR6894 ab 126605 (1:5000)). The next day membranes were incubated in anti-Rabbit and anti-Mouse secondary antibody. Knock-down was quantified on the LICOR. Each sample from protein shRNA RD cells was compared to the scrambled shRNA transduced control RD cells.

2.16 Sub-genomic Replicase Assay

Performed according to published protocol [186]. Huh7 or RD cells were seeded at 100,000 cells/well in a 12-well plate. The next day they were observed to reach 70% confluency. For each well, 250 ng of the sub-genomic CHIKV RNA was added to 50 µL of Opti-MEM™. Separately for each well, 1 µL of Lipofectamine-2000 (ThermoFisher) was added to 50 µL of Opti-MEM™. They were independently incubated at room temperature for 5 minutes. Then the RNA mixture was gently added to the Lipofectamine-2000 mix and incubated at room temperature for 20 minutes. The cells were washed with 1x PBS and 400 µL of Opti-MEM™ was added to each well. After the 20 minute incubation, the RNA and Lipofectamine-2000 mixture (transfection mixture) was added dropwise onto each well. The cells were

incubated with the transfection mixture for 4- 6 hours. Then the mixture was removed, the cells were washed with 1x PBS, and replaced with cDMEM.

After the experimental window of time, generally 24 hours, the media was removed, the cells were washed again with 1 x PBS, and the cell monolayer was lysed in Passive Lysis Buffer (PLB, Biotium). The samples were stored at -20 °C until analysis. To analyse the lysates for luciferase signal, they were thawed, and 10 µL of the lysate was mixed with 50 µL of firefly working solution (Biotium) in a white bottom 96-well plate. The firefly luciferase activity levels were assessed using the FLUOstar Plate Reader (BMG LABTECH).

2.17 *Trans* replicase Assay

Performed according to published protocol [187]. Huh7 cells were seeded at 100,000 cells/well (500,000 cells/well for C636 cells) in a 12-well plate the day before. The next day they were observed to reach 70% confluency. For each well, 500 ng of the reporter plasmid and replicase plasmid were added to 50µL of Opti-MEM™ (250ng was optimized for transfection of C636 cells). For each well, 1 µL of Lipofectamine-2000 (ThermoFisher) was added to 50 µL of Opti-MEM™. They were independently incubated at room temperature for 5 minutes. Then the DNA mixture was gentled added to the Lipofectamine-2000 mix and incubated at room temperature for 20 minutes. The cells were washed with 1x PBS and 400 µL of Opti-MEM™ was added to each well. After the 20-minute incubation, the DNA and Lipofectamine-2000 mixture (transfection mixture) was added dropwise onto each well. The cells were incubated with the transfection mixture for 4- 6 hours. Then the mixture was removed, the cells were washed with 1x PBS, and replaced with media.

After the experimental window of time, generally 24 hours, the media was removed, the cells were washed again with 1 x PBS, and the cell monolayer was lysed in Passive Lysis Buffer (PLB, Biotium). The samples were stored at -20 °C until analysis.

To analyse the lysates for luciferase signal: 10 µL of the lysate was mixed with 50 µL of firefly working solution (Biotium) in a white bottom 96-well plate

to determine the firefly signal. Additionally, 10 µL of the lysate was mixed with 50µL of the *Renilla* working solution (Biotium) to determine the Gaussia signal. The relevant luciferase activity levels were assessed using the FLUOstar Plate Reader (BMG LABTECH).

2.18 In silico Methods

2.18.1 Mapping m^{6}A Sites

The full length wild-type CHIKV RNA sequence was input into the Cui Lab online SRAMP tool [188]. The mature mRNA mode was used as a FASTA format sequence not containing introns and the generic predictive model was used.

2.18.2 RNA Structure Mapping

307 nucleotides of the natural CHIKV sequence present in the *trans* complementation assay system were used to predict the structure of this region using an 'RNA structure' software web page interphase[189] (link below)

https://rna.urmc.rochester.edu/RNAstructureWeb/Servers/Fold/Fold.html (2010)

WT CHIKV 5' region
ATGGCTGCGTGAGACACACGTAGCCTACCAGTTTCTTACTGCTCTAC TCTGCAAAGCAAGAGATTAATAACCCATCATGGATCCTGTGTACGTG GACATAGACGCTGACAGCGCCTTTTTGAAGGCCCTGCAACGTGCGTA CCCCATGTTTGAGGTGGAACCAAGGCAGGTCACACCGAATGACCAT GCTAATGCTAGAGCGTTCTCGCATCTAGCTATAAAACTAATAGAGCAG GAAATTGACCCCGACTCAACCATCCTGGATATCGGCAGTGCGCCAGC AAGGAGGATGATGTCGGACAGGAAG
$96^{A>G}$ mutant CHIKV 5' region
ATGGCTGCGTGAGACACACGTAGCCTACCAGTTTCTTACTGCTCTAC TCTGCAAAGCAAGAGATTAATAACCCATCATGGATCCTGTGTACGTG GGCATAGACGCTGACAGCGCCTTTTTGAAGGCCCTGCAACGTGCGT ACCCCATGTTTGAGGTGGAACCAAGGCAGGTCACACCGAATGACCAT GCTAATGCTAGAGCGTTCTCGCATCTAGCTATAAAACTAATAGAGCAG GAAATTGACCCCGACTCAACCATCCTGGATATCGGCAGTGCGCCAGC AAGGAGGATGATGTCGGACAGGAAG
Table 8. CHIKV sequence for secondary structure computational modelling The first 307 nucleotides with the $^{A}96^{G}$ mutation highlighted in yellow.

The resultant .ct file was then converted to a dot bracket file. The dot bracket file along with the sequence was then visualized using VARNA software[190] (linked below)

https://varna.lri.fr/index.php?lang=en&page=downloads&css=varna

2.19 Q5 Mutagenesis of m^{6}A Sites

To mutate the two potential m^{6}A sites in both the infectious clone plasmid and the *trans* complementation reporter plasmid the Q5® Site-Directed Mutagenesis Kit (NEB, E0554) was used according to the manufacturer's

instructions. Primers which substituted an $96^{A>G}$ and $11749^{A>G}$ (viral genome position) were generated using the online tool accompanying the kit[191].

https://nebasechanger.neb.com/

Transformed NEB 5-alpha competent *E. coli* cells were picked from selection plates to inoculated 10mL of LB+Amp overnight at 37 °C, the plasmid was isolated, and their sequence confirmed by Sanger sequencing. Confirmed plasmids were then double digested by restriction enzymes.

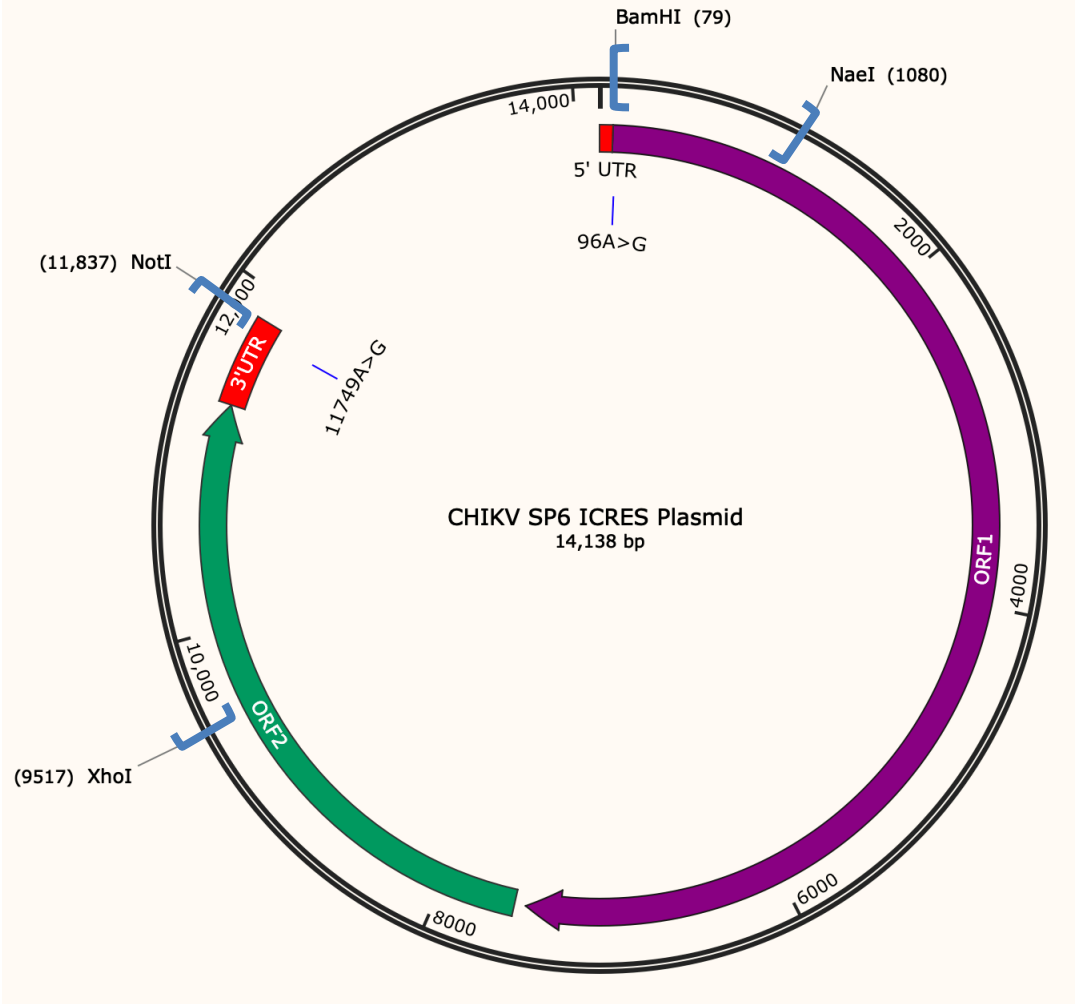

Figure 15. Infectious clone CHIKV plasmid showing $96^{A>G}$ and $11749^{A>G}$ substitutions

Blue brackets show the regions that were cut from the mutated plasmid by restriction enzymes listed, purified, and sub-cloned back into the original plasmid backbone. $96^{A>G}$ and $11749^{A>G}$ substitutions are marked in blue. CHIKV ORF1 coding region shown by purple arrow. CHIKV ORF2 coding region shown by green arrow. Figure generated in SnapGene.

A

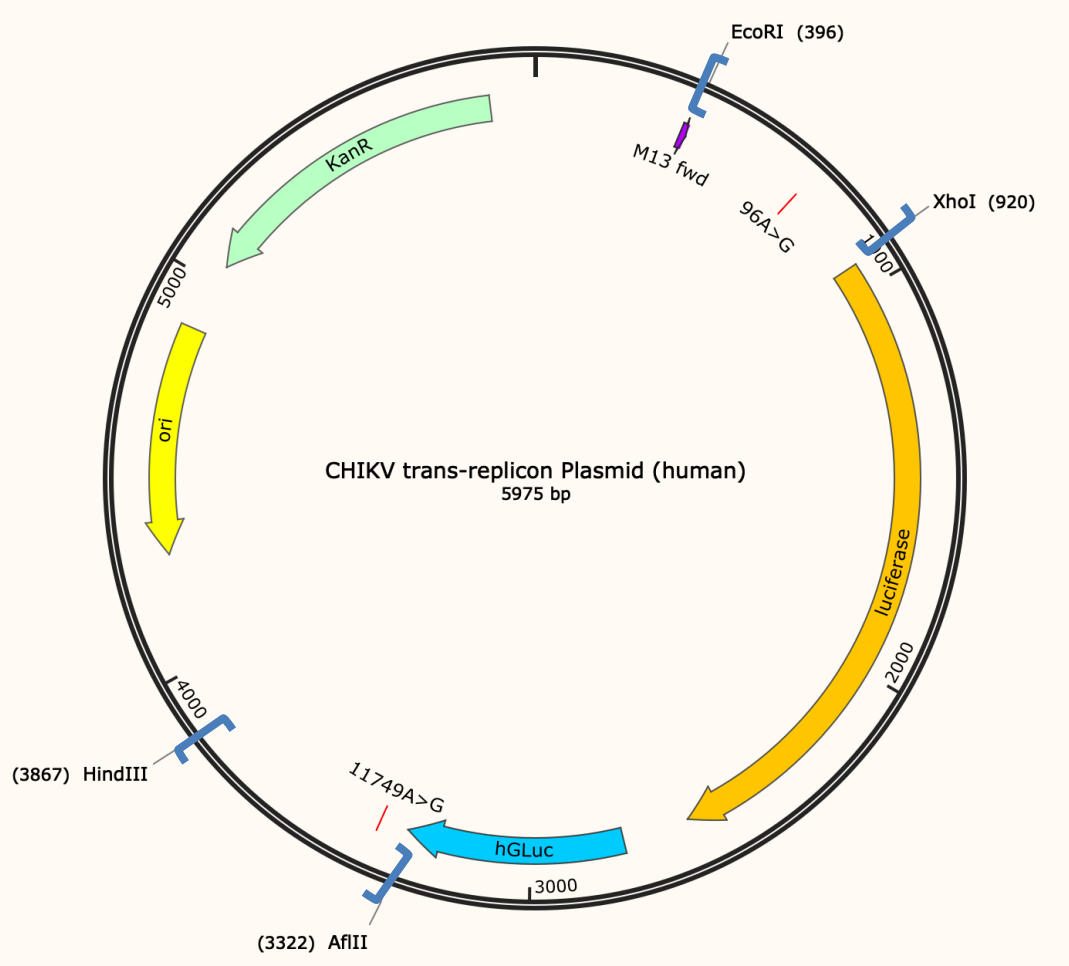
EcoRI (396)
M13 fwd
96A>G
XhoI (920)
1000
2000
luciferase
3000
hGLuc
11749A>G
(3322) AflII
4000
(3867) HindIII
ori
5000
KanR
CHIKV trans-replicon Plasmid (human)
5975 bp

B.

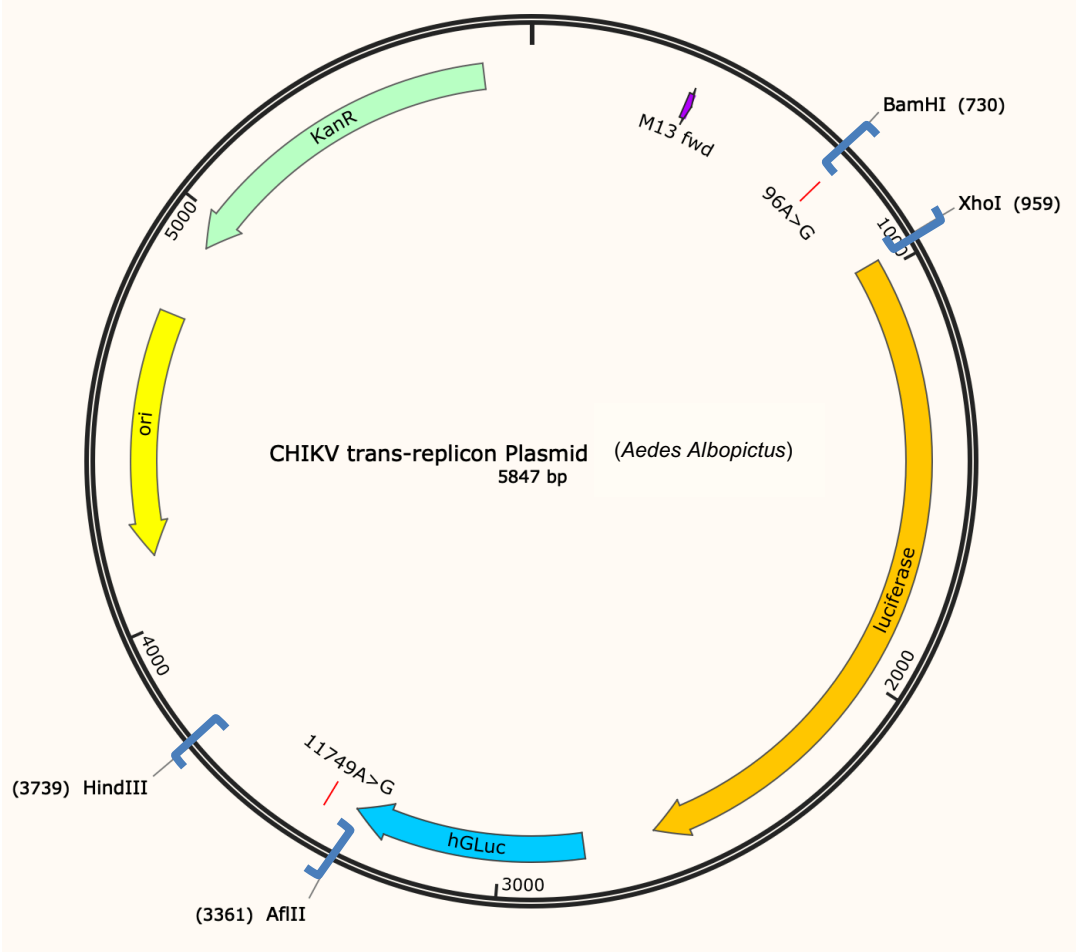

Figure 16. *Trans* replicon CHIKV plasmid showing $96^{A>G}$ and $11749^{A>G}$ substitutions

A. *human.trans* plasmid - HsPolII-Gluc-Fluc: Human compatible reporter plasmid
B. A.ae.*trans* plasmid - Ubi-Gluc-Fluc: *Aedes Albopictus* compatible reporter plasmid

Blue brackets show the regions that were cut from the mutated plasmid by restriction enzymes listed, purified, and sub-cloned back into the original plasmid backbone. $96^{A>G}$ and $11749^{A>G}$ substitutions are marked in red.

M13 fwd sequence shown by purple arrow, firefly luciferase coding sequence shown by orange arrow, gaussian luciferase coding sequence shown by blue arrow, origin of DNA replication sequence shown by yellow arrow, and finally the kanamycin resistance coding sequence shown by green arrow.

Figure generated in SnapGene. Construct design described in Utt et al. 2019 [187]

For the $96^{A>G}$ substitution in the ICRES plasmid the region of interest was digested with *BamH1* and *Nae1* to generate a 1001 bp fragment which was ligated back into the original backbone plasmid (Figure 15). For the $11749^{A>G}$ substitution in the ICRES plasmid the region of interest was cut with *Xho1* and *Not1* to generate a 2320 bp fragment which was ligated back into the original backbone plasmid (Figure 15).

For the $96^{A>G}$ substitution in the *human.trans* plasmid the region of interest was digested with *EcoR1* and *Xho1* to generate a 524 bp fragment which was then sub-cloned back into the original backbone plasmid (Figure 16.A). For the $11749^{A>G}$ substitution in the *human.trans* plasmid region of interest was digested with *HindIII* and *AflI* to generate a 545 bp fragment which was sub-cloned back into the original plasmid backbone (Figure 16.A).

For the $96^{A>G}$ substitution in the A.ae.*trans* plasmid the region of interest was digested with *BamH1* and *Xho1* to generate a 229 bp fragment which was sub-cloned back into the original backbone plasmid (Figure 16.B). For the $11749^{A>G}$ substitution in the A.ae.*trans* plasmid the region of interest was digested with *HindIII* and *AflI* to generate a 378 bp fragment which was sub-cloned back into the original plasmid backbone (Figure 16.B).

The digested plasmids were then analysed by 1% denaturing agarose gel, and isolated using the NEB Monarch® DNA Gel Extraction Kit according to manufacturer's instructions. The original plasmid backbone was treated with calf intestinal alkaline phosphatase (NEB), and ligated with the confirmed mutated insert. Ligation was performed using the Quick ligation protocol.

Components	20 µL Total
Quick Ligase Reaction Buffer 2x	10 µL
Vector DNA	50 ng
Insert DNA	37.5 ng
Nuclease-free Water	Up to 20 µL
Quick Ligase	1 µL
Room temperature (25 °C) for 5 mins.	

Table 9. NEB Quick Ligase protocol

These conditions were used to subclone the mutated insert back into the plasmid backbone. A 3:1 (insert:vector) was used for ICRES plasmid and for the *human.trans* replicon plasmid.

For the *A.ae.trans* plasmid an alternative ligation method was used after trials with NEB Quick Ligase were unsuccessful. Instant Sticky-end Ligase (NEB) was used at a 3:1 (insert:vector).

These mutated plasmids were then retransformed into competent *E. coli* cells according to the methods discussed in 2.2, the plasmid was isolated, and the desired mutated sequence was confirmed by Sanger sequencing.

2.20 Sanger Sequencing

Between 750 ng and 1.5 µg of plasmid DNA was sequenced by Sanger sequencing with 10 pmol primer in a total volume of 20 µL using Eurofinn Genomics Sanger sequencing service.

2.21 Nanopore

To assess the sequence of the 5' region of CHIKV NGS was used. The Oxford Nanopore Technology, PCR tiling of SARS-CoV-2 virus with rapid barcoding (SQK-RBK-110) was adapted for this purpose. To generate eleven 1,200 bp amplicons primers were designed using Primal Scheme[192]. Two pools of primers were combined to make a 100 µM stock (**Table 10**).

Primer Pool 1	
CHIKV ICRES 1 LEFT	AGACACACGTAGCCTACCAGTT
CHIKV ICRES 1 RIGHT	TGTTCGTATTCCGTTGCGTTCT
CHIKV ICRES 3 LEFT	TGTAAGAAGGAAGAAGCCGCAG
CHIKV ICRES 3 RIGHT	AATAGCCCGCTGTCTAGATCCA
CHIKV ICRES 5 LEFT	CGCAAAAACAGTTATGTGCGGT
CHIKV ICRES 5 RIGHT	TGTTTCTTGTACGACCGGACAC
CHIKV ICRES 7 LEFT	ACCCACTTTGGACTCAGCAGTA
CHIKV ICRES 7 RIGHT	ACCTATTTAGGACCGCCGTACA
CHIKV ICRES 9 LEFT	ATCCCAGTTATGTGCCTGTTGG
CHIKV ICRES 9 RIGHT	CGGCCAATACTTATACGGCTCG
CHIKV ICRES 11 LEFT	TTCATTGTGGGGCCAATGTCTT
CHIKV ICRES 11 RIGHT	TTGTTACTATTCAGGGGTTTTATAGCC
Primer Pool 2	
CHIKV ICRES 2 RIGHT	TCCGAAGACTCCTATGACTGCA
CHIKV ICRES 2 LEFT	AATGTCATTCTCGGTGTGCACA
CHIKV ICRES 4 RIGHT	CTTTGCGACTTCTCGATAGGCA
CHIKV ICRES 4 LEFT	TTGTTGGGCTAAGAGCTTGGTC
CHIKV ICRES 6 RIGHT	CTGCTGCTTTTGGCCCTTTTAG
CHIKV ICRES 6 LEFT	GGTAATGAGCACCGTACCTGTC
CHIKV ICRES 8 RIGHT	CGGTGGGGAGAACATGTTAAGG
CHIKV ICRES 8 LEFT	ATGGCAACGAACAGGGCTAATT
CHIKV ICRES 10 RIGHT	GCCAAATTGTCCTGGTCTTCCT
CHIKV ICRES 10 LEFT	AACACTCCTGTCCTACCGGAAT

Table 10. NGS Primers designed using Primal Scheme [192]

The number indicates the amplicon that is being amplified, left indicates the forward primer and right indicates reverse primer.

2.21.3 Library Preparation

Two reverse transcription reactions were done in duplicate using extracted cellular RNA or in-vitro transcribed 5’ capped CHIKV RNA. Each sample was

reverse transcribed using 8 µL of extracted cellular RNA was mixed with 2 µL of the LunaScript™ RT SuperMix (New England Biolabs). These samples were then placed in a thermocycler at 25°C for 2 minutes, 55°C for 10 minutes and 95°C for 1 minute, and then held at 4°C.

A mastermix was prepared for two separate PCR reactions of: RNase free H_20, primer pool 1 or 2 (100 µM) and Q5® Hot Start 2x Master Mix (New England Biolabs). The primer pool 1 or 2 mastermix was added to clean RNase free PCR tubes and then mixed with 2.5 µL of the cDNA generated from the RT step. PCR reactions were performed under these conditions:

Cycle Number	**Temperature**	**Time**	**Step**
1 cycle	98 °C	30 sec	Polymerase Activation
35 cycles	98 °C	15 sec	Denaturation
	65 °C	5 mins	Anneal/Extension
Hold	4 °C	Indefinite	Final Hold

Table 11. Q5® Hot Start 2x Master Mix Thermocycler Conditions

The entire contents of both primer pool reactions were then mixed. Then 7.5 µL of both primer pool PCR products was combined with 2.5 µL of each barcode from the Rapid Barcoding Plate (Oxford Nanopore Technology). The sample was then incubated at 30°C for 2 minutes and 80°C for 2 minutes to attach the “barcodes”, after which the samples were pooled together. A 1:1 ratio of pooled sample with AMPure XP SPRI beads (Beckman Coulter) was incubated at room temperature for 5 minutes. To pellet the magnetic beads a magnetic rack was used and the supernatant removed. The pellet of beads and barcoded cDNA was washed twice with 1 mL 80 % ethanol. To evaporate the ethanol from the beads they were allowed to dry at room temperature for 5 minutes. Elution buffer (Oxford Nanopore Technology) was added and incubated with the beads for 10

minutes at room temperature. The beads were pelleted and the elution was collected to a fresh tube.

The eluted cDNA was mixed with 1 µL of Rap F (Oxford Nanopore Technology), incubated at room temperature for 5 minutes and then stored on ice. The flow cell priming mix was prepared by mixing the Flush Buffer (Oxford Nanopore Technology) with the Flush Tether (Oxford Nanopore Technology). Finally, the prepared library was mixed with Sequencing Buffer II and Loading Beads II.

2.21.4 Sequencing Run

To prime the flow cell, 800 µL of priming mix was added to the priming pore and incubated at room temperature for 5 minutes. The sample pore was then opened and a further 200 µL of priming mix was added to finish priming the flow cell. Finally, the prepared DNA library gentle loaded into the sample port.

The sequencing run was set up at the recommended voltage, for 72 hours and with basecalling, barcoding enabled, and mid-read barcoding was also enabled. The minimum barcoding score was overridden to 60, and the minimum mid-read barcoding score set at 50.

2.21.5 NGS Analysis

Real time basecalling was performed using Guppy that is integrated within MinKNOW; the 'Fast' basecalling option was selected. Guppy was also used to demultiplex samples based on their "barcodes". Post-run analysis to align the FastQ files generated by Guppy to a reference genome used the InterARTIC web application, so that single nucleotide variations could be detected relative to the CHIKV reference genome[193]. The Medaka workflow was chosen for detection, and consensus genome sequences were generated. The consensus FASTA files (.bed files) were used for downstream analysis on IGV 2.13.0. This allowed for determination of population percentages of bases at specific nucleotide positions.

3 Chapter 3- Global m^{6}A knockdown inhibits CHIKV replication

m^{6}A is a common reversible methylation of an adenosine primarily at a DRACH consensus sequence on mRNAs. m^{6}A in human cells is catalysed by the m^{6}A writer complex using the methyl donor SAM. Homologs for the m^{6}A methyltransferase in yeast, *Drosophila melanogaster (D. melanogaster)*, and bacteria have also been identified [194]. The m^{6}A signature is read by a diverse family of reader proteins such as YTH-domain containing proteins, which dictate the RNA's localization within the cell, splicing, stability, translation, and secondary structure [123]. The connection between m^{6}A and virus biology is thought to be well established including examples of both DNA and RNA viruses [155]. Members of the *Flaviviridae* family, which are positive RNA viruses and which replicate solely in the cytoplasm, have also been, shown to have their RNA genomes m^{6}A methylated [116,115]. This points to redistribution of m^{6}A methyltransferases and demethylases to the cytoplasm from the nucleus.

Work on m^{6}A in CHIKV infection suggested that the packaged CHIKV genome within the virion is m^{6}A -methylated [140]. They also propose that known m^{6}A readers YTHDF1 and YTHDF3 interact with genomic CHIKV RNA[140]. This peer-reviewed and published work suggests that m^{6}A plays a pro-viral or antiviral role, depending on which m^{6}A reader protein is recruited to the transcript. YTHDF1 and YTHDF3 bind the viral genome and reduce CHIKV replication, while YTHDF2 binds the viral genome and stimulates viral replication [156]. A preprint study which has not yet been through peer review by Dr Belinda Baquero *et al.* 2023 looking at m^{6}A in relation to CHIKV and DENV in Huh7 and 293T cells suggests otherwise [195]. Their study using LC-MS/MS of RNA, Oxford Nanopore Direct RNA sequencing, and m^{6}A methyltransferase knockdown showed no evidence to support the m^{6}A methylation of the viral transcript or any effect of m^{6}A on viral replication [195]. They also say that there is no redistribution of proteins involved in m^{6}A to the cytoplasm following CHIKV infection, unlike what was observed for HCV [195,196]. Conflicting reports suggest a complex but developing understanding

of the landscape of m^{6}A proteins within the cell and their interaction with viruses throughout the lifecycle of the virus.

3.1 Aims

The aim of the work described in this chapter was to establish if m^{6}A plays a role in CHIKV replication. These experiments sought to reduce cellular m^{6}A levels by two methods: a small molecule inhibitor of an enzyme necessary for the regeneration of SAM the methyl donor in the m^{6}A addition and shRNA knockdown of proteins in the host m^{6}A pathway. Important considerations of the limitations of these widely used methods in m^{6}A methylation studies will be discussed in following sections. Infection with CHIKV and transfection with CHIKV replicon constructs were performed in two human cell lines and one mosquito cell line where m^{6}A was reduced using established experimental techniques in these cells. An m^{6}A modified RNA immunoprecipitation (MeRIP) was also trialled on RNA extracted from CHIKV infected Huh7 cells, to see if the viral genome could be detected by qPCR in the cDNA generated from RNA bound to the anti-m^{6}A antibody.

Huh7 cells (a human hepatoma cell line) were used due to their high reported CHIKV replication titres and CHIKV's natural tropism for liver cells in both acute infection and as a persistent reservoir of CHIKV [197, 198,199, 200,201]. Additionally, in humans, hepatitis has been reported in acute infection with CHIKV [202]. In a non-human primate macaque model of CHIKV infection, the liver was found to be a main late-stage reservoir of CHIKV, with viral load still detectable 2 months post infection [203].

To determine if there were differences in the role of m^{6}A methylation in CHIKV replication across human cell types, a second culture system, derived from a different tissue of origin was used. The second human tissue culture system used to investigate CHIKV replication was RD cells (a human muscle Rhabdomyosarcoma cell line). As CHIKV symptoms include severe myalgia [204] (muscle pain), muscle derived cells were identified as a relevant second cell type in which to study m^{6}A and CHIKV. The findings in RD cells are described here but with the understanding that Sudeep et al. (2019) in their study of susceptibility of different vertebrate and invertebrate cell lines

to CHIKV infection, found that RD along with A-594 (a human lung cell line) cells produced the lowest titre virus [205]. This shows variation in CHIKV production across cultured cell lines and therefore potential variation in effects of m^{6}A methylation on the lifecycle of CHIKV across cell lines.

To look at the relationship between CHIKV and m^{6}A methylation in CHIKV's mosquito host, C636 cells which are an *A. albopictus* larval cell line, were used. C636 cells have been reported to be the most sensitive mosquito cell line tested and produce the highest titre CHIKV virus [205].

3.2 Small molecule m^{6}A inhibitor (c3Ado) decreases CHIKV replication in Huh7 cells

The cellular m^{6}A methyltransferase protein requires SAM to act as the methyl donor in the catalytic methyltransferase reaction onto RNA [80]. A lowered amount of SAM or its reaction product SAH available in the cell can cause an overall decrease in m^{6}A by reducing the available pool of the essential methyl donor within the cell [206]. 3-Deazaadenosine (c3ADO) acts as a chemical inhibitor of cellular m^{6}A methylation by inhibiting the S-adenosylhomocysteine hydrolase (SAHH) competing with SAH for binding, which in turn interrupts the essential degradation of SAH and generation of SAM [206].

3.2.1 Introduction to c3Ado

SAM is generated through the cyclic balanced degradation and addition of chemical building blocks. It acts as a crucial methyl donor in many ubiquitous and important chemical reactions necessary for metabolism and cell viability, including the methylation of RNA in the m^{6}A reaction as well as RNA cap methylation. Part of the degradation of the downstream SAM by-product, SAH, is the enzyme SAHH which hydrolyses the adenosine component from the homocysteine component of SAH (**Figure 17**)[206]. The chemistry of adenosine and c3Ado are analogous allowing c3Ado to act as a potent competitor for SAH and as a SAHH sink. m^{6}A differs from adenosine by the methylation at the nitrogen 6 position, but is otherwise chemically

identical (**Figure 17 A**). They are both purine rings composed of a six membered pyrimidine ring and a five membered imidazole. The SAHH inhibitor, c3Ado, instead has a six membered pyridine ring and a five membered imidazole (**Figure 17 A**). The amino group at the carbon 6 position is consistent with the adenosine present in SAM.

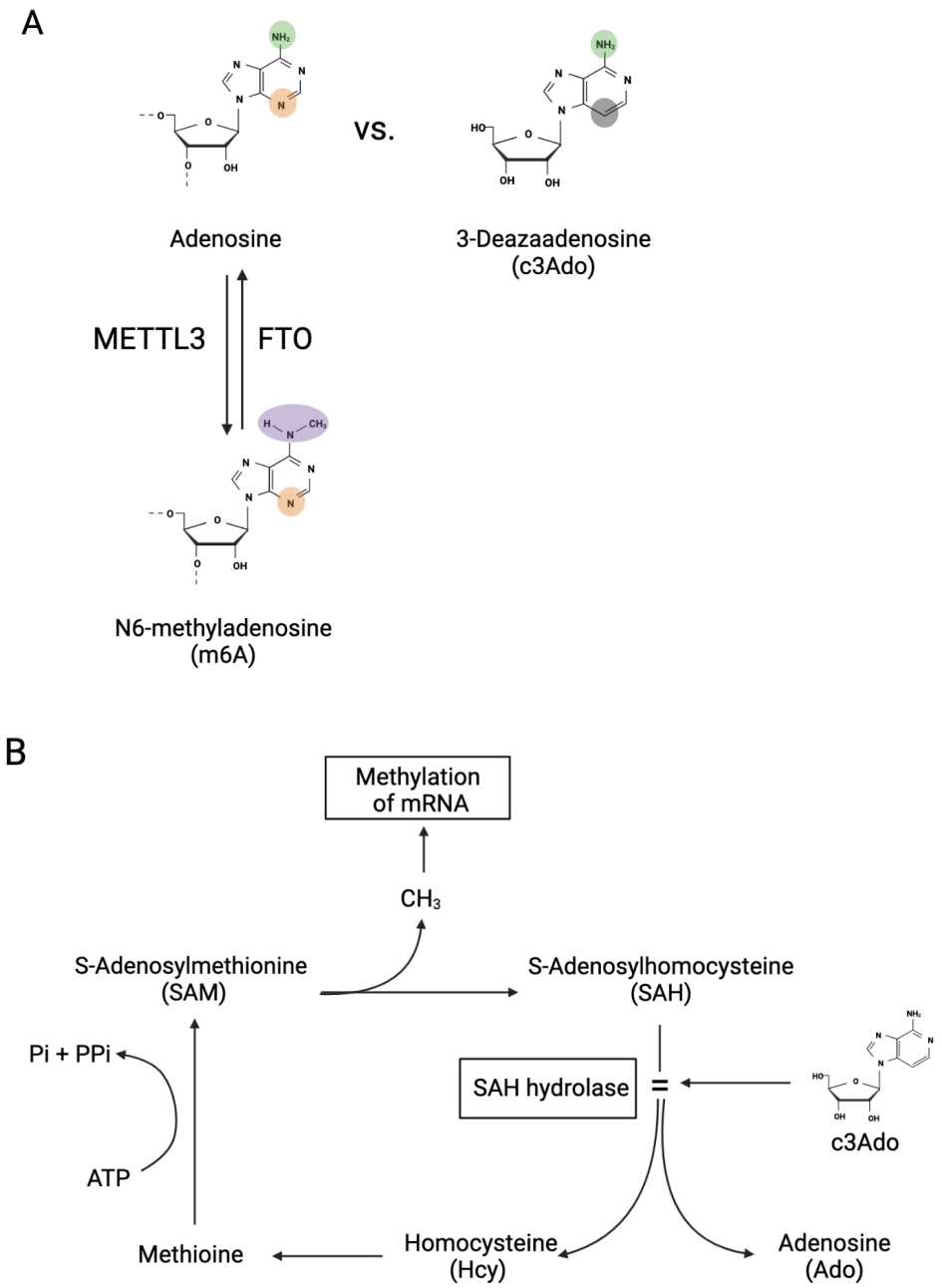

Figure 17. 3-Deazaadenosine (c3Ado) is an adenosine analogue that interrupts the generation of SAM.

A. Adenosine and c3Ado share chemical structural similarities that explain c3Ado's ability to reduce SAM. m^6A differs from adenosine only at the methylation at the n6 position (purple), and can be added by METTL3 and removed by FTO.

B. Schematic representation showing the generation and essential degradation of SAM to its by-products with c3Ado interrupting the enzyme SAHH. Adapted from De Clercq [206] Figure created using BioRender.

c3Ado is a member of a class of drugs, adenosine analogues, decades in use in both research and therapeutics. Its antiviral effects have been studied including against other RNA viruses, including the negative strand RNA virus Ebola virus [206], [207]. Baquero-Perez *et al.* (2019) used c3Ado at a concentration of 200μM to reduce m^6A in HEK-293 cells for the study of m^6A and KSHV[127]. They showed it was not cytotoxic at that concentration [127]. To control for cell type variation in c3Ado cytotoxicity a cytotoxicity assay was performed for each cell line. This allowed the results of c3Ado treatment to be put into the context of the SAM requirements of each cell line studied. Sedding et al. (2009) have also shown that c3Ado prevents migration and proliferation of human vascular smooth muscle cells *in vivo*, presenting a possibly anti-oncogenic effect as well [208]. Xu *et al.* (2020) showed that the tumorgenicity of colon cancer cells is in part due to an increase in METTL3, the major m^6A methyltransferase [209]. In their work they used c3Ado (also referred to as DAA) as an inhibitor of m^6A methylation, citing other papers such as the work of Fustin *et al*. (2013) on m^6A and the circadian clock as their justification for c3Ado use [210].

SAM acts as a methyl donor in many cellular reactions. The 5' end of the CHIKV positive strand RNA has the ubiquitous 5' m7G cap [36]. Zhang *et al*. (2022) show the molecular basis of the capping and methylation by CHIKV nsP1 of the CHIKV RNAs [36]. In this reaction SAM acts as the methyl donor. However, work by Mundgal *et al.* (2020) shows that c3Ado does not affect the essential methyltransferase activity of CHIKV nsP1 *in vitro*, which alleviates a potential concern in using this drug in the study of m^6A and CHIKV [211]. However, that assay was not done in the context of live viral replication where c3Ado influenced SAM reduction could cause a decrease in CHIKV genomic RNA with a fully methylated cap. However, given an understanding of the limitations and published literature stating that c3Ado treatment did not impact methyltransferase activity of CHIKV nsP1 an assay using c3Ado could show that any reduction in CHIKV replication would be less likely due to a decrease in essential capping activity by nsP1, but rather the intended reduction of SAM in the cell.

Given its widespread use c3Ado was chosen for this work as a cellular methylation inhibitor to assess its effect on CHIKV replication in a human liver derived cell line Huh7.

3.2.2 c3do reduces CHIKV replication in Huh7 cells

Firstly, it was necessary to determine a maximum non-toxic dose of c3Ado to use in experiments with Huh7 cells. m^6A methylation and other SAM dependent methylation reactions are essential cellular processes, so the aim was to reduce the amount of SAM in the cell without that treatment being too cytotoxic to the cells.

The MTT assay is commonly used to determine cell viability. Only viable cells are detected, as their mitochondrial reductase should be able to break down MTT reagent (3-(4,5-dimethylthiazol-2-yl)-2,5-diphenyl-2H-tetrazolium bromide) to the purple dye formazan which has a detectable absorbance near 570nm [212]. Huh7 cell cytotoxicity survival was assessed at a range of c3Ado concentrations from 0 to 100 μM, 25 hours post treatment using the MTT assay (**Figure 19**). A 25 hour time point was used to ensure that there was coverage for the 24 hour long infection experiment with a one hour drug pre-incubation time used in the follow-on experiments. A maximum concentration of 100 μM was used. This choice of concentration range to investigate was informed by the previous work with c3Ado in another human cancer derived cell line, HEK293 cells, by Baquero *et al*. (2019) [127]. At 50 μM, c3Ado (dissolved in DMSO) treatment of Huh7 cells had a 71.4% survival rate normalized to cells exposed to the same volume of DMSO but with no c3Ado (**Figure 19.A**). Sedding *et al*. (2009) showed that c3Ado at 50 μM has no effect on VSMC necrosis or apoptosis suggesting that the concentration range chosen was consistent with published literature [208]. Consequently, 50 μM c3Ado was used as the maximum non-toxic dose for analysis of the effect of m^6A methylation inhibition on CHIKV replication in Huh7 cells. In their work, Baquero *et al.* (2019) used the cut off of 80% survival when assessing the effects of c3Ado on HEK-293 cells so the aim was to have a similar level of survival but in Huh7 cells which is a more relevant cell line system in which to study CHIKV [127].

However, it is important to note that 71.4% survival still presents substantial cell death and that the MTT assay does not provide insight into whether the surviving treated cells remain unaffected in ways that could impact viral replication unrelated to SAM dependent m^6A methylation of RNA. Infectious CHIKV was generated in BHK cells, a CHIKV permissive mammalian cell culture system. BHK transfection by electroporation with capped *in vitro* transcribed CHIKV RNA was used to generate virus stocks at approximately $1x10^7$ plaque forming units per millilitre (PFU/mL). Huh7 cells were pre-treated with 50 µM c3Ado for 1 hour prior to infection with CHIKV at an MOI of 1. Supernatant was collected at 24 hpi and productive CHIKV replication was measured by plaque assay (Figure 18).

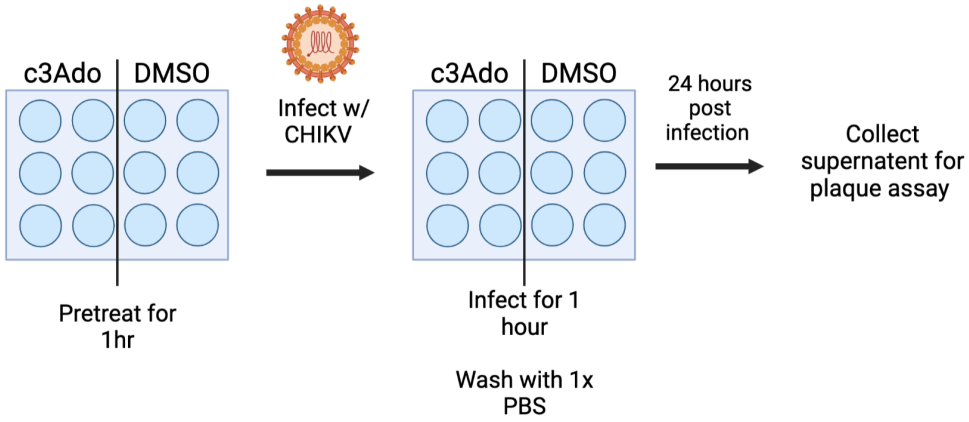

Figure 18. c3Ado with CHIKV Experimental Workflow

Work flow of disruption of methylation in cell culture using the SAH hydrolase inhibitor molecule, c3Ado, 3-Deazaadenosine. Cells undergoing c3Ado treatment had the drug present at all stages of the experiment. Cells were pre-treated for one hour with either c3Ado or DMSO (negative control), infected with CHIKV for one hour in media containing the drug, washed with 1x PBS, and media containing the drug replaced to leave for incubation for 24 hours. Supernatant was collected for plaque assay assessment of infectious released virus.

Figure created using BioRender.

DMSO only treated Huh7 cells had a released virus titre of $1.57x10^6$ plaque forming units/mL (PFU/mL) compared to cells treated with 50 μM c3Ado which had a released virus titre of 4.68×10^4 PFU/mL, nearly a two-log decrease (**Figure 19.B**). These results demonstrated that treatment with the maximum non-toxic dose of c3Ado at 50 μM significantly (p=0.0356) inhibited productive CHIKV replication in Huh7 cells (**Figure 19.B**).

Importantly, c3Ado treatment could be having a negative impact on essential cellular functioning and overall health of the remaining cells, through effects on host transcript methylation or other SAM-dependent cellular processes. As a result, the conclusions that can be drawn from these results are limited by the lack of specificity of c3Ado to m^6A methylation. However, at 50 μM approximately 71.4% of Huh7 cells plated will have survived until the 25 hours post treatment. From after the first hour of treatment when the cells were then infected with WT CHIKV until 24 hours later when the supernatant is assessed there is a nearly two-log decrease in virus produced by the surviving Huh7 cells. This suggests there was an inhibition of CHIKV replication by c3Ado treatment as measured by production of infectious virus in Huh7 cells. It would be unlikely that a 30% decrease in cell number would result in such a large reduction in virus production.

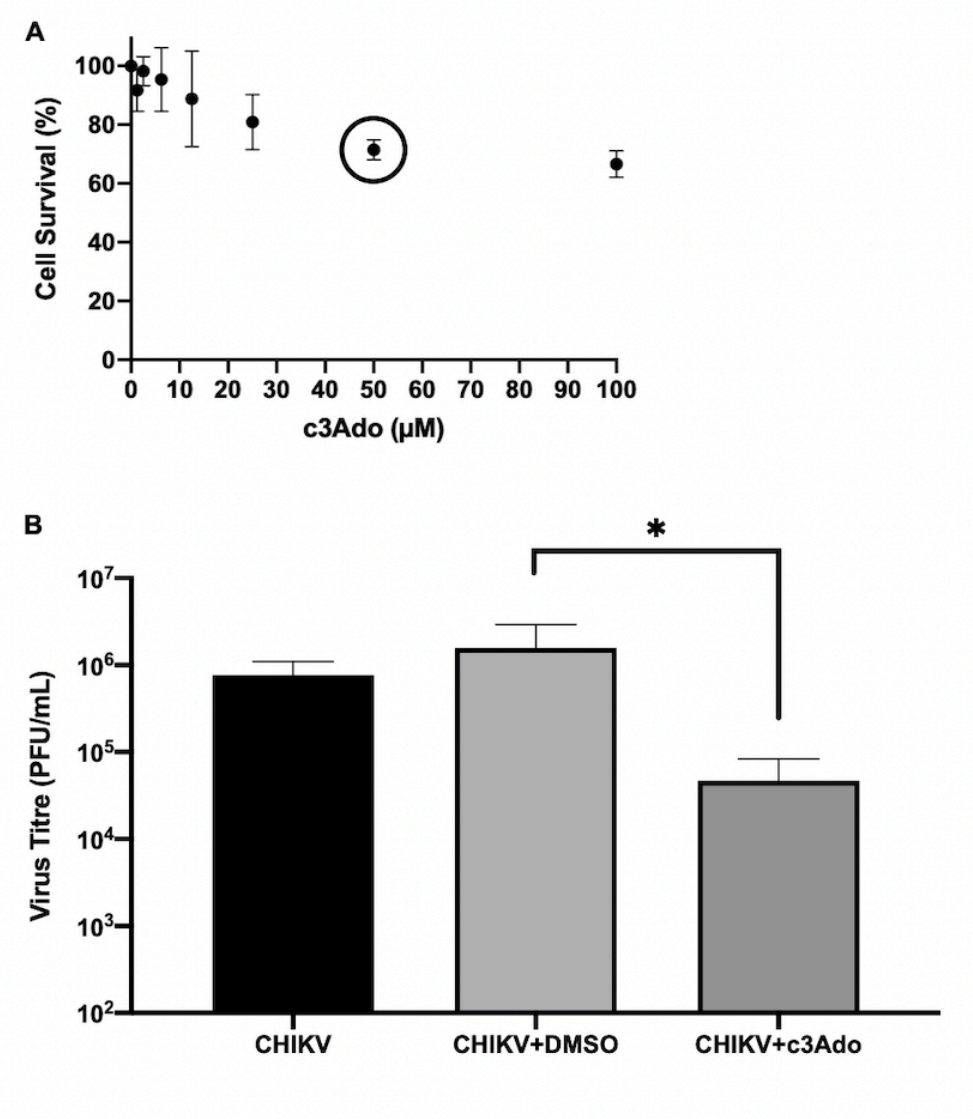

Figure 19. Small molecule inhibitor c3Ado which reduces SAM availability in the cell, inhibits CHIKV replication in Huh7 cells

A. Huh7 cells were treated with a range of c3Ado concentrations and cell viability was determined. Using an MTT Cytotoxicity assay a maximum non-cytotoxic dose of 50 μM (ring on figure) c3Ado dissolved in DMSO yielding greater than 70% Huh7 cell survival, c3Ado+DMSO values were normalized to same DMSO volume negative control n=3, error bars represent standard deviation from the mean. Experiments were repeated in both technical duplicate and biological triplicate.

B. Huh7 cells treated with 50 μM c3Ado show a significant decrease in infectious CHIKV produced by treated cells 24 hours post treatment. Treatment of Huh7 cells with c3Ado resulted in a significant decrease in released virus titre, viral replication as assessed by plaque assay. n=5, p-value= 0.0356 < 0.05*, error bars represent standard deviation. Experiments were repeated in both technical duplicate and biological quintuplicate.

As this assay assessed released virus titre, it was not possible to pinpoint at what stage in the viral lifecycle the reduction in SAM has its effect. The c3Ado could be impacting SAM dependent methylation which would include m^6A deposition without discrimination for host cellular transcripts or viral transcripts. Reduced SAM could interrupt normal functioning of innate immunity impacting early or even late stage replication of the virus. c3Ado could influence RNA structure or protein interaction. As a result, the effect on methylation of host and/or viral transcripts and recruitment by proteins could also be playing a role in the reduction of CHIKV. To begin to assess the role of m^6A more specifically on CHIKV replication within the cell a more targeted knockdown of m^6A machinery, rather than just the ubiquitous methyl donor, SAM, was performed.

3.3 WTAP shRNA knockdown in Huh7 cells

The above results suggest that SAM dependent methylation, possibly also including m^6A methylation, reduced within the cell by treatment with the small molecule inhibitor c3Ado leads to a decrease in CHIKV replication. To better understand the role of m^6A methylation in CHIKV replication an essential member of the m^6A methyltransferase multiprotein complex was targeted for knockdown. Wilms Tumour 1 Associated Protein (WTAP) was chosen. WTAP is thought to recruit appropriate RNA to the complex for methylation by METTL3 and is required for methyltransferase activity [95]. Although WTAP generally localizes to the nucleus guiding RNAs to the nuclear speckles for m^6A methylation, recent work has shown that infection with Hepatitis C Virus (HCV) redistributes WTAP protein to the cytoplasm[196]. This suggested that under viral infection previously identified nuclear localization of WTAP can be shifted[196]. Their work showed by immunofluorescence and WTAP siRNA depletion methods that WTAP colocalizes to the cytoplasm with an HCV NS5A and that WTAP depletion impacts METTL3 and HCV RNA interaction. However, this work does has not shown conclusively the functional role of the WTAP redistribution beyond a possible interaction with METTL3[196]. As a result, this work alone cannot

show conclusively that cytoplasmic WTAP is playing a role in m^{6}A methylation in the cytoplasm for all cytoplasmic replicating viruses, such as CHIKV. The patterns of m^{6}A methylation of RNAs could differ from virus to virus and cell type to cell type.

3.3.1 Producing shRNA knockdown cell lines

To produce the WTAP depleted Huh7 cell line an shRNA-based system was used. shRNA is an experimental molecular biology tool that utilises the cell's endogenous RNA interference (RNAi) mechanism[141].

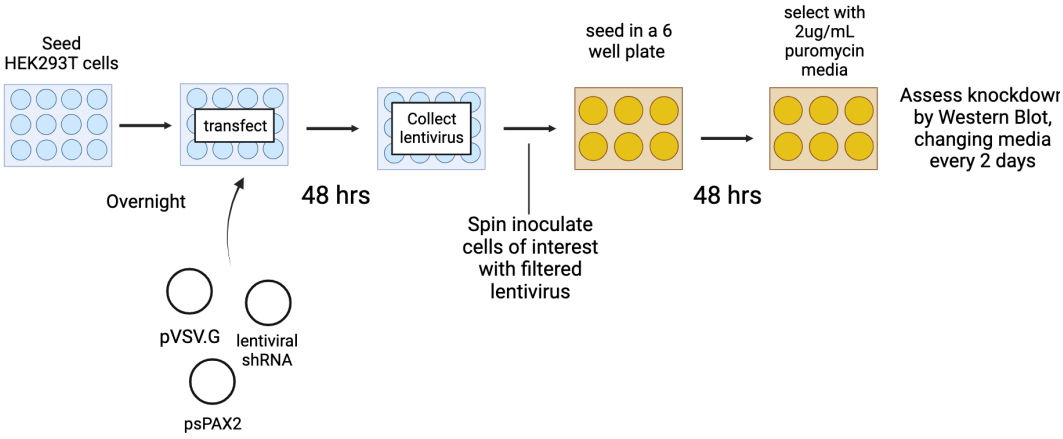

Figure 20. Lentiviral shRNA knockdown workflow

HEK293T cells were seeded and transiently transfected with the plasmids vectors that compose the lentivirus virion as well as the specific shRNA construct. The lentivirus was collected after 48 hours and inoculating in the centrifuge the cell line of interest with the lentivirus, selected with 2µg/mL puromycin, and the protein expression knockdown assessed by western blot.

Figure created using BioRender.

The lentiviral shRNA method was used to generate stable WTAP knockdown Huh7 cell lines using Puromycin resistance. In Figure 20, the workflow from transfection of lentiviral plasmids to transduction of cell line of interest is shown. Traditional transfection of siRNAs into the cell suffers from transfection efficiency concerns and as the experiments required infections and subsequent transfections, this was chosen as the option to assess knockdown of m^{6}A proteins on CHIKV replication.

3.3.2 WTAP shRNA knockdown in Huh7 cells

As discussed above, WTAP is involved in m^6A methylation of host transcripts. It was possible that essential host RNAs would be dysregulated in WTAP knockdown cell lines so these cells were transduced, observed, and assessed for WTAP knockdown. WTAP knockdown cells were observed to grow more slowly than the cells transduced with the scramble shRNA lentivirus. However, WTAP constructs numbered 424, 425, and a combination of the two shRNA constructs resulted in Huh7 cells that still proliferated to an extent that they could be seeded and passaged. Glyceraldehyde 3-phosphate dehydrogenase (GAPDH) protein levels were consistent between transduced and untransduced cells (Figure 21). However, it should be noted that if WTAP knockdown affected cell proliferation this could obviously influence viral replication. WTAP protein knockdown was assessed by western blot, to determine a window of time appropriate for an infection experiment with CHIKV. This time window was day 6-8 post transduction with WTAP shRNA lentivirus. WTAP protein expression began to return by day 11, in comparison to scramble shRNA treated cells (Figure 21).

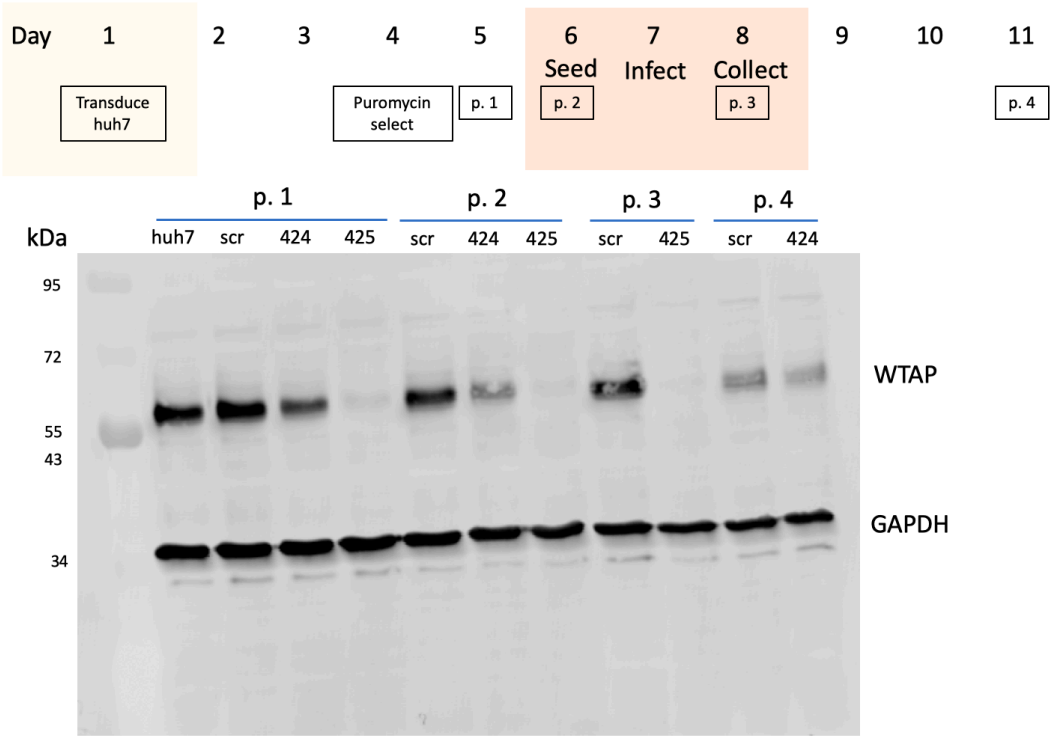

Figure 21. shRNA knockdown for WTAP in Huh7 cells.

Huh7 cells transduced with lentivirus generated from WTP shRNA constructs 424 and 425 were assessed by western blot over 11 days post transduction. This showed a reduction in WTAP protein (55 kDa) production post puromycin selection. GAPDH (36 kDa) is used as a loading control. Cells were assessed from the first passage (p.1) which involved the cells being lifted from the flask with trypsin treatment and plated into a larger cell culture dish to accommodate cell proliferation. Cells were taken from that first passage (p.1) through subsequent passages up to passage 4 (p.4). Timeline at the top of the figure, relevant days have been highlighted. Transduction in yellow and the experimental days in orange.

3.3.3 WTAP knockdown reduced CHIKV replication

To assess the effect of WTAP knockdown in Huh7 cells on CHIKV replication the knockdown cells were infected with CHIKV and assessed for productive viral replication. All three virus infection experiments were conducted from passage 2 to passage 3 post transduction and from independent transductions with lentivirus generated for each individual experiment. The knockdown Huh7 cells were collected on day 6 to seed, infected with CHIKV at a multiplicity of infection (MOI) of 1 on day 7, and the supernatant and lysed monolayers were collected on day 8, 24 hpi, as highlighted by the orange box in Figure 21**.**

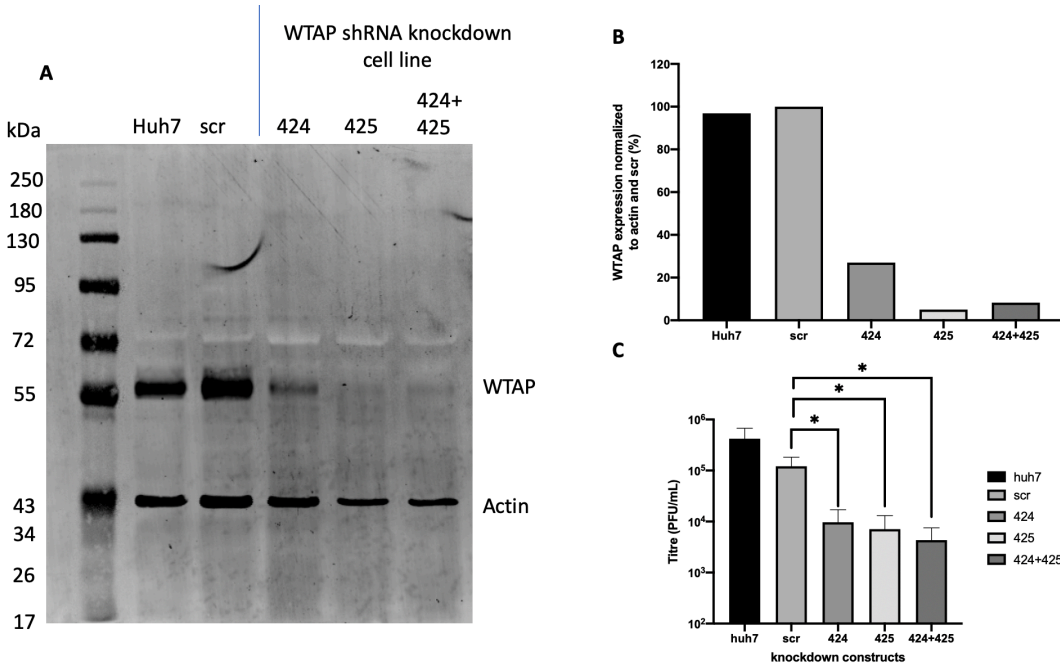

Figure 22. Knockdown of WTAP, Component of m^{6}A methyltransferase complex, in Huh7 cells reduces CHIKV replication.

WTAP shRNA knockdown cell lines were generated three independent times, each time seeded at passage 2 and infected with CHIKV MOI 1 and assessed for productive virus after 24 hours and for WTAP protein knockdown which corresponds to passage 3. A. Representative western blot showing that WTAP protein was reduced as compared to scrambled knockdown for the shRNA knockdown Huh7 cell lines, n=3. B. Quantification of WTAP expression from A. normalized to actin and then to scramble control as assessed by densitometry in ImageJ. This showed 27%, 8% and 5% expression in 424, 425, and 424+425 respectively. C. Productive CHIKV replication measured by plaque assay for WTAP shRNA knockdown Huh7 cells 24 hpi with MOI 1 CHIKV, n=3, Student T-test performed. Scramble to 424: p= 0.0338 <0.05*; Scramble to 425: p= 0.0313 <0.05*; Scramble to 424+425: p= 0.0287 <0.05*, error bars represent standard deviation from the mean.

Depletion of WTAP by 95% in Huh7 cells showed significant one log reduction in CHIKV replication (p=0.0313) (Figure 22). This further supports the above c3Ado experiments in Huh7 cells (Figure 19) showing that that perhaps m^6A methylation plays a role in viral replication in Huh7 cells. This effect must happen at some point in the virus's lifecycle, either methylation of the viral genome itself or of proviral transcripts. However, it is important to note that the cells with WTAP knockdown were less fit than scramble negative control Huh7 cells due to the reduction of an important protein. This reduction in cell fitness is difficult to distinguish from the reduction of viral fitness, as they are both so intimately linked.

WTAP is essential for recruitment of the METTL3/METTL14 complex to nuclear speckles and regulates the binding affinity of METTL3 to RNAs[95]. However, the CHIKV lifecycle occurs entirely in the cytoplasm. Work on other cytoplasmic replicating viruses such as ZIKV and HCV, has shown that a reduction in essential m^6A machinery increases viral replication and that virus infection can be associate with redistribution of m^6A proteins to cytoplasm[117,116]. By reducing WTAP levels, less methylation of potentially pro-viral and anti-viral host transcripts or even the 5' capped CHIKV genomic RNA or 26S RNA might be expected. The vast majority of RNAs recruited to the complex are mRNAs, so reduction in WTAP only shows us that a reduction in m^6A methylated WTAP recruited transcripts leads to a significant decrease in CHIKV replication. Although METTL3 catalysed m^6A is overwhelmingly predominant, this does not account for METTL16 catalysed m^6A within the cell; notably METTL16 has not been found in complex with WTAP like METTL3[93]. Together these results indicate that m^6A may play a role in CHIKV replication in Huh7 cells but do not distinguish whether the effect of reduced m^6A is acting on viral RNAs or on cellular mRNAs. However, CHIKV replicates in the cytoplasm and its viral RNAs are not thought to have a nuclear localisation during its lifecycle in the cell. So this antiviral effect from WTAP knockdown in Huh7 cells would most likely be an effect on the host mRNAs which require WTAP for m^6A methylation or an overall decrease in health due to off target effects of this WTAP knockdown.

3.4 Small molecule m^{6}A inhibitor (c3Ado) does not affect viral replication in RD cells

To determine if the effect of c3Ado on CHIKV replication was cell type specific, experiments were also performed in RD cells (a human derived muscle cell line). This system was chosen as CHIKV often causes muscular pain and arthritis, sometimes lasting months or even years in infected patients[202].

An MTT cell viability assay was performed to determine toxicity of the drug, c3Ado. The results indicated that the maximum non-cytotoxic dose of c3Ado was similar to Huh7 cell viability results at 50 μM, with 83% RD cell survival (Figure 23.A). Similar to the results in Huh7 cells, although 83% of the RD cells survived this did not mean the remaining cells were not affected by the c3Ado treatment. Infections with WT CHIKV at MOI 0.01 and MOI 0.1 for 24 hours showed similar levels of viral replication, as assessed by plaque assay of supernatant. For the experiment infecting with an MOI 0.1, qRT-PCR was also used to measure CHIKV genomic transcripts in the cells.

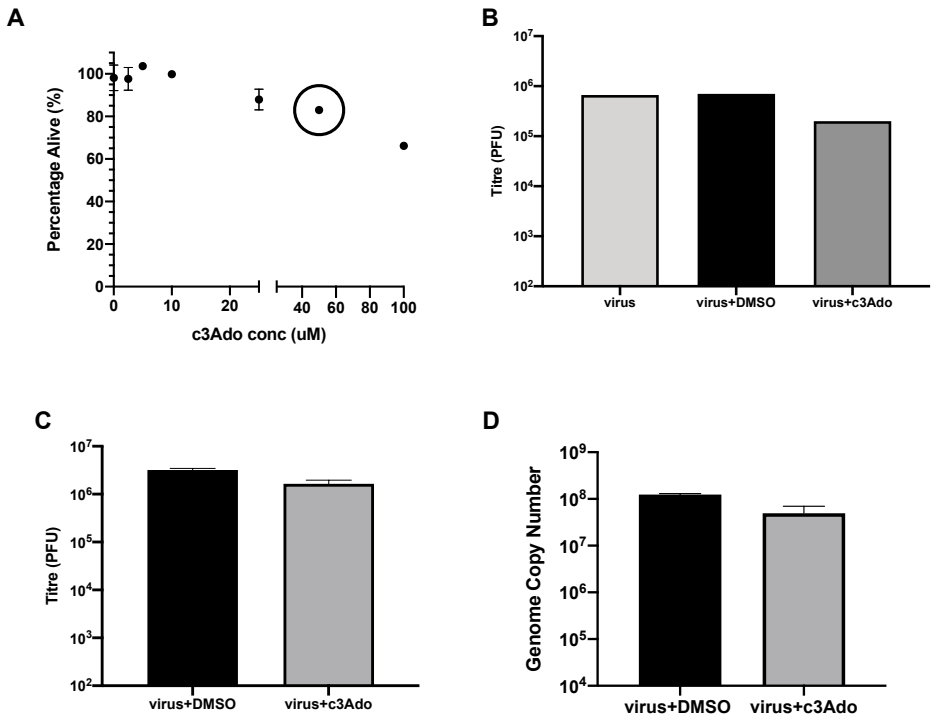

Figure 23. Small molecule inhibitor c3Ado which reduces SAM availability in the cell does not impact CHIKV replication in RD cells

RD cells were treated with a range of c3Ado concentrations and cell viability was determined by MTT assay.

A. MTT Cytotoxicity assay in RD cells suggests a maximum cytotoxic dose of 50μM c3Ado dissolved in DMSO (circled), c3Ado+DMSO values are normalized to same DMSO volume negative control n=2, error bars represent standard deviation from the mean.

B. RD cells were pre-treated for one hour with 50 μM c3Ado and 50 μM c3Ado was present throughout the incubation. Treated cells were infected at an MOI of 0.01 with WT CHIKV and released virus titre assessed by plaque assay 24 hours post infection, n=1 showing no significant difference between treated and untreated infected cells

C. RD cells were pre-treated for one hour with 50 μM c3Ado and 50 μM c3Ado was present throughout the incubation. Treated cells were infected at an MOI of 0.1 with WT CHIKV and released virus titre assessed by plaque assay 24 hours post infection, n=1 showing no significant difference between treated and untreated infected cells n=2, error bars represent standard deviation from the mean.

D. Monolayer of RD cells from same experiment displayed in C, where RD cells were treated with 50 μM c3Ado and infected with WT CHIKV at an MOI 0.1 were lysed. The CHIKV genome copy number was determined by RT-qPCR alongside at a standard curve of *in-vitro* transcribed CHIKV RNA of known concentration and then normalized to Actin Ct value, n=2, error bars represent standard deviation from the mean.

These experiments were all performed either once or twice. There was no detectable reduction in CHIKV replication, measured by released virus titre or intracellular genome copy number. Consequently, the next step was to pursue a more targeted knockdown of m^6A proteins in RD cells to determine if there was indeed an effect of m^6A on CHIKV replication in RD cells. This would help distinguish an effect that could not be characterised using the c3Ado experiment given potential off target effects.

3.5 FTO shRNA knockdown in RD cells

The c3Ado treatment of RD cells indicated there was no clear role for SAM dependent methylation in CHIKV replication in these cells. shRNA knockdown of FTO in RD cells was performed to look at the effect of reducing the amount of a cellular m^6A eraser protein on CHIKV replication. The same lentiviral shRNA knockdown system described in section 3.3.1 was used.

3.5.1 FTO knockdown in RD cells

METTL3 is the catalytic subunit of the primary m^6A methyltransferase complex and FTO is a known m^6A demethylase. In the case of FTO knockdown, cellular m^6A would still be deposited but would not be removed as readily. This would result in an overall increase in m^6A present relative to cells with normal levels of WTAP.

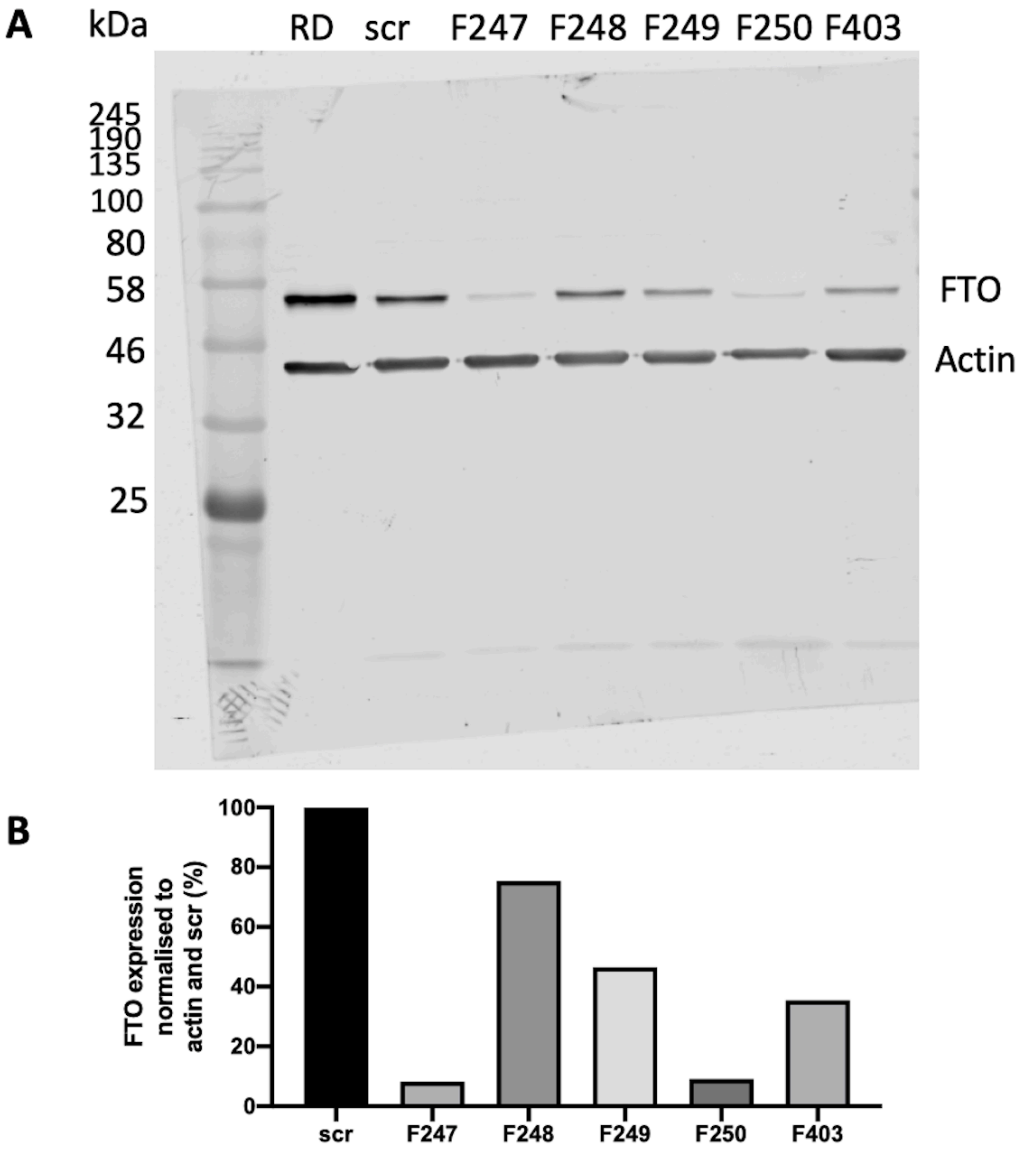

Figure 24. Relative shRNA knockdown of FTO in RD cells to a scrambled shRNA control

RD cells were transduced with lentivirus containing shRNA constructs against the FTO (m^6A demethylase).

A. Western blot showing that FTO protein was reduced as compared to scrambled knockdown for the shRNA knockdown RD cell lines.

B. Quantification of FTO expression from A. normalized to actin and then to scramble control as assessed by densitometry in ImageJ. FTO shRNA knockdown RD cell lines shows 8%, 75%, 46%, 9%, and 35% FTO protein expression for F247, F248, F249, F250, and F403 normalised to scramble shRNA control cells, n=1.

Five different shRNA constructs were used for the FTO knockdown and four different constructs were used for METTL3. There was at most a 46% and 89% reduction in FTO, as assessed by western blot in shRNA RD cell lines compared to the scramble control (Figure 24).

3.5.2 CHIKV sub-genomic replicon does not change in RD cells knock downed for protein in m^{6}A pathway

To assess the effect of FTO knockdown on CHIKV genome replication, a CHIKV sub-genomic system (CHIKV-Fluc SGR) developed and initially described in Pohjala *et al.* (2011) was used. It has subsequently been used to look at the role of CHIKV RNA structure and the requirement of cellular chloride channels during early stages of the virus replication cycle [66,186,182]. This CHIKV-Fluc SGR assay system has the structural proteins in ORF-2 replaced by a Firefly luciferase gene allowing the assessment of viral RNA replication (Figure 25). The functional replicase formed of the nsPs binds at the sub-genomic promoter just upstream of the firefly sequence (Fluc) on the positive strand full-length RNA. This generates the equivalent of the 26S RNA from which the firefly protein is produced. This system isolates viral genome replication and viral protein translation from other stages of the CHIKV lifecycle such as entry or egress.

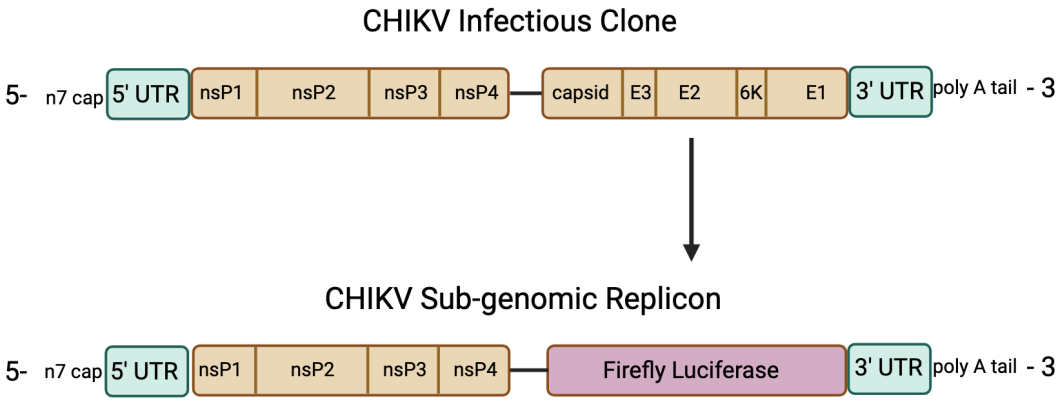

Figure 25. Sub-genomic CHIKV Replicon

The CHIKV sub-genomic replicon has a Firefly luciferase reporter gene (Fluc) in place of the structural proteins to assess viral genome replication and viral protein translation through transfection of in-vitro transcribed RNA into cell lines of interest and detection of reporter protein.

Figure created using BioRender.

Transient transfections were performed with the CHIKV sub-genomic replicon and Firefly expression was assessed at both 6 hours post transfection and 24 hours post transfection to determine both early and late CHIKV genome replication. For the three FTO shRNA knockdown cells with the greatest reduction in protein levels, there was no clear decrease in sub-genomic replicon replication, as measured by Firefly luciferase protein production at either 6 hours or 24 hpt (Figure 26).

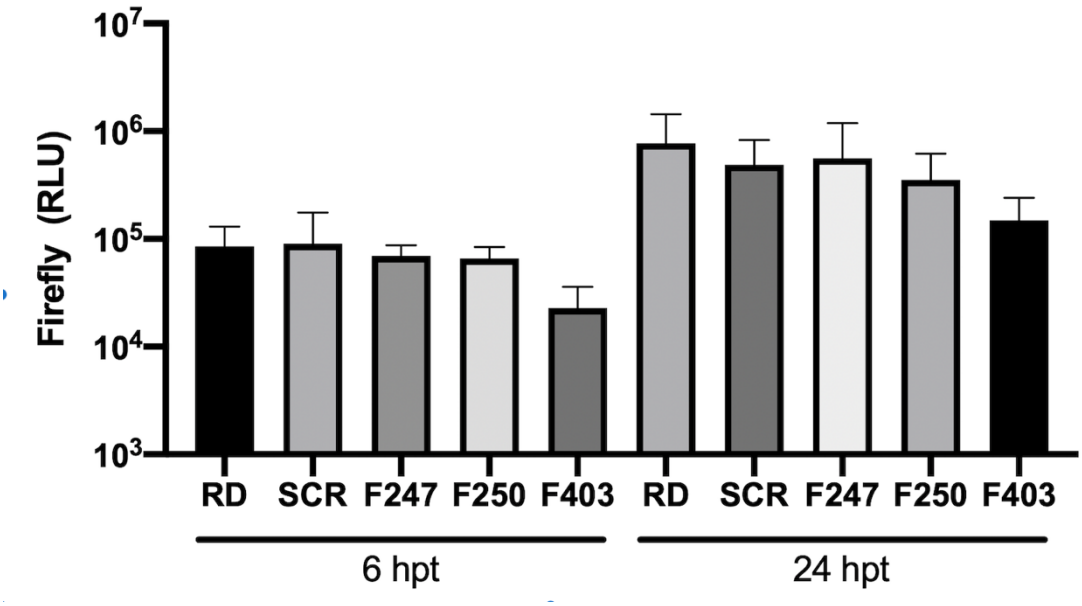

Figure 26. Knockdown of protein component of m^{6}A modification, FTO, has no significant impact on CHIKV sub-genomic replication in RD cells

FTO shRNA knockdown cell lines were generated one time and transfected with the CHIKV sub-genomic replicon system and assessed after 6 hours and 24 hours for Firefly luciferase expression as a proxy for viral replication. Shows no significant change in luciferase expression when transfected into FTO knockdown RD cells, N=1.

These results suggest that the proteins involved in m^{6}A methylation may not play a role in the stages of the CHIKV replication cycle measured by the sub-genomic replicon in RD cells. Consequently, Huh7 cells were used as the primary model system for studying the role of m^{6}A methylation in CHIKV replication in human host cells. Experiments were attempted in two human cell lines to begin to unravel the likely complicated relationship between m^{6}A and CHIKV infection in their human hosts. To obtain a more complete picture of the viral lifecycle analogous experiments in the vector host, mosquito, were performed. Given that there was no observable potential role for m^{6}A in RD cells while there was in Huh7 cells that would suggest that CHIKV's m^{6}A dependency may be cell type specific in humans. As a result of this m^{6}A methylation may not be universally important to the biology of CHIKV in these cells but rather cell type specific. This selective importance suggests a more complex and interesting relationship between m^{6}A methylation and CHIKV.

3.6 Small molecule m^{6}A inhibitor (c3Ado) affects viral replication in C636 cells

The METTL3 homolog encoding gene IME4 which produces a protein which binds SAM and is essential to development has been identified in *Drosophila melanogaster*[194,213]. SAM is also the methyl donor substrate in *D. melanogaster* for the m^{6}A methyltransferase protein with a METTL3 homolog also identified in *Anopheles* mosquito species[153]. c3Ado is an adenosine analogue as previously described in section 3.2.1. c3Ado would be expected to have a similar action of reduced SAM in cultured mosquito cells given its mode of action. C636 cells were used as a representative model of the role of m^{6}A in the CHIKV lifecycle in one of its mosquito hosts, *Aedes. albopictus*.

Like in the mammalian system, the concentration of c3Ado to use in C636 experiments needed to be established. The MTT assay used above is ubiquitous and relatively accessible, but Ghasemi *et al.* (2021) do point out its limitations while also recommending using it as a cell viability proxy only under optimized conditions. In their work they recommend a 3 hour

incubation at 4 mg/mL with the human cell culture seeded at a density of 20,000 cells/well[214]. Santana-Roman *et al.* (2021) used 50 µg/ well (5 mg/mL) of MTT reagent to assess the effect of DENV infection on C636 mitochondrial function but they did not report the incubation time with MTT[215]. However, five independent attempts with the MTT assay for C636 cells (which included trials of 1, 3, and 4-hour incubations with 1 mg/mL and 5 mg/mL MTT reagent) all proved insufficient to yield a usable difference in signal between cells grown in regular media, which should not have any reduced mitochondrial activity, and those grown in toxic 50:50 DMSO and media.

As a result, a different cell viability system, the ATP-lite (Perkin-Elmer) cytotoxicity kit, was used. While in their literature they state it is for mammalian cell culture it was optimised in C636 cells as detailed in this section. This assay relies on the reaction of a viable cell's ATP with reporter luciferase protein. Unlike in the MTT assay which requires uptake by the living cell, this assay requires cells to be lysed to release their ATP. The cell breakdown process was observed by light microscopy when the lysis reagent was placed on the C636 cells according to the kit instructions. The cell membrane broke down and ultimately no intact cells were visible.

Using the ATP-lite kit to asses cytotoxicity at a range of higher c3Ado concentrations the maximum noncytotoxic dose was determined to be 500 µM c3Ado for experiments in C636 cells (Figure 27.A).

To determine the effect of c3Ado on CHIKV replication in C636 cells the same workflow as described for experiments in human cells was used (Figure 18). This included a one hour pre-treatment, one hour infection, and incubation for 24 hours post infection with the drug present at 500 µM throughout the whole experiment. c3Ado treated C636 cells had an approximately two log decrease in infectious virus released into the supernatant 24 hpi, however the difference in titres was not significant (Figure 27.B). Whilst not significant, such a large difference was notable and lack of significance is likely due to further needed biological repeats. The c3Ado treated titres were normalized to the DMSO treated titres, which showed a very significant effect by c3Ado on CHIKV replication (Figure

27.**C**). This prominent decrease is likely pointing to a role of m^6A in CHIKV infection in C636 cells but variability between the three independent experiments meant that it was not possible to get the power needed to document a significance in these two-log reductions.

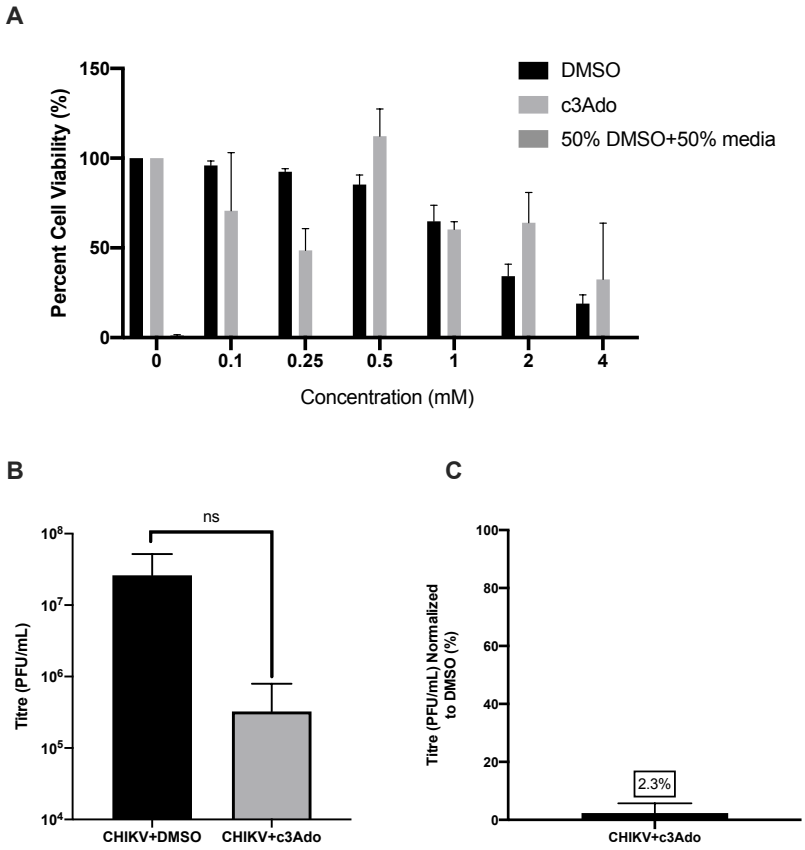

Figure 27. Small molecule inhibitor c3Ado which reduces SAM availability in the cell, inhibits CHIKV replication in C636 cells

Mosquito cells were treated with a range of c3Ado concentrations and cell viability was determined.

A. ATP-lite cytotoxicity assay for c3Ado in C636 cells 48 hours post treatment, showed that at 500 μM there was no detectable cytotoxicity, Cells were either treated in media with c3Ado dissolved in DMSO, a DMSO only volume control for each concentration n=3, error bars represent standard deviation the mean.

Cells were then treated with 500 μM of c3Ado and infected with CHIKV for 24 hours.

B. C636 cells were infected at an MOI 1 with WT CHIKV in the presence of 500 μM of c3Ado at 24 hpi released virus titre was reduced by ~1 log, n=3, not significant, p=0.15>0.05, error bars represent standard deviation from the mean.

C. Results from 24.B normalized against the DMSO control titre, show only 2.3% of the untreated CHIKV replication at 24hpi following incubation in the presence of c3Ado n=3, p=0.0002<0.0005**, error bars represent standard deviation the mean.

Experiment 24.A designed and supervised by myself and performed by MSc student, Sarah Menzes.

These results suggest that m^{6}A could play a role in CHIKV replication in its mosquito host as well as mammalian host, but further repeats are needed to establish significance. Changes to m^{6}A methylation signatures or an effect on other SAM dependent reactions reducing the overall health of remaining cells could lead to the observed result of a decrease in viral replication in c3Ado treated C636 cells. This result in C636 cells mirrored the result of c3Ado treated of Huh7 cells but not RD cells.

To begin to distinguish whether this reduction in methylation by two methods: c3Ado and essential m^{6}A protein knockdown could be detected as reduced methylation of the viral RNA itself or host transcripts *in silico* and antibody-based detection methods were trialled.

3.7. Optimizing detection of m^{6}A methylation within the CHIKV genome

The work outlined in this section focused on trialling a commonly and widely used method, Methylated RNA Immunoprecipitation (MeRIP), to detect m^{6}A sites within the CHIKV genome. MeRIP utilises an m^{6}A specific antibody that recognizes m^{6}A modifications on an RNA molecule. This method requires fragmentation of the RNA before immunoprecipitation with anti-m^{6}A antibody coated beads and subsequent analysis by qRT-PCR. This allows the mapping of m^{6}A methylation to specific regions of the transcript. The region of methylation is determined by the length of the fragment, as one can only determine if there is methylation within a fragment, rather than at single-nucleotide resolution. In recent work by Kim *et al.* (2020) they identified m^{6}A enrichment in the first 5000 nts of CHIKV genomic RNA extracted from virions by fragmenting to 1000 nt fragments of RNA [140]. MeRIP of other viral transcripts, such as of KSHV, used fragmentation of RNA to establish smaller regions of ~100-150 nts, providing higher resolution data across the transcript of interest in which to identify the m^{6}A site[127]. However, work by Schwartz *et al.* (2013) showed that 50% of m^{6}A peaks in analysis of yeast transcripts were false positives and enriched in purine rich sequences. Additionally, more recent work in 2020 showed a reanalysis of published MeRIP datasets and found low reproducibility [216]. They found 30-60%

variation in peaks between experiments [216]. That notwithstanding, MeRIP has been used in a majority of analysis of the relationships between m^{6}A and viruses. This includes of CHIKV and m^{6}A and as a result this method was attempted here [154].

3.7.1 *In silico* m^{6}A mapping of CHIKV genome

Potential m^{6}A sites in the CHIKV genome were *in silico* mapped using an m^{6}A predictor to understand the landscape of potential m^{6}A sites across the transcript and to ultimately inform MeRIP primer design. The SRAMP m^{6}A site predictor was used to map 35 predicted m^{6}A sites in the whole CHIKV genome (Figure 28, Supplementary Figure 1).

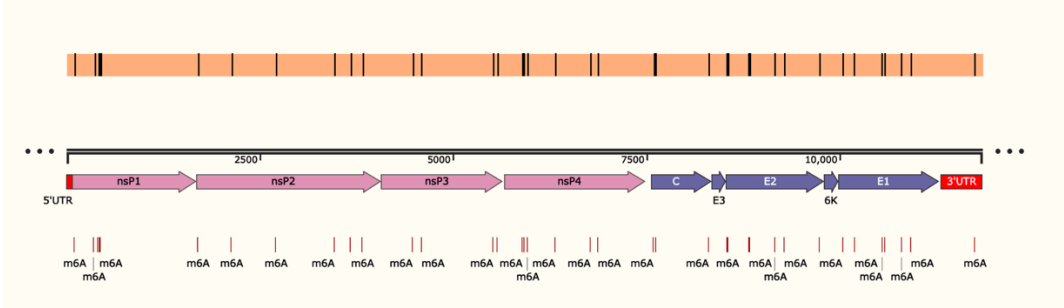

Figure 28. *In silico* mapped m^{6}A sites in the CHIKV genome

35 potential m^{6}A sites mapped by SCRAMP within the CHIKV genome[188]. The orange bar on top with black lines struck throughout indicated the m^{6}A sites location along the transcript. Double black lines showed nucleotide position along the transcript. Below that 5'UTR and 3' UTR are in red, nsPs are indicated by the pink arrows, structural proteins are indicated by purple arrows. The m^{6}A sites are also shown in red below the transcript to align with protein position more easily.

SRAMP provided a tool to begin investigation into potential m^{6}A sites in the CHIKV genomic transcript, CHIKV vRNA. Using the sequence context (30 nt flanking either side of the m^{6}A site) informing algorithm trained on other transcripts the tool was able to predict where in the genome the most likely m^{6}A sites occurred[188]. Results from *in silico* m^{6}A analysis using SRAMP indicated a spread of potential m^{6}A sites throughout the viral genome, with

some clustering at the start and end of new protein coding regions (Figure 28).Central areas of protein coding regions of nsP1, nsP2, and nsP3 show a noticeable lack of predicted m^6A sites (Figure 28).There was only one predicted m^6A site in a non-protein coding region at the end of the genome in the 3'UTR and none in the 5'UTR. ORF1 contained 20 predicted m^6A sites in comparison to ORF2 which contained 14 sites (Figure 28, Figure 29.A). The portion of the RNA molecule that encoded viral proteins which had the highest amount of predicted m^6A sites internally were nsP2, nsP4, and E1 (Figure 28). The whole CHIKV genome when *in silico* mapped using the SRAMP tool, showed that there were 35 predicted m^6A sites within the virus genome spread throughout the genome including outside of the first 5000 nts. This was in contrast to the experimental work published by Kim et al. 2020 on CHIKV genomes extracted from virions, which showed m^6A enrichment only in the first 5000 nts of the genome [156]. This discrepancy could be explained by the fact that m^6A methylation is a dynamic process and that methylation at individual residues may vary throughout the virus lifecycle. Kim et al. captured a snapshot of the m^6A methylation signatures on the CHIKV genome once it had been packaged into an infectious virion and released from the cell. The Cui Lab, SRAMP tool was built using a model trained on cellular eukaryotic transcripts. Using it on a relatively large nearly 12 kb viral genome was using it on a transcript that the programme had not been trained to recognise. Only the primary RNA sequence was considered for the *in-silico* analysis. Secondary structure was not taken in to account by the software into the analysis performed. The CHIKV genome has extremely important and dynamic secondary structure throughout that would not have been accounted for at all. Secondary structure would be an important consideration when predicting m^6A methylation. m^6A is a dynamic post transcriptional modification that m^6A site occupancy would change throughout the CHIKV lifecycle by m^6A machinery for recognition by m^6A reader proteins. Therefore, understanding the dynamic landscape of m^6A within the cell during CHIKV replication could provide better understanding of essential proviral and antiviral processes that could be exploited for treatment.

A

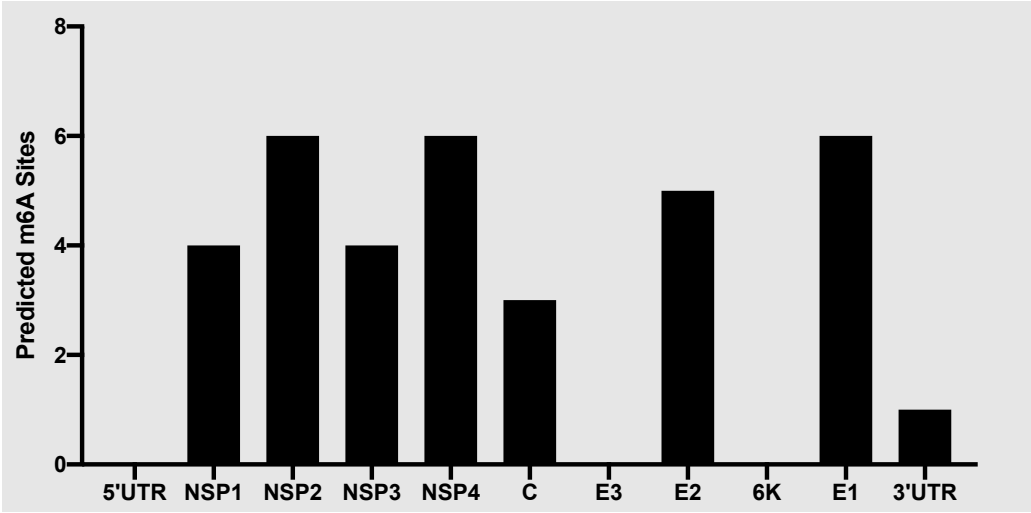

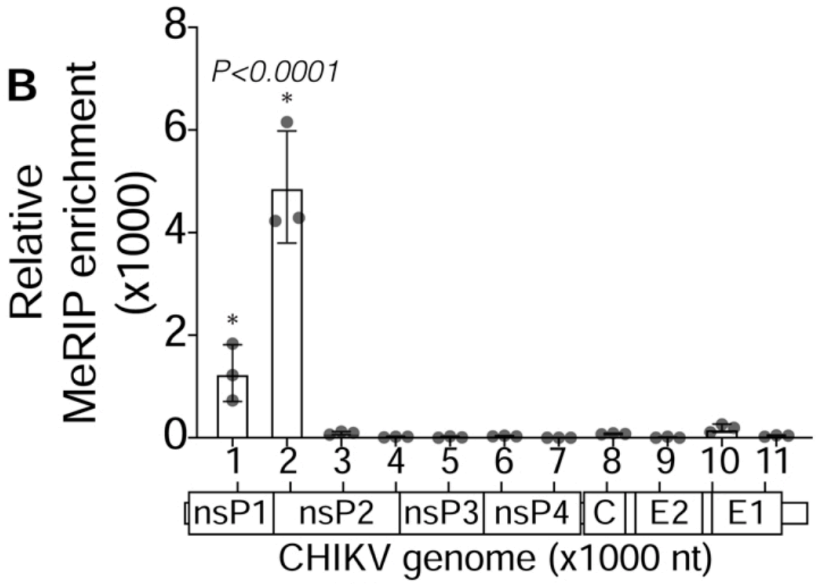

Figure 29. Distribution of m^{6}A sites across CHIKV genome elements.

A. Number of predicted m^{6}A sites across the different elements of the CHIKV genome as predicted by SRAMP[188] (Figure 28).

B. MeRIP of CHIKV RNA isolated from CHIKV virions as reported in Kim *et al.* (2020) [140], showing the distribution of m^{6}A sites in CHIKV genome, original labelled Figure 5B in their published paper.

Previously discussed work by Kim *et al*. (2020) used MeRIP to map the m^{6}A sites in the CHIKV genome which was fragmented into 1000 nt fragments[140]. They found that in virion packaged RNA, MeRIP enrichment was only present in the first 5000 nt of the CHIKV sequence, which covers the 5' UTR, nsP1 and nsP2 coding regions [140]. This suggested that perhaps other sites could be m^{6}A methylated at other points during the CHIKV lifecycle and are removed before packaging or that these proposed m^{6}A sites are not in fact m^{6}A methylated and as a result were not detected by their MeRIP. Therefore, the aim of the work here was to design a MeRIP of CHIKV RNA extracted from infected cells with fragmentation to smaller windows. Attempts in this study to fragment to 100bp were successful. However, all attempts to qRT-PCR from the RNA eluted from the antibody-coated beads by either advised or published methods yielded low Ct values as well as inconsistent results that were not robust enough for interpretation.

3.7.2 Unfragmented MeRIP shows CHIKV vRNA enrichment

Huh7 cells were infected with CHIKV at an MOI 1 for 24 hours and the RNA was extracted for MeRIP analysis to determine if the viral transcript could be immunoprecipitated by the m^{6}A antibody. Although detection of methylated transcripts in the MeRIP using fragmented RNA was attempted many times but results were inconsistent and/or unsuccessful despite repeated attempts with various modifications to the protocol. So, the MeRIP was instead repeated using unfragmented RNA in parallel to the fragmented RNA.

To calculate the Fold Enrichment of transcripts of interest over the negative control, the following equations were used. The Ct_{IP} was the Ct result from either the anti-m^{6}A sample (positive) or the IgG antibody sample (negative). ΔCt for both conditions was the change in Ct from input which used the Ct of the 10% input RNA. Fold enrichment was a product of the change in Ct of the positive m^{6}A sample minus the change in Ct of the negative IgG sample[217].

$$\Delta Ct = Ct_{IP} - (Ct_{input} - \log_2 10)$$

$$\Delta\Delta Ct = \Delta Ct_{positive} - \Delta Ct_{negative}$$

$$Fold\ Enrichment = 2^{-\Delta\Delta Ct}$$

Equation 1. Fold Enrichment calculation for MeRIP

Although using unfragmented RNA would not allow identification of specific m^{6}A sites with the CHIKV genome, the intention was to help optimise steps downstream of the fragmentation step in the MeRIP. As a positive control, solute carrier family 6 member 19- Slc6a19 (SLC) a human mRNA was used. SLC is a well characterised and well established positive control that has regions of known m^{6}A methylation [218]. Both poly(A) selected RNA and total RNA, when left unfragmented, yielded high MeRIP fold-enrichment of 5 x 10^5 and 1 x 10^3 respectively while the fragmented sample gave 1 and 7 fold enrichment respectively (Figure 30**.A and C)**. This suggested that the

fragmentation step was possibly leading to reduced sensitivity and reproducibility of the assay Another indication that the results for fragmented RNA were unreliable was that the dissociation curve with fragmentated RNA showed a different pattern of melting temperature from RNA that was left not fragmentated (Figure 30.B and D**)**. This suggested that the product being amplified at higher Ct means it was low abundance. One explanation for this is that it corresponds to non-specific amplification.

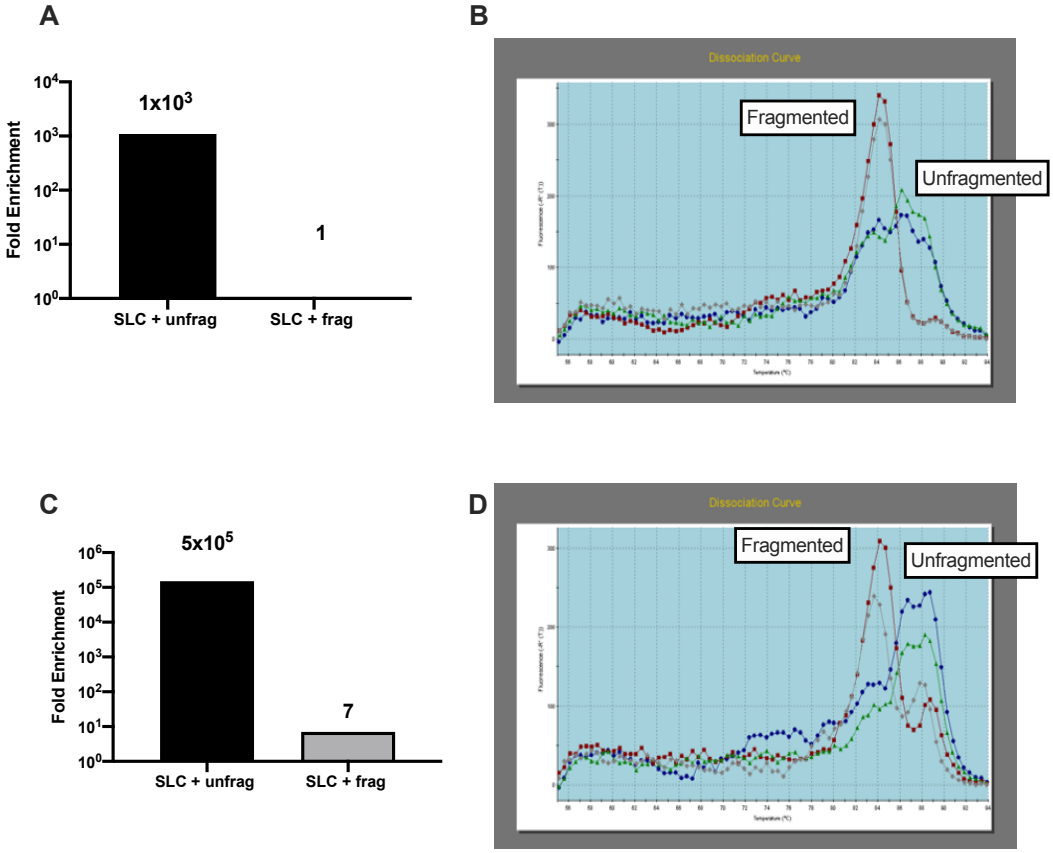

Figure 30. Unfragmented SLC transcript enriched in MeRIP for both total RNA and poly A selected RNA

A. MeRIP fold enrichment over IgG control for SLC+ from total RNA

B. Corresponding dissociation curves for the qRT-PCR product amplified by the SLC+ primers for fragmented (red and grey) and unfragmented RNA (blue and green).

C. MERIP fold enrichment over IgG control for SLC+ from poly A selected RNA

D. Corresponding dissociation curves for the qRT-PCR product amplified by the SLC+ primers for fragmented (red and grey) and unfragmented RNA (blue and green).

(N=1)

The results for the positive control SLC primer set showed ~5 x 10^5 fold enrichment over the IgG control, suggesting that the MeRIP was working as expected (Figure 30.C). GAPDH acts as an overall negative control, as it is

not known to be m^6A methylated and is used as a negative control in other published studies [219],[220]. Fold enrichment over the IgG control for SLC in the total RNA sample was $1x10^3$ (Figure 30.A, Supplementary Figure 10). For poly(A) selected RNA there was $5x10^5$ fold enrichment, for the positive control SLC (Figure 30.C).

The unfragmented samples were analysed using primers against the E1 coding region of the CHIKV genome, to determine MeRIP fold enrichment for CHIKV vRNA over the IGG control. For samples from total RNA there was ~$3x10^3$ enrichment compared to the positive control $1x10^3$ enrichment (Figure 31.A). For samples which had undergone poly(A) selection before the MeRIP step there was $1.25x10^5$ enrichment compared to the positive control $5x10^5$ enrichment (Figure 31.B).

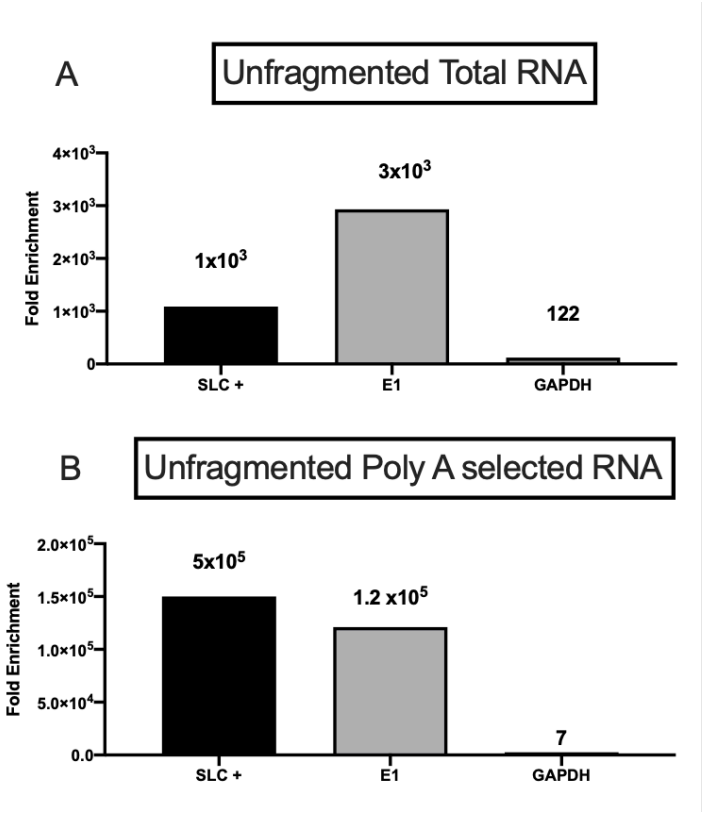

Figure 31. CHIKV RNA was detected in MeRIP with unfragmented RNA

Huh7 cells were infected at an MOI of 1 with WT CHIKV and total RNA was extracted after 24 hours. MeRIP and qRT-PCR of eluent RNA was performed for positive control transcript SLC, CHIKV E1, and negative control GAPDH.

Fold enrichment for transcripts from MeRIP of unfragmented total RNA

Fold enrichment for transcripts from MeRIP of unfragmented poly(A) selected RNA

(n=1)

These results suggest that the CHIKV RNA could be detected in the eluted RNA from an MeRIP. This leads to the possibility that the CHIKV vRNA could be m^{6}A methylated in Huh7 cells. There was enrichment of CHIKV and the positive control SLC RNA following poly(A) selection before MeRIP as the fold enrichment of poly(A) selected RNA was ~2 logs greater than that of the total RNA (Figure 19). However, because the RNA had not been fragmented, the location of the m^{6}A sites could not be distinguished and may have occurred at any point within the vRNA. Assuming multiple methylated residues are present throughout the genome, fragmentation of the RNA

would lead to an overall decrease of the number of m^{6}A sites on each segment of RNA. Where an intact RNA transcript could be highly methylated meaning that all of the sites present provided opportunities to bind to the anti-m^{6}A antibody coated beads. However, following fragmentation when only the m^{6}A methylated residues present within the 100 nt fragment could bind, so the overall the sensitivity of MeRIP would decrease. Although this would not account for the changes in dissociation curve, it may suggest that fragmentation to a larger size, like the 1000 nt fragments used in MeRIP performed by Kim *et al. (*2020), may be necessary or optimization of the downstream steps with fragmented RNA is necessary[140].

3.8 Discussion

In this chapter, SAM dependent methylation including targeting of m^{6}A protein machinery for knockdown resulted in a significant decrease in viral replication in Huh7 cells and C636 cells. This suggested that CHIKV may have evolved a pro-viral utility for m^{6}A during infection in both its human and mosquito hosts. Interestingly, there was differences in tolerance of cell lines to c3Ado. 50 µM of c3Ado lead to 71% survival of Huh7 cells 83% survival of RD cells (Figure 19, Figure 23). Whereas at 500 µM C636 cells had no detectable cytotoxicity (Figure 27). As CHIKV is a positive strand RNA virus. As a result, m^{6}A methylation of the full-length genome, negative strand intermediate, or 26S RNA could have led to the pro-viral utility of the methylation reported. This could be due to interaction with proteins such as YTHDF2[156] or other yet to be identified pro-CHIKV m^{6}A reader proteins. Additionally, host transcripts and their methylation signatures as well as the redistribution of m^{6}A machinery proteins such as WTAP (as is the case for cells under HCV infection[115]) could also influence the replication of CHIKV and contribute to the observed pro-viral role of m^{6}A in Huh7 and C636 cells.

The pro-viral effect was not observed in the preliminary work in RD cells, another human cell culture line, perhaps suggesting that this effect is cell type specific. For EV71, Hao *et al. (*2017) found a strong pro-viral link between m^{6}A and viral replication by both knockdown of METTL3, FTO, and YTHDF1-3 as well as by viral mutagenesis work in Vero and 293T cells[159]. However in RD cells they found knockdown for m^{6}A reader protein,

YTHDC1, resulted in increased viral titre suggesting an antiviral role[159]. This shows other studies have observed a difference in phenotype across cell lines and even specifically in RD cells. Further work, in other tissue cell lines, could yield interesting information on CHIKV and m^{6}A cell type specificity. Work in U87-MG (human epithelial glioblastoma astrocyte-like cells) would be an interesting next step. U87-MG are non-neuronal cells still essential for functioning of the central nervous system, present in both vertebrates and invertebrates. In CHIKV infected patients organs such as the liver act as reservoirs for virus in late-stage infection[221]. Just as m^{6}A signatures also differ across cell types it would reason that the relationship between CHIKV and m^{6}A would also differ across cell types [113]. Work into resolving m^{6}A signatures with single-cell resolution have even shown variability across populations of same cell types [144]. This also extends to work in the mosquito host and its different cell types. It would be interesting to look at the role of m^{6}A in infected mosquito tissues such as the midgut. The work in C636 cells used c3Ado but future work knocking down essential m^{6}A machinery, such as methyl transferase *IME4* or WTAP homolog *Fl(2)d*, would support the relationship between m^{6}A and CHIKV in the mosquito host[222]. CHIKV infection in mosquito versus mammalian cell culture have radically different phenotypes[223]. In mammalian cells the infection is lytic, while in mosquito cells CHIKV establishes a non-lytic persistent infection. The C636 mosquito cells under microscope were observed to not change their morphology and continue to replicate normally. This is still true of c3Ado treated C636 cells infected with CHIKV. However, we still see a significant decrease in released CHIKV virus in the supernatant of c3Ado treated cells suggesting that even in the host cell which tolerates infection well CHIKV is downregulated due to a reduction in m^{6}A.

Further work undertaken for mammalian cell culture in this thesis was predominantly performed in either in Huh7 cells or BHK cells, with exception of preliminary m^{6}A immunoprecipitation undertaken in RD cells. Mosquito cell culture work was done in C636 cells.

Ideally the fragmented RNA immunoprecipitated in the MeRIP would have been analysed by RNA-seq. This would have allowed investigation of both host and viral RNAs and mapping m^{6}A sites within all of those transcripts.

The intention of the pipeline was to generate material for a strategy similar to Baquero-Perez *et al.* 2019, in which they mapped the m^{6}A sites in the KSHV transcripts[127]. They fragmented their RNA to 100-150 nt allowing for relatively small windows within which the m^{6}A site could be on the transcript aligning it with a DRACH site but they also validated 12 of their peaks from RNA-seq by qRT-PCR[127]. To initially test whether the MeRIP worked on the CHIKV infected samples, qRT-PCR was used to detect known m^{6}A methylated transcripts and regions of the CHIKV genome with predicted m^{6}A sites. However, notably (as addressed in the introduction) a majority of viral RNA m^{6}A studies have utilized antibody-based m^{6}A detection which suffers from issues of up to 50% false positive peaks and low reproducibility of peaks and peak changes in MeRIP-seq analysis [224],[216].

MeRIP on RNA extracted from CHIKV infected Huh7 cells suggested that the full length CHIKV genome was m^{6}A methylated. Although a conclusive picture of where on the CHIKV genome these sites were located could not be established without fragmentation, these results suggested the CHIKV genome could be m^{6}A methylated and led to further work optimizing this workflow to determine which region of the genome was undergoing methylation. Ultimately infection of four flasks of 70% confluent Huh7s with CHIKV at an MOI of 1 for 24 hours was determined to be optimal. Phenol-chloroform purification, poly(A) selection and chemical fragmentation steps were all optimized to yield approximately 4 µg of fully processed material for the MeRIP. However, attempts to detect m^{6}A on fragmented RNA from CHIKV infected cells did not prove conclusive, despite a range of optimization techniques and modifications. This included the use of alternative negative controls, using primers designed in regions of the virus genome that predicted by *in silico* mapping to be devoid of m^{6}A sites and any permutation of the DRACH sequence. However, the results were inconsistent and unreliable, even for the positive control host transcripts SLC and EEAF1 (another positive control transcript supplied with the MeRIP kit). It was possible the final step of using the Qiagen miniRNeasy column, which in their published literature captures >200 nt fragments or Phenol/Chloroform RNA purification led to loss of already low abundance material and to inconclusive results. Other RNA-spin columns such as the Monarch RNA

clean-up kit which has a cut off of >15 nts could be tested in future to ensure that a spin column could concentrate the RNA that was eluted from the MeRIP beads by m^{6}A salt [225]. An Agilent 2100 Bioanalyser could also be used to assay RNA fragmentation length and integrity throughout the MeRIP workflow. A Bioanalyzer can detect as little as 5 ng of RNA and is 100-200x more sensitive that a denaturing agarose MOPS gel, which needs at least 500 ng to visualize the RNA band [226].

In an alternative approach to detect m^{6}A sites in the CHIKV genome, RNA extracted from CHIKV infected Huh7 cells was also used in a trial of the *in vitro* DART-seq method described in Meyer *et al.* 2019 [142]. Unfragmented total RNA was tested but no CHIKV RNA was able to be detected by qRT-PCR following incubation with the YTH-APOBEC protein. Possibly degradation of the transcript had occurred but future trials of this alternative m^{6}A mapping method could be worthwhile. Any of the alternative methods for m^{6}A detection for extracted RNA *in vitro, such as* Nanopore direct RNA-sequencing (RNA-seq) [146], would be ideal, as the issue with the DART-seq method in live cells was the timing for transfection of the APOBEC-YTH constructs alongside relatively short lived infection cycles for CHIKV in mammalian cell culture.

Whilst results from this chapter were inconclusive, there was indication that the CHIKV genome could be immunoprecipitated in an m^{6}A specific IP and that a reduction in SAM by a small molecule inhibitor and reduction of m^{6}A machinery by shRNA led to a reduction in infectious CHIKV produced in Huh7 cells. During the study there was confirmation in the published literature that the CHIKV genome was m^{6}A methylated within the first 1000 nts of its genome [156]. Consequently, the next step of this study was to try to characterize the functionality of some of the *in silico* mapped m^{6}A sites by site directed mutagenesis.

4 Chapter 4- m^{6}A is essential for initiation of CHIKV genome replication

4.1 Introduction

Initiation of CHIKV genome replication is temporally controlled within the virus lifecycle. RNA structure and RNA binding proteins interact in a nucleotide specific manner, and post-transcriptional modification contribute to this regulation [40,41,66,67,156]. Kendall *et al.* showed that RNA structure elements within the 5' UTR and adjacent ORF1 region are essential for initiation of genome replication[66]. m^{6}A sites were mapped by *in silico* analysis within the positive stand CHIKV genome, to determine positions of potential interest for further investigation (Figure 28). As shown in the previous chapter, the CHIKV genome was not conclusively immunoprecipitated by MeRIP but work by Kim *et al.* suggested that the packaged CHIKV genome was m^{6}A methylated within the first 5000 nts[156]. This included areas of particular interest in the CHIKV genome, including but not limited to the potential pseudoknot SL85 identified by Kendal *et al.* [30] and other essential 5'UTR secondary structures confirmed by Madden *et al.* [227].

4.2 Aims

The overall aims of the work described in this chapter were to understand when in the CHIKV lifecycle m^{6}A could play a role and whether proposed m^{6}A sites in the CHIKV genome had functional significance to viral replication and vRNA replication. Firstly, the small molecule inhibitor c3Ado was used in the *trans* replicon system, which includes limited regions of the CHIKV genome, and measured CHIKV genome replication in isolation of all the other stages of the virus replication cycle. These experiments were conducted in both a human and mosquito cell line. Following this, experiments were performed to investigate the potential role of specific predicted m^{6}A sites within the CHIKV genome itself . Here, mutagenesis was performed of two nucleotide sites in the CHIKV genome which had been *in silico* predicted to be m^{6}A sites. The first nucleotide site chosen was within the window reported by Kim *et al.* to be m^{6}A methylated while the second

one was not. These two sites were mutated in both the ICRES infectious virus system and the *trans* replicon system. The reverse genetic mutants' fitness was also assessed in both mammalian and mosquito cell lines, in line with similar experiments performed for the picornavirus, EVA71[159].

4.3 c3Ado inhibits CHIKV *trans*-complementation replicon assay

To investigate the relationship between CHIKV RNA replication and m^{6}A methylation a CHIKV *trans*-complementation replicon assay was used [228,229]. This assay allowed us to investigate specifically the requirement for SAM on CHIKV genome replication in isolation from other stages of the virus replication cycle, such as entry, egress or viral protein translation (Figure 32). Sequences encoding two fluorescent reporter proteins, flanked by CHIKV genomic sequence of interest, was replicated by the CHIKV replicase which was supplied in *trans* from a 2nd co-transfected (codon-optimised) plasmid. This allowed the impact of drug treatment of cells or mutation of CHIKV sequence of interest on virus genome replication to be measured in isolation of other stagers of the virus replication cycle, such as translation.

The assay supplied the CHIKV replicase in *trans*, which was expressed on a separate plasmid with a CMV promoter, allowing it to be expressed constitutively at high levels in the cell (Figure 32.B). This meant that the replicase protein was not a limiting factor in the assay This plasmid had been codon-optimized to ensure that the CHIKV replicase complex was expressed but the CHIKV RNA primary sequence changed to encode the same amino acid but to disrupt any natural secondary structure. In this way the generation of the CHIKV replicase itself was not an experimental factor and thus transcription and not translation of the viral RNA elements could be measured. Notably, CHIKV genomic nucleotide sequence forms critical RNA structures [66,227] and contains sequence specific protein binding sites such as for Musashi RNA binding protein [230]. An experimental negative control to assess background or translation of initial reporter, required transfection of a plasmid supplying "inactive" replicase; this was the same sequence except

that it contained a mutation in the RdRp (nsP4) active site GND to GDD (Figure 32.B).

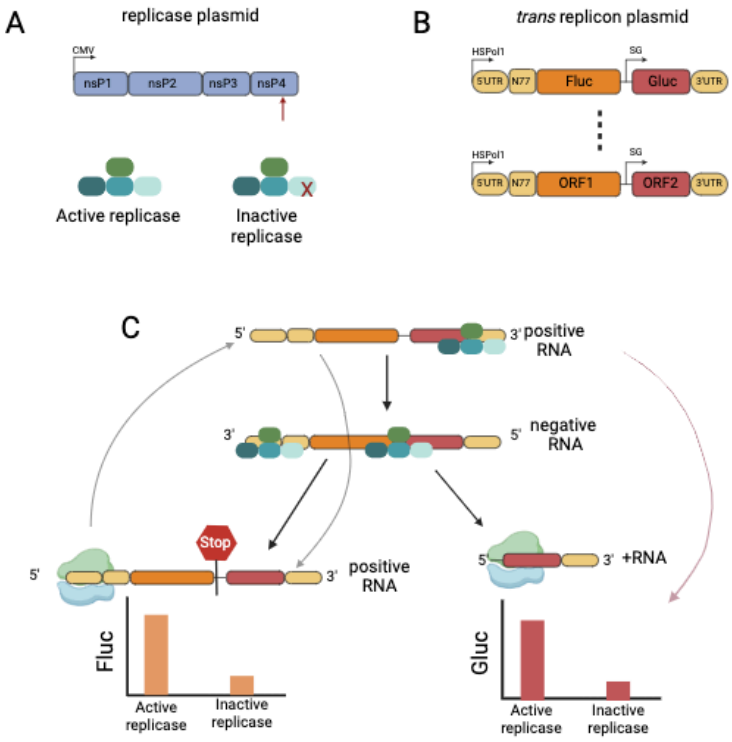

Figure 32. CHIKV *trans*-complementation Assay

CHIKV *trans* complementation assay is designed to assess the replication of viral genome independent of translation of the viral replicase.

A. Codon-optimized CHIKV replicase plasmid designed to encode the four non-structural proteins to produce active replicase complex. Expression of these proteins is driven by transcription from the powerful CMV promoter upstream of the protein coding sequences. An inactive replicase is generated from GDD>GAA mutation in the active site of nsP4

B. *Trans* replicon plasmid: Reporter plasmid containing the DNA complement of natural CHIKV RNA sequence including the 5' UTR, 77 nucleotides into the nsP1 coding sequence, and the 3' UTR. In comparison to the CHIKV genomic RNA, Firefly Luciferase sequence (Fluc) is in place of ORF1 and Gaussia Luciferase sequence (Gluc) in place of ORF2. Initial transcription of the transcript is driven by human polymerase I (HSPolI) binding to the promoter in the plasmid while subsequent rounds of replication are taken over by the viral RdRp encoded by plasmid shown in A.

C. Right side- ORF1 expression is a direct product of full-length positive strand RNA by the ribosome pictured here; a stop codon means that only Firefly can be generated from the full length positive.
Left side- ORF2 expression is a product of the sub genomic 26S RNA from the ribosome.

Created using BioRender and based on [229],[19].

The second plasmid which was co-transfected into the cell line of interest was the reporter plasmid, it contained either an optimized HSPol1 (human) or Ubi (*Ae ageypti*) promoter upstream of protein coding sequences for Firefly luciferase (Fluc) in place of ORF1 and Gaussia luciferase (Gluc) in place of ORF2 (Figure 32.A). The human cell line compatible reporter plasmid will be referred to as *human.trans* and the *Ae aegypti* cell line compatible plasmid will be referred to as *A.ae.trans*. These reporter protein sequences were flanked by the wild type CHIKV 5'UTR and adjacent upstream region of ORF-1(encompassing nts 1-330), the untranslated intragenic region between the ORFs and the authentic 3'UTR **(**Figure 32.A**)**. Generation of the Firefly luciferase (Fluc) was dependent on full-length negative strand transcription and subsequent replication of the full-length genomic positive strand. The genomic strand was used as a template for both ORF-1 translation, leading to the production of Fluc protein, and replication of more negative strand RNA (Figure 6). An authentic ORF-1 stop codon at the 3' end of ORF-1 was present, meaning that only Fluc could be expressed from the genomic strand. Consequently, FLuc expression was a measure of full-length positive and negative strand genome replication. Generation of the Gluc signal was also dependent on full-length negativse and positive stands but required the additional step of transcribing the sub genomic 26S RNA from the negative strand template – from which ORF-2 encoded Rluc could be expressed (Figure 32). This *trans*-replicon system thus allowed the opportunity to assess the importance of a comparatively small region of the CHIKV genome for virus genome replication, in isolation for all other stages of its life cycle. It has been shown by a combination of northern blot and luciferase assay that expression of the reporter proteins from the positive strand viral RNA correlates to both positive and negative strand RNA synthesized by the viral replicase supplied in *trans*[187].

4.3.1 *Trans*-complementation assay in Huh7 cells

The small molecule inhibitor c3Ado was used in the *trans*-complementation replicon assay to investigate the effect of cellular SAM reduction on CHIKV

RNA replication. c3Ado, a small molecule inhibitor reduced the available methyl donor SAM. Therefore c3Ado treatment would also be expected to result in reduced m^6A methylation of RNAs in the cell. The results from Chapter 3 demonstrated that overall virus replication was inhibited by c3Ado. Transfection of the *trans*-complementation replicon assay system into c3Ado treated cells allowed for the analysis of the effect of reduced SAM on CHIKV RNA replication.

When treated with 50 µM of c3Ado (Figure 19.A) Huh7 cells transfected with the *trans* complementation assay system showed a significant decrease for both Fluc and Gluc expression, indicating a decrease in replication of full length and sub-genomic RNA to act as template for host ribosomes to translate Fluc and Gluc (Figure 33).

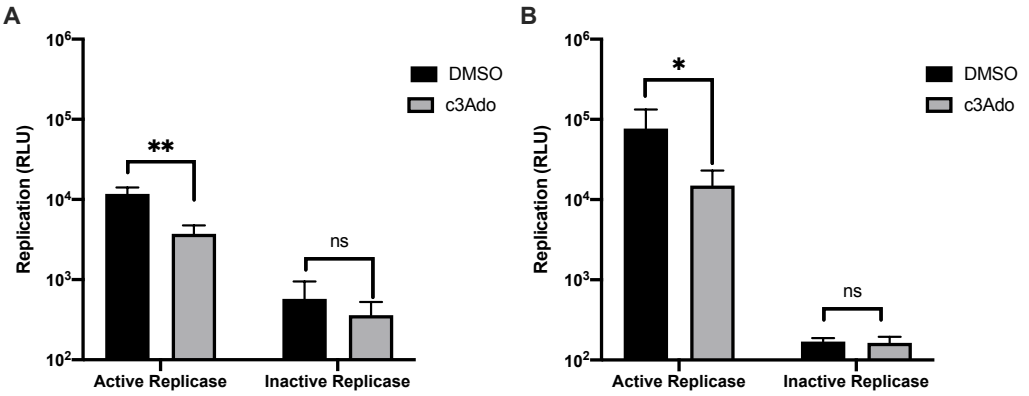

Figure 33. 5' Expression of Fluc and Gluc reduced in c3Ado treated Huh7 cells

Huh7 cells were transfected with the CHIKV *trans* complementation-assay and incubated in the presence of 50 μM c3Ado for 24 hours. Expression of Renilla luciferase and Firefly luciferase fluorescent protein was assessed as a proxy for reporter nucleic acid replication, showing reduced replication of both genomic and sub genomic RNAs when treated with 50 μM c3Ado.

A. Fluc expression is significantly reduced upon the addition of 50μM of c3Ado measured at 24 hpi. (Active replicase: p=0.0059< 0.05; Inactive replicase: p= 0.414 > 0.05)
B. Gluc expression is significantly reduced with the addition of 50μM of c3Ado measured at 24 hpi (Active replicase: p=0.0407< 0.05; Inactive replicase: p= 0.693> 0.05)

*one star indicates p<0.05-0.01

**two stars indicates p<0.01-0.005

N=3, Experiments were done in biological triplicate and analysed in technical duplicate, using a two-tailed students t-test significance was measured, Error bars represent standard deviation from the mean.

The decrease in Fluc expression would be consistent with inhibition of either the full length negative intermediate or genomic transcript replication. As c3Ado affected total cellular methylation, this could have been consistent with inhibition of methylation of either viral RNA, or cellular transcripts or inhibition of other SAM dependent methylation reactions. This decrease in

Fluc expression could also be due to reduced cell survival which was 71.4% in 50 μM c3Ado treated Huh7 cells after 25 hours (Figure 19.A). Treatment with c3Ado at 50 μM could also impact the overall health of the remaining Huh7 cells and lead to a decrease in translation of the Fluc protein from the replicated transcript. However, it does suggest that CHIKV requires SAM for efficient RNA replication as captured by this assay summarized in Figure 32. However, the synthesis of the 26S sub genomic RNA cannot be isolated from full-length RNA, as the generation of both positive and negative sense full-length species would go on to impact the amounts of 26S equivalent RNA available too (Figure 33.B). The 26S equivalent RNA is synthesized from the full-length negative intermediate which uses the full length positive strand as template as displayed by the cyclical arrows in Figure 32.C.

4.3.2 *Trans*-complementation replicon assay in C636 cells

Plasmids that had been designed for replication in mosquito cells were used for *trans* complementation assays in C636 cells. The approach was the same as that previously outlined for Figure 32 but with the HSPol1 promoter (Figure 32.A) was replaced by an *Ae. aegypti* polyubiquitin promoter (Ubi) [229]. In their design of these plasmids, the authors observed that Fluc expression was low and although significantly higher with the active replicase, was only ever ~ 2 fold higher than with the inactive replicase control. However, Gluc expression demonstrated a significant ~55 fold increase when compared to the inactive replicase (refer to Figure 32) [229]. Following optimisation of transfection efficiency in C636 cells (Supplementary Figure 16.) the *trans*-complemental replicon assay was performed in C636 cells. ORF1 expression was not detected, which was consistent with results by Utt *et al.* 2019. However, levels above background were observed for the Gluc signal, allowing for the assessment of genome replication. This is likely due to the fact that Gluc expression is influenced by levels of negative, genomic, and sub-genomic positive strand synthesis. C636 cells were treated with c3Ado at 1000 μM.

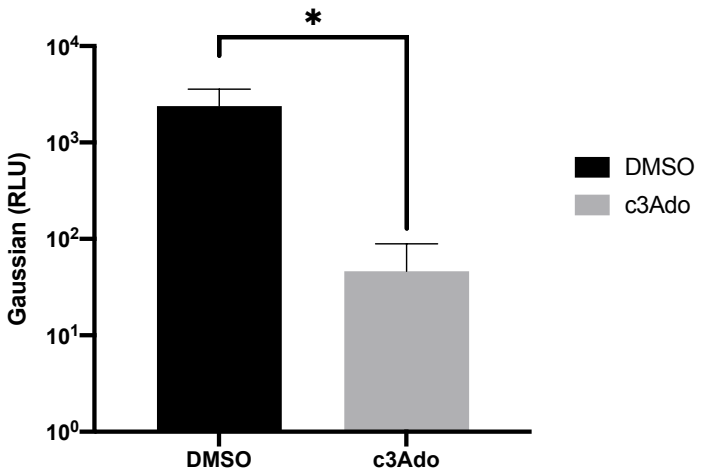

Figure 34. Expression of Gluc reduced in c3Ado treated C636s transfected with *Trans* complementation assay

C636 cells were transfected with the CHIKV *trans* complementation-assay and incubated in the presence of 1000 µM c3Ado for 24 hours. Expression of fluorescent protein was assessed as a proxy for reporter nucleic acid replication, and showed a significant decrease in Gluc expression 24hpt, n=3. p= 0.0269 < 0.05 (*)

N=3, Experiments were done in biological triplicate and analysed in technical duplicate, error bars represent standard deviation from the mean.

The *trans* replicon assay showed that Gluc expression was reduced by ~2 logs when treated with 1000 µM c3Ado, when compared to a DMSO control (Figure 34). These results showing decrease at the level of RNA replication support the previously demonstrated significant inhibition observed in released virus titre in 500 µM c3Ado treated C636 cells (Figure 27.C).

One important caveat with these results was that the 1000 µM c3Ado concentration was double that of 500 µM determined at a later point to be the maximum non-cytotoxic dose using the ATP-lite kit (Figure 27.A). At 1000 µM, there was 50% cell survival, which may have contributed to the above c3Ado results and produced the significant decrease in Gluc expression when treated at 1000 µM concentration (Figure 27.A). However, the reduction seen is greater than 10-fold which might not be fully accounted for by the 50% reduction in cells. The same consideration made with the infectious viral replication in c3Ado treated cells is notable here as well. The health of the remaining cells could be compromised. This result shows the

importance of SAM in insect cells. However, the insect cells tolerate c3Ado treatment at a much higher concentration than mammalian cells.

4.4 Reverse genetic analysis of predicted 5' and 3' m^6A sites in CHIKV Infectious Clone

Two m^6A sites, predicted using the Cui Lab SRAMP [188] tool were of particular interest because they were in the sequence contained within the *trans* replicon system (Figure 28). In the work that follows, these two proposed m^6A sites, at positions 96^A and 11749^A , were targeted for site directed mutagenesis introducing an A> G substitution within the predicted m^6A DRACH methylation sites. This minimal approach to mutagenesis was taken to maintain the primary nucleotide sequence as much as possible and to minimise disruption of any essential RNA secondary structural elements. The first m^6A site was in the 5' region of ORF-1 - 19 nucleotides into the coding region of nsP1 (96^A). Nucleotide 96^A forms essential secondary structure base pairing within both of the published structures of the CHIKV genome (Figure 35). In the Kendall *et al.* Model 96^A, was positioned at the apex of base paired stem SL85, adjacent to the single stranded terminal loop, where it can base pair with nt 89^U. The authors, proposed that this region was dynamic and could potentially form an alternative pseudoknot interaction with complementary sequence on the adjacent double stranded RNA[66]. In the Madden *et al.* structure, they proposed that 96^A was in a single stranded bulge of the long arm that makes up stem loop SL3. Bulges form regions of single stranded flexibility around which the RNA can hinge, as well as forming important sites of ssRNA recognition for RNA binding proteins[231]. The two published models of the 5' CHIKV genome differed. However, this could be due to the dynamic nature of this region, the SHAPE conditions used by each group, and different modelling software used. Still both models experimentally showed that 96^A was highly reactive by SHAPE which meant that 96^A was likely free and unpaired. As a consequence, disruption to the RNA structure through experimental mutation of this

singular nucleotide at position 96 was not predicted to disrupt important RNA structure.

The other predicted m^{6}A site of interest was 11749^A which was in the 3'UTR, for which there was no structural information at the time. Interestingly, m^{6}A sites have been reported to be found most often in the 3' UTRs of eukaryotic transcripts [90]. However, results from Kim *et al.* (2020) showed that MeRIP enrichment precipitated the first 5000 nts and did not report enrichment in the 3'UTR of the CHIKV RNA genome[156]. This made 11749^A of particular interest for mutation. The *trans* replicon system introduced at the beginning of the chapter contains both sequence of the 5' UTR and the 3'UTR sequences (Figure 32). Therefore, the effect of mutating these two predicted m^{6}A sites within the UTRs of the ICRES system mirrored work in the *trans* replicon systems. Sites 96^A and 11749 ^{A} were therefore targeted for site-directed mutagenesis and their relative importance in viral replication was assessed using the ICRES infectious clone system.

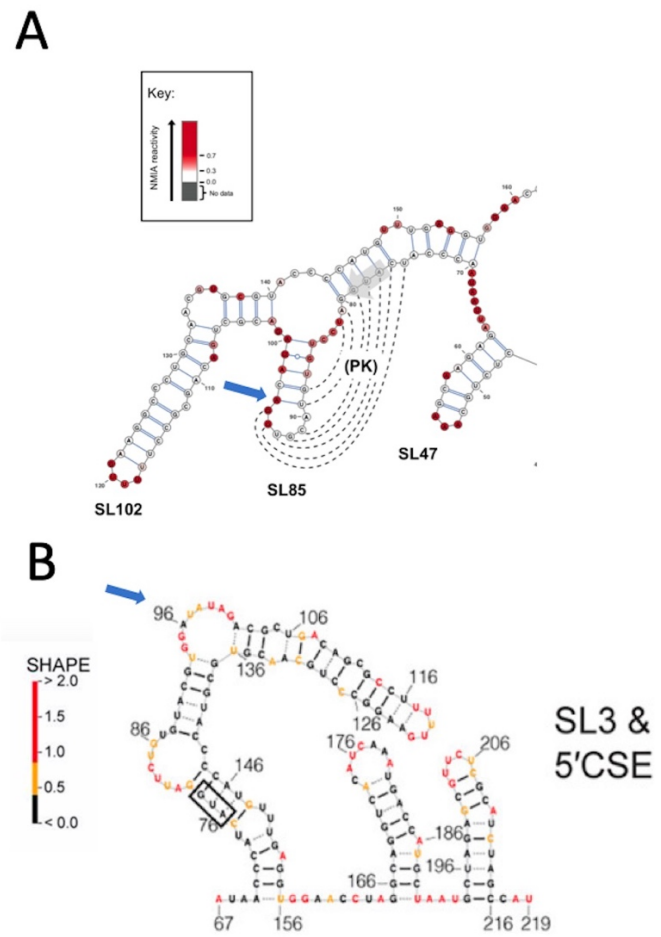

Figure 35. Two alternative predictions for RNA Structure of the CHIKV 5' Region

A. Kendall *et al.* (2019) secondary structure prediction using UNAFOLD[232] proposing a thermodynamically unstable SL85 forming but shows 96^{A} coloured red (blue arrow) to indicate SHAPE reactivity work showing that that position is highly reactive and unlikely to be base paired, even in this proposed structure that is *in-silico* mapped showing a potential base pair with 89^{U}. PK indicates a proposed pseudoknot between sequence in SL85 and an adjacent double stranded RNA region[66]. The analysis done on this structure shows increasing nucleotide reactivity (which suggests that nucleotide is not base paired) from white, pink, to red.

B. Madden *et al.* (2020) secondary structure prediction using SHAPE-MaP of the same region showing a long arm (SL3), with 96^{A} coloured black (blue arrow) which for their colour scheme indicates SHAPE reactivity work showing that that position is highly reactive and is unlikely base paired due to it being in a bulge. Blue box indicates the AUG start codon. The 51 nucleotide alphavirus 5' conserved sequence element (CSE) are the two stem loops on the right[67]. The analysis done on this structure shows increasing nucleotide reactivity (which suggests that nucleotide is not base paired) from yellow, orange, to red.

To generate mutant ICRES plasmids which encoded for viral RNA which could not be m^6A methylated by the cellular machinery at sites A^{96} and A^{11749} the DRACH consensus sequence at these sites were disrupted. Mutating this residue within the DRACH sequence was intended to block m^6A methylation with the least possible effect on RNA structure. m^6A has been reported to occasionally occur outside of a DRACH consensus but an A was essential to m^6A methylation regardless of the surrounding nucleotides[155]. The next consideration was which nucleotide should be used to replace the A. In the Kendall *et al.* 2019 structure, 96^A was proposed to be base paired with 89^U. Consequently, a C or a U at position 96 would have broken up the RNA. However, G^{96} has the potential to base pair with 89^U and thus was predicted to maintain the local RNA structure. For consistency and because the considerations for RNA structure were similar, the same mutation was used for both 96^A and 11749^A.

Using a NEB Q5 site directed mutagenesis kit and associated primer design tools, mutant CHIKV ICRES plasmids were generated altering $96^{A>G}$ and $11749^{A>G}$ within the 5' and 3' regions respectively (Table 1). The substitutions were confirmed using Sanger sequencing. The mutated region was then sub-cloned back into the wild type ICRES plasmid backbone and *in vitro* transcribed to generate capped infectious viral RNA.

The RNA generated from three independent plasmid templates and *in vitro* transcription reactions was analysed by denaturing MOPS agarose gel electrophoresis. Results showed that the most prominent RNA species was at the predicted size, of ~12 kB (Figure 36). WT, $96^{A>G}$ and $11749^{A>G}$ ICRES RNA was then transfected into BHK cells and C636 cells to produce infectious wild type and mutant virus.

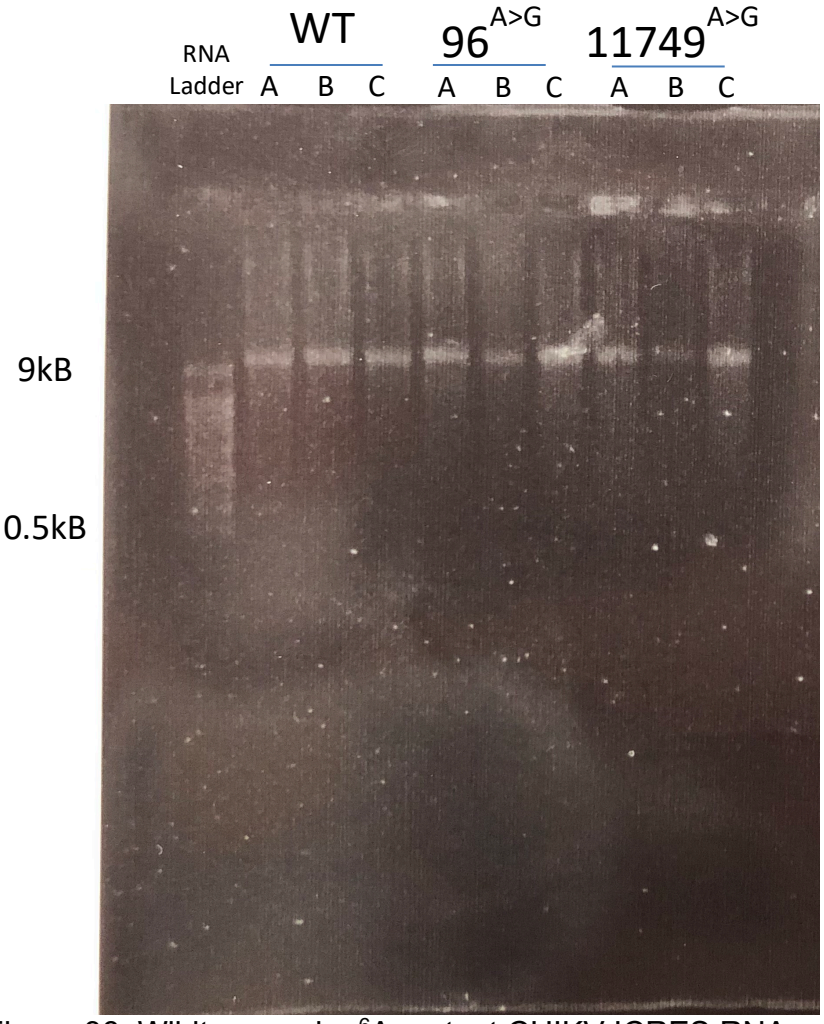

Figure 36. Wildtype and m^{6}A mutant CHIKV ICRES RNA

1% MOPS- Agarose gel showing 1ug of RNA for WT, 96$^{A>G}$, and 11749$^{A>G}$ ICRES plasmids (A, B, and C). Capped RNA was *in vitro* transcribed from three independent plasmids and sequence confirmed by Sanger sequencing of the region of interest. The gel shows that the RNA has is consistent size (approx. 12kB) and is intact. Invitrogen Millennium^{TM} RNA ladder loaded alongside RNA samples in the first lane.

5.4.1 $96^{A>G}$ and $11749^{A>G}$ ICRES CHIKV In Mammalian Cells

The WT, $96^{A>G}$, and $11749^{A>G}$ ICRES RNA was transfected into BHK-21 cells as three independent biological repeats, to control for experimental variation in transfection efficiency or variability between DNA and RNA preparations. At 24 hpt supernatant was collected and virus titres measured by plaque assay on BHK-21 cells. $11749^{A>G}$ ICRES (average: $3.33x10^6$ PFU/mL) was observed to replicate to a similar titre as WT ICRES (average: $9.47x10^6$ PFU/mL) following transfection with relevant RNA, both at approximately 10^6 (Figure 37). However, $96^{A>G}$ ICRES was rescued at ~5 logs lower (average: 2.71x102 PFU/mL) than WT or $11749^{A>G}$ ICRES (Figure 37). The p-value for the difference between infectious virus produced from transfection of $96^{A>G}$ ICRES and WT ICRES was $p=0.07 > 0.05$, using a 2-tailed students t-test. As a result, this difference was not statistically significant.

The results suggested that the 96^{A} site was important for CHIKV replication, in contrast no effect was seen with 11749^{A}. The clear drastic decrease for productive virus from $96^{A>G}$ ICRES was in stark contrast to the productive virus from the $11749^{A>G}$ ICRES. Transfections were repeated with both 1µg and 2µg of RNA for each condition but no effect from amount of RNA transfected was identified (Figure 37).

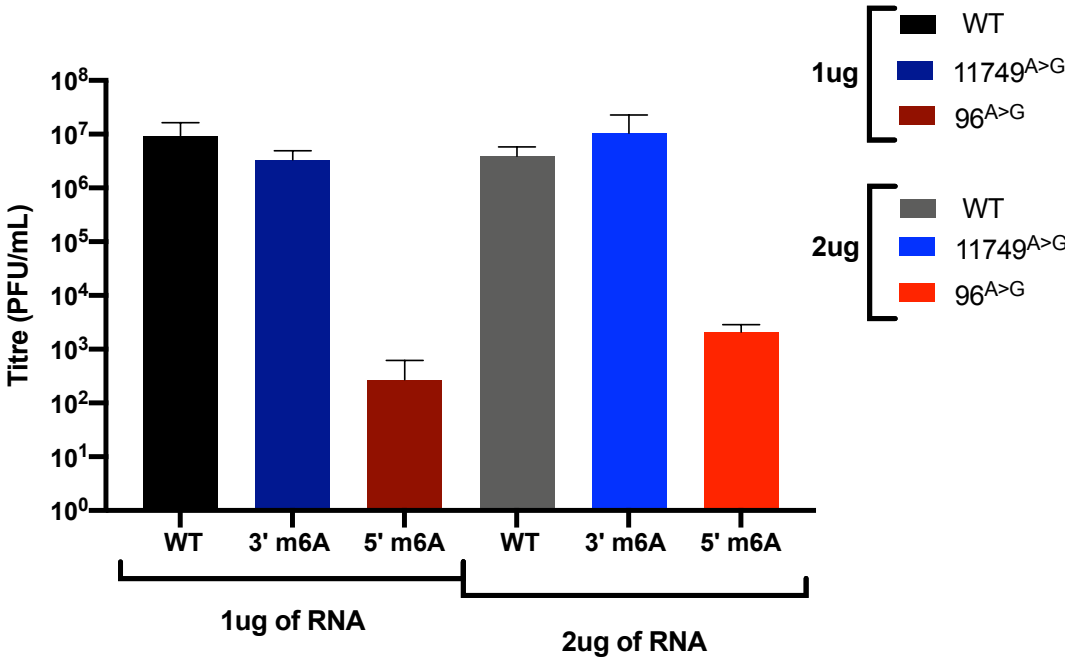

Figure 37. In BHK-21 cells the mutation of Adenosine to Guanosine at site 96 in the CHIKV genome reduces CHIKV replication while same mutation at site 11749 does not.

Productive virus titres measured by plaque assay of the supernatant of BHK-21 cells transfected by electroporation with either 1µg or 2µg of WT, $11749^{A>G}$ ICRES, and $96^{A>G}$ ICRES RNA 24 hour post transfection.

p= 0.07 > 0.05, N=3, Experiments were done in biological triplicate and analysed in technical duplicate, error bars represent standard deviation from the mean of the biological replicates.

Supernatant was collected from the transfected flasks with the intention of performing a one-step growth curve in Huh7 cells at MOI 1. This one-step growth curve would allow us to determine the relative fitness of the mutated viruses in a human cell line. Unfortunately, due to the low $96^{A>G}$ ICRES RNA produced virus the growth curve could not be performed. However, the low but detectable titre for the $96^{A>G}$ ICRES suggested that there was viral replication occurring, but it was being severely impacted by this mutation.

In order to investigate growth of $96^{A>G}$ ICRES selected revertant mutants, total RNA was isolated from the $96^{A>G}$ ICRES RNA transfected BHK-21 24hpt and CHIKV sequences analysed by Nanopore sequencing of cDNA generated from RNA extracted from the monolayer of transfected BHK-21

cells 24 hours post transfection (sequencing performed and analysed by Dr Kate Loveday (Table 12)). In all three independent experiments 98-99% of the extracted CHIKV RNA sequenced had reverted back to the wild type 96^{A} (Table 12).

A.

$96^{A>G}$ ICRES *in vitro* trans RNA	Plasmid A		Plasmid B	
	Total count: 367		Total count: 351	
Base	Count	Percent	Count	Percent
A	28	8%	33	9%
C	1	0%	3	1%
G	335	91%	313	89%
U	3	1%	2	1%
N	0	0%	0	0%

B.

$96^{A>G}$ ICRES 24 hpt	Plasmid A		Plasmid B		Plasmid C	
	Total count: 791		Total count: 789		Total count: 507	
Base	Count	Percent	Count	Percent	Count	Percent
A	781	99%	776	98%	500	99%
C	0	0%	0	0%	0	0%
G	6	1%	5	1%	1	0%
T	4	1%	8	1%	6	1%
N	0	0%	0	1%	0	0%

Table 12. RNA sequencing showing reversion from mutated 96^{G} back to WT 96^{A} sequence

BHK-21 cells were transfected by electroporation with 1µg of WT, $11749^{A>G}$ ICRES, and $96^{A>G}$ ICRES RNA. 24hour post transfection RNA was extracted from the lysed monolayer of transfected cells, cDNA was generated, and that cDNA was sequenced by Nanopore sequencing. Sequencing was performed by Dr Kate Loveday.

A. Original input RNA used in the transfection show that the $96^{A>G}$ mutant *in vitro* transcribed RNA show overwhelming G at the 96 position. N=2 Plasmid A and B refer to independent plasmid preps which were transfected into BHK-21 cells in Figure 36.

B. $96^{A>G}$ mutant RNA was transfected into BHK cells after 24 hours a majority of the viral RNA within the cell has reverted back to an A at the 96 position, in all three instances of

transfection. N=3 Plasmid A, B, and C refer to independent plasmid preps which were transfected into BHK-21 cells in Figure 36.

This suggested that the A at site 96 was the preferred nucleotide over G. This was shown by the fact that the overwhelming species of full length CHIKV RNA present in the cell at 24 hours were able to replicate and had reverted back to 96^{A}. This restored the DRACH site and thus the potential for m^6A methylation at residue 96^{A}. This experiment shows the importance of having an A at this position. This could be explained by a number of reasons, including requirement for m^6A, importance to secondary structure or an RNA protein binding site

Measurement of productive replication by plaque assay was assessed. The results suggested that after 24 hours' worth of rounds of replication the $96^{A>G}$ ICRES RNA was replaced with the 96^{A} ICRES RNA (Table 12). This could have occurred when reversion was selected for and became the predominant sequence. The infectious virus then produced and released by the cell was likely WT 96^{A} ICRES RNA sequence and replicated accordingly. Due to the time it took for reversion to occur viral RNA replication was now a few rounds of replication behind. As a result, the $96^{A>G}$ transfected cells produced a much lower titre virus by 24 hpt (Figure 37).

Importantly reversion was only possible if active replication is taking place, so the $96^{A>G}$ ICRES RNA was able to be replicated by the RdRp but much less efficiently than the WT RNA. These results could suggest that the $96^{A>G}$ ICRES viral RNA itself was less fit. Alternatively, the minority WT sequence (8% and 9%) RNA species in the *in vitro* transcribed RNA samples could have outcompeted the mutated sequence RNA (Table 12). According to the sequencing data of the in vitro transcribed RNA both RNA preps from the two independent plasmids A and B had 8% and 9% had an Adenosine at position 96 while 91% and 89% had Guanosine (Table 12). It is possible that WT sequence species although fewer in number eventually outcompeted the mutated for replication. The results could correspond to the T7 polymerase introduced variation at the *in vitro* transcription level of the RNA from DNA

plasmid or from viral RdRp introduced error that eventually produced a more fit WT revertant sequence.

5.4.2 $96^{A>G}$ and $11749^{A>G}$ ICRES CHIKV in Mosquito Cells

The results in BHK-21s were consistent with rapid reversion to the WT sequence for the $96^{A>G}$ ICRES. Chemical transfection of C636 cells with $96^{A>G}$ and $11749^{A>G}$ ICRES RNA was performed to determine if there was a similar phenotype in mosquito cells as was observed in mammalian cells. For C636 cells there was more variability in transfection efficiency across experiments than for BHK-21 cells (Figure 38). For the first experiment the WT ICRES and $11749^{A>G}$ ICRES both produced titres of ~10^8 PFU/mL but experiments 2-4 resulted in lower titres of between 10^3 – 10^5 PFU/mL. Similar to the pattern observed for BHK-21 cells, the WT ICRES and the $11749^{A>G}$ ICRES had similar titres within and not between the independent biological replicates (Figure 38). Unlike in the mammalian cell transfections, the $96^{A>G}$ ICRES never produced any detectable infectious virus from the mosquito cell transfection. This suggested a complete block on virus replication, rather than low levels of replication, that enabled reversion and rescue, as observed in the BHK-21 cells (Figure 38). This could argue against the hypothesis that the viral RdRp was responsible for the A to G mutation at site 96 as the same RNA which had 8-9% WT sequence was also transfected into the C636 cells with no productive virus detectable in the supernatant after 24 hours. This is unless there is cell type variability in that A to G mutation occurring at position 96.

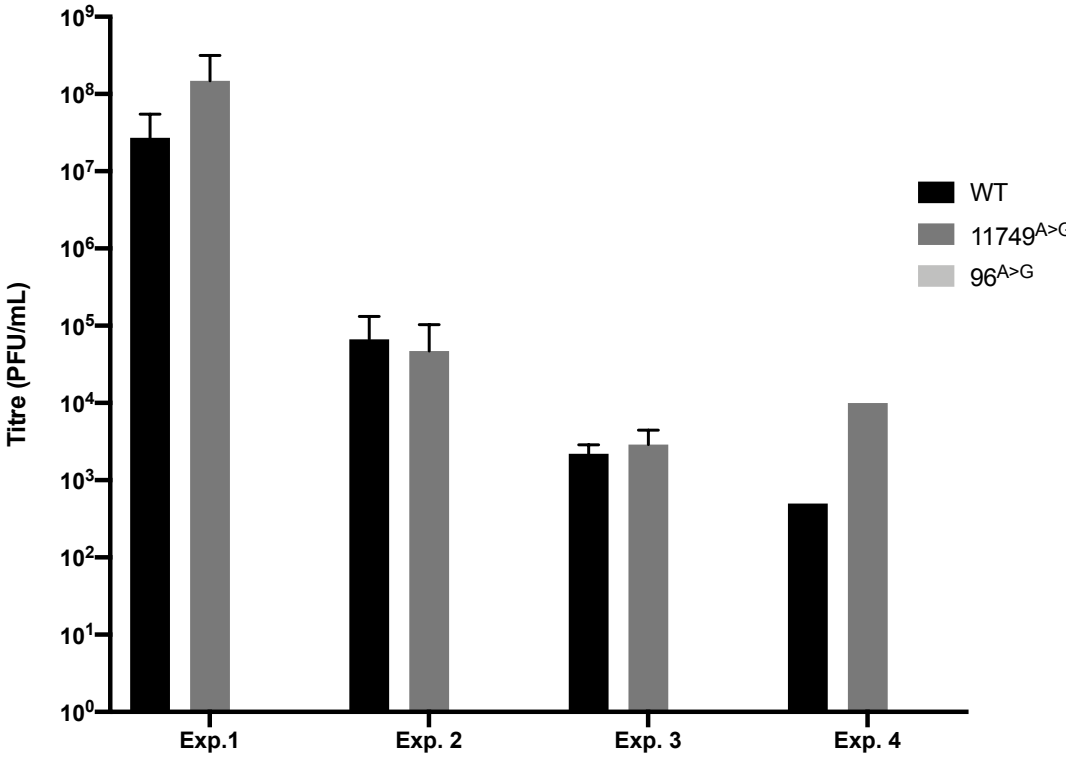

Figure 38. In C636 cells $96^{A>G}$ reduces CHIKV replication while mutation at $11749^{A>G}$ has no effect in four independent experiments

Titres were calculated from supernatant collected from chemically transfected C636 cells 24 hours post transfection in four independent experiments (Exp.1-4). Due to large differences in titre likely due to transfection efficiency these results could not be easily combined. However, these results show no infectious virus detected for the $96^{A>G}$ RNA transfected into C636 cells but similar virus titres were detected for both WT and$11749^{A>G}$ RNA transfected into C636 cells.

N=4, Experiments were done in biological duplicate, except for experiment 4 which was only done only a single time, error bars represent standard deviation from the mean.

As addressed above, the same RNA preparations, but different aliquots stored stably at -80 °C, which were used for the BHK-21 work were used for the mosquito cell assays, meaning the RNA size and integrity were the same (Figure 36Figure 36). These results suggested that the A^{96} site was also essential for CHIKV replication in mosquito cells while the A^{11749} site had no effect.

4.5 Reverse genetic analysis of $96^{A>G}$ and $11749^{A>G}$ in CHIKV *Trans*-complementation assay

While previous knockdown and c3Ado inhibitor-based assays results were consistent with m^6A methylation being required for efficient CHIKV genome replication, these experiments could not differentiate between methylation of the virus genome or host cell transcripts (Figure 33, Figure 34). To determine the significance of two potential *in-silico* predicted m^6A sites to CHIKV RNA transcription the previously described site directed mutagenesis outlined above in Section 4.4, was repeated within the context of the *trans* complementation replicon assay (Figure 39).

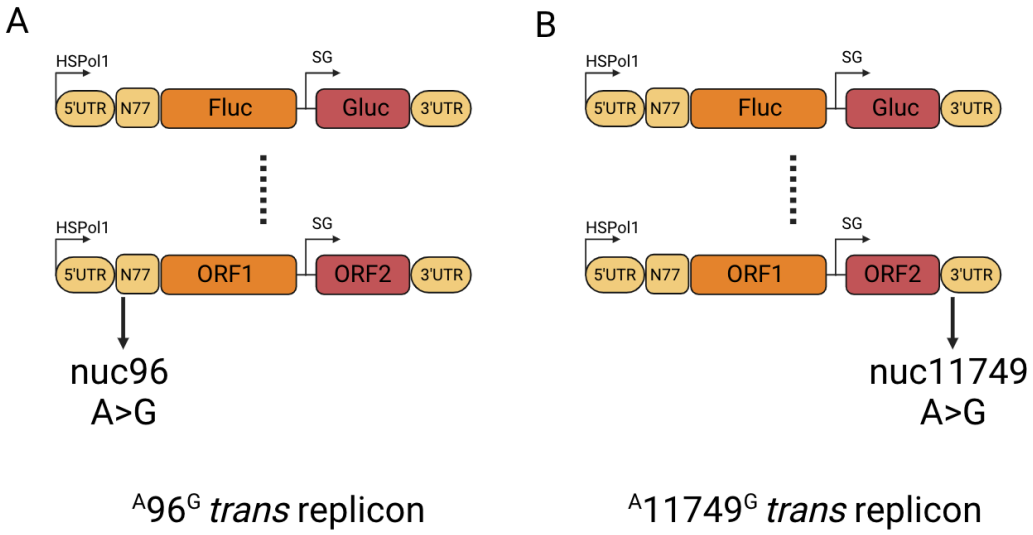

Figure 39. Mutation of the CHIKV *trans* replicon expression construct

Mutation was made to the CHIKV *trans* replicon expression construct. Initial transcription of the transcript is driven by Human Polymerase I (HSPolI) binding to the promoter in the plasmid while subsequent rounds of replication are taken over by the viral RdRp encoded by plasmid shown in Figure 32 A.

A. Mutation was an A>G at position 96 in the CHIKV sequence of the *trans* replicon construct
B. Mutation was an A>G at position 11749 in the CHIKV sequence of the *trans* replicon construct

This assay was designed and described in Utt *et al. (*2018) [229].

Figure created using BioRender.

In the infectious virus system, IC96$^{A>G}$ significantly inhibited productive CHIKV replication, in both mammalian (BHK-21) and mosquito (C636) host cells, suggesting this site is important to the viral lifecycle. Whereas mutating the IC11749$^{A>G}$ had little effect on the viral lifecycle (Figure 37).

Using the *trans*-replicon system allowed characterization of truncated CHIKV-specific sequence and two potential m^{6}A sites independent of other elements of the viral lifecycle, as well as other potential m^{6}A sites on the viral RNA, and m^{6}A methylation of host transcripts.

4.5.1 $96^{A>G}$ inhibits vRNA replication in Huh7 cells while $11749^{A>G}$ does not inhibit vRNA replication in these cells

To determine if 96^{A} and 11749^{A} were important to RNA replication in human cells the WT, *human.trans*$96^{A>G}$ and *human.trans*$11749^{A>G}$ reporter plasmids were transfected into Huh7 cells, alongside either the active or inactive *trans*-replicase expressing plasmids, and Fluc and Gluc expression was measured 24 hpt.

A significant reduction of ~ 3 log in expression of both Fluc and Gluc was observed (p=0.0082) 24 hpt, for *human.trans*$96^{A>G}$ relative to WT *human.trans* replicon assay expression levels (Figure 40).

Although a statistically significant difference (p= 0.0053) was observed for Fluc expression between WT and *human.trans*$96^{A>G}$ in the cells which were transfected with the inactive replicase, the values were closer to background expression levels at ~10^3 RLU (Figure 40.A). The active replicase in contrast reached signal levels of ~10^5 RLU. No significant difference (p=0.67) was observed for Gluc expression with the inactive replicase, which would be consistent with this difference even in the “negative control” being within background levels of expression. As a result, this should not invalidate the significant active replicase results in Gluc (p=0.0068) (Figure 40.B).

As a result, the reduction for both Fluc and Gluc expression in the *trans* replicon assay showed that mutation of the potential m^6A site 96^{A} in the 5’ end of the CHIKV genome led to a decrease in transcription of the positive and negative viral transcripts.

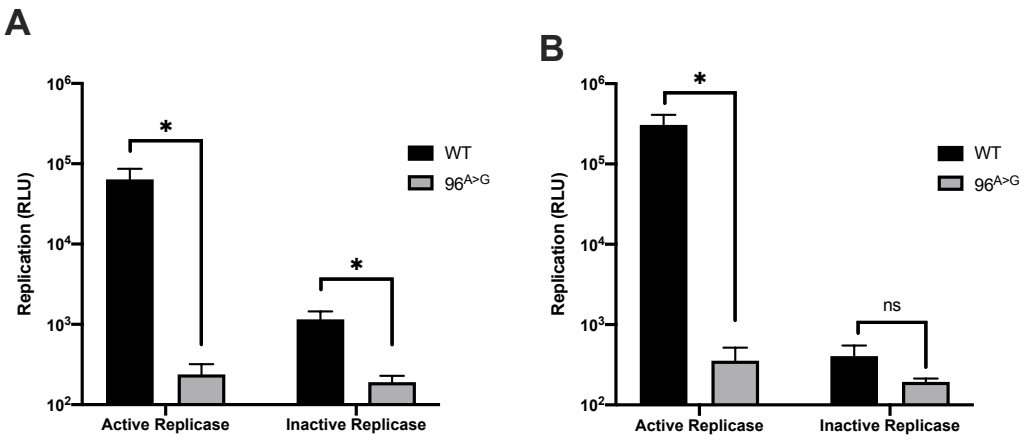

Figure 40. *human.trans*$96^{A>G}$ mutation drastically reduces ORF1 and ORF2 expression in Huh7 cells

Huh7 cells were transfected with *human.trans* replicon, WT sequence and 96A>G and 24 hour post transfection the cells were lysed and the Fluc and Gluc was quantified as a proxy for replicon replication by either active or inactive replicon (constitutively expressed and as a result should not be limiting in this assay).

A. Fluc expression is significantly reduced with *human.trans*$96^{A>G}$ 24 hpt. (active replicase: p=0.0082< 0.05*; inactive replicase: p= 0.0053 < 0.05*)

B. Gluc expression is significantly reduced with *human.trans*$96^{A>G}$ 24 hpt. (active replicase: p=0.0068< 0.05*; inactive replicase: p= 0.67> 0.05)

N=3, Experiments were done in biological triplicate and analysed in technical duplicate, error bars represent standard deviation from the mean.

Experiment designed and supervised by myself and performed by MSc student, Katie Allott.

To determine if another potential m^6A site played a role in vRNA replication mutagenesis in the human *trans* replicon was performed at nt site 11749. *human.trans*$11749^{A>G}$ was assessed relative to WT *human.trans* expression levels. This was performed three times, but only one experiment yielded detectable levels of Fluc signal. In the one experiment that could be read, there is a ~ 1 log reduction for Fluc expression, but because this was only one experiment statistical significance could not be analysed due to access to working reagent to read the Firefly signal (Figure 41.A).

All three experiments could be analysed for Gluc expression. Gluc expression was assessed using a separate reagent for detection of Gluc

rather than the Fluc. For Gluc expression with the active replicase there was a statistically significant ~1 log reduction (p=0.000018) in expression for *human.trans*11749$^{A>G}$ relative to *human.trans*WT (Figure 41.B). The inactive replicase also gave a statistically significant difference between *human.trans*11749$^{A>G}$ compared to *human.trans*WT replicon assay for ORF 2 expression but the expression was at 10^3 and was in the range of expected background levels which was also observed for *human.trans*11749$^{A>G}$ assessment in Figure 40.

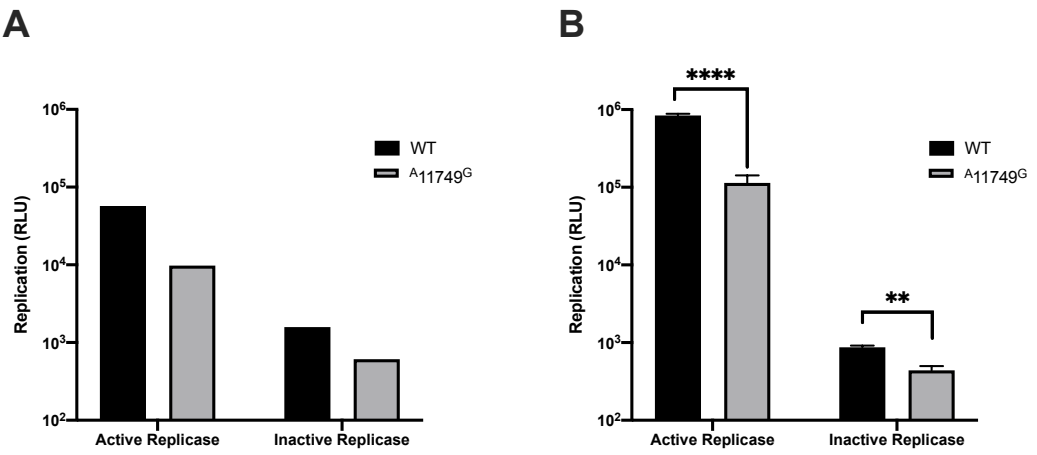

Figure 41. $^{A}11749^{G}$ mutation in *trans* replicon reduces ORF1 and ORF2 expression in Huh7 cells

Huh7 cells were transfected with *human.trans* replicon, WT sequence and 11749A>G and 24 hour post transfection the cells were lysed and the Fluc and Gluc was quantified as a proxy for replicon replication by either active or inactive replicon (constitutively expressed and as a result should not be limiting in this assay).

A. Fluc expression was reduced with *human.trans*$11749^{A>G}$ 24 hpt. (n=1)

B. Gluc expression was significantly reduced with *human.trans*$11749^{A>G}$ 24 hpt. (n=3) (active replicase: p=0.000018 < 0.00005 ****; inactive replicase: p= 0.000585< 0.005 **)

Experiments were performed in biological triplicate and analysed in technical duplicate, error bars represent standard deviation from the mean.

Experiment designed and supervised by myself and Figure 42.B performed by MSc student, Katie Allott.

For the *human.trans*$11749^{A>G}$ compared to *human.trans*WT replicon assay ORF1 expression was only able to be detected for one sample of three, this was likely due to out of date reagent used for detection of the firefly luciferase (Figure 41.A).

These results suggested that in Huh7 cells both $96^{A>G}$ and $11749^{A>G}$ significantly decreases viral RNA replication but the effect was only ~ 1 log inhibition for $11749^{A>G}$ versus the ~ 3 log inhibition for $96^{A>G}$. These results suggested a more crucial role for 96^{A} in CHIKV RNA replication than 11749^{A}.

4.5.2 Reverse Genetic *Trans* Replicon Assay in Mosquito Cells

In order assess the role of 96^{A} and 11749^{A} in C636 cells, site-directed mutagenesis was performed in the mosquito compatible *trans* replicon plasmids, *A.ae.trans* replicon. As previously described (Figure 27) no ORF-1 expression was detected, which was consistent with Utt *et al.* 2019 Replication with the inactive replicase was ~ $10^{1.5-2}$ RLU which was consistent with background levels of expression[229]. With the active replicase ~ 10^{4} RLU was observed but no difference in Gluc expression was observed between $96^{A>G}$ (Figure 42.A) or $11749^{A>G}$ (Figure 42.B) and WT. This suggested that methylation of neither site was important for viral genome replication in mosquito cells.

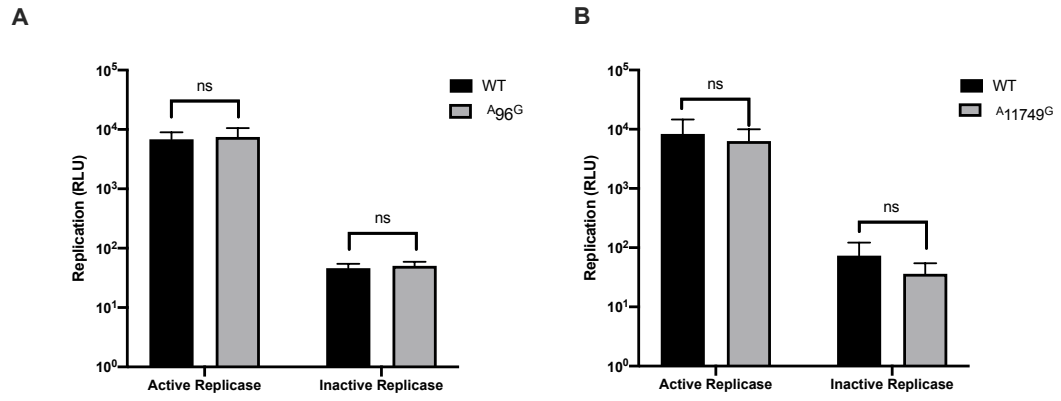

Figure 42. Neither $96^{A>G}$ or $11749^{A>G}$ changes GLuc expression in *trans* replicon transfected C636 cells

C636 cells were transfected with *A.ae.trans* replicon, WT sequence, 96A>G, and 11749A>G and 24 hour post transfection the cells were lysed and the Gaussia luciferase was quantified as a proxy for replicon replication by either active or inactive replicon (constitutively expressed and as a result should not be limiting in this assay).

A. Gluc expression with *trans*$96^{A>G}$ was not significantly changed from levels obtained from transfection with WT trans replicon 24 hpt. (ns = no significant difference)

B. Gluc expression with *trans*$11749^{A>G}$ was not significantly changed from levels obtained from transfection with WT trans replicon 24 hpt. (ns = no significant difference)

Error bars represent standard deviation from the mean, n=3

Experiment designed and supervised by myself and performed by MSc student, Sarah Menzes.

4.6 5' CHIKV RNA Structure Mapping

The reverse genetic analysis enabled investigation into the effect of blocking m^6A methylation at specific nucleotides to be assessed. However, the substitutions could result effects unrelated to m^6A methylation, such as disrupting the stability of essential RNA structures within the viral genome. Such RNA elements have previously been shown to play a vital role in initiation of CHIKV genome replication [66]. CHIKV predicted structure from SHAPE constrained *in silico* thermodynamic analysis published by Kendall *et al.* 2019 showed 96^A has the highest recorded reactivity[30]. This suggested that under *in vitro* folding conditions 96^A does not base pair (Figure 35.A). A paper by Madden *et al.* 2020 also predicted that 96^A was highly reactive and

exists in the single stranded bulge of a stem-loop, suggesting that an A>G substitution did not disrupt essential base paring (Figure 35.B).

To confirm that the substitution made to 96^{A} had no predicted effect on RNA folding, *in-silico* mapping was used to model both WT ICRES RNA and $96^{A>G}$ ICRES RNA. The RNAstructure software was used to model the first 307 nucleotides of the CHIKV genomic RNA present in the *trans* replicon system[189]. This software used was a free energy minimisation algorithm which used base stacking energies and hydrogen bonding to predict the most stable (lowest free energy or LFE) structure for individual RNA molecules. The temperature parameter was set to either 37°C or 28°C to *in silico* predict this region under either mammalian or mosquito host body temperatures respectively.

The mutation $96^{A>G}$ did not change the structure and only slightly increased the minimum free energy predicted for that structure for either sequence at 37 °C . WT and $96^{A>G}$ had -110.1 to 113.7 kcal/mol respectively (Figure 43,Figure 44). Both showed a similar long arm reported by Madden *et al.* in their published CHIKV 5' end structure[67]. These results showed similar structure and minimum free energy predictions. They also align well with the SHAPE mapping by Kendall *et al.* and Madden *et al.* (Figure 35) showing that 96^{A} has high reactivity and is thus not likely base paired. The $96^{A>G}$ predicted structure does show 96^{G} base paired with 143^{C} does whereas the WT structure shows 96^{A} not base paired which could perhaps stabilize the stem loop (Figure 43, Figure 44). This analysis suggested that the substitution $96^{A>G}$ may but should not have major impacts on overall RNA structure at 37 °C, disruption of which could have influenced viral replication [30,227]. The structure mapping was also performed for both the WT and $96^{A>G}$ sequence but at 28 °C (Figure 43-47). The WT LFE structure at 28 °C was -130 kcal/mol and had a dissimilar shape to the WT LFE structure at 37 °C (Figure 45 and Figure 43). The predicted $96^{A>G}$ structure which was most similar to WT structure at 28 °C was the second LFE structure which was extremely close to the LFE at -129.4 kcal/mol (Figure 46 and Figure 43). At 28 °C the second LFE WT structure and the LFE structure for $96^{A>G}$ showed the same long arm reported by Madden *et al.* It is perhaps interesting that by *in silico* mapping at 28 °C there is a more likely WT structure which does not

match either the LFE structure predicted for the WT sequence at 37 °C or the LFE structure predicted for $96^{A>G}$ at 28 °C. It is possible that at this lower temperature the mutation from A>G at position 96 has a more profound effect on structure. However, as this is all *in-silico* mapping and the energies associated with the first and second free energies are only 0.6 kcal/mol different, it is not likely a profound effect. However, it of course cannot be discounted.

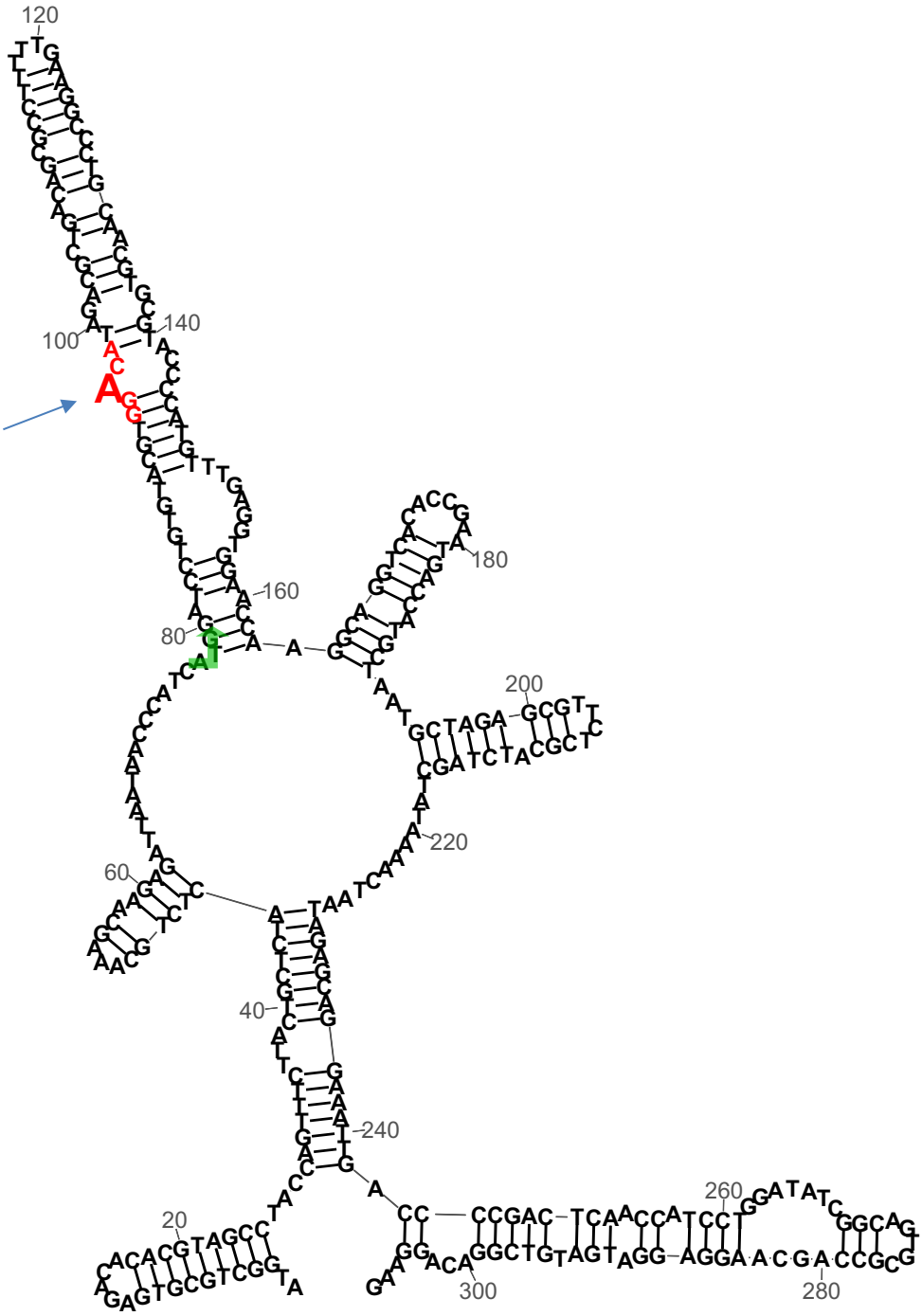

Figure 43. RNAstructure software[189] LFE folding of the WT CHIKV RNA at 37 °C

First 307 5' nucleotides of WT CHIKV at 37 °C at the Lowest Free Energy -110.1 kcal/mol, DRACH sequence in red with 96^{A} in bold red indicated by the blue arrow and ATG start codon highlighted in green. Visualized using RNACanvas[233].

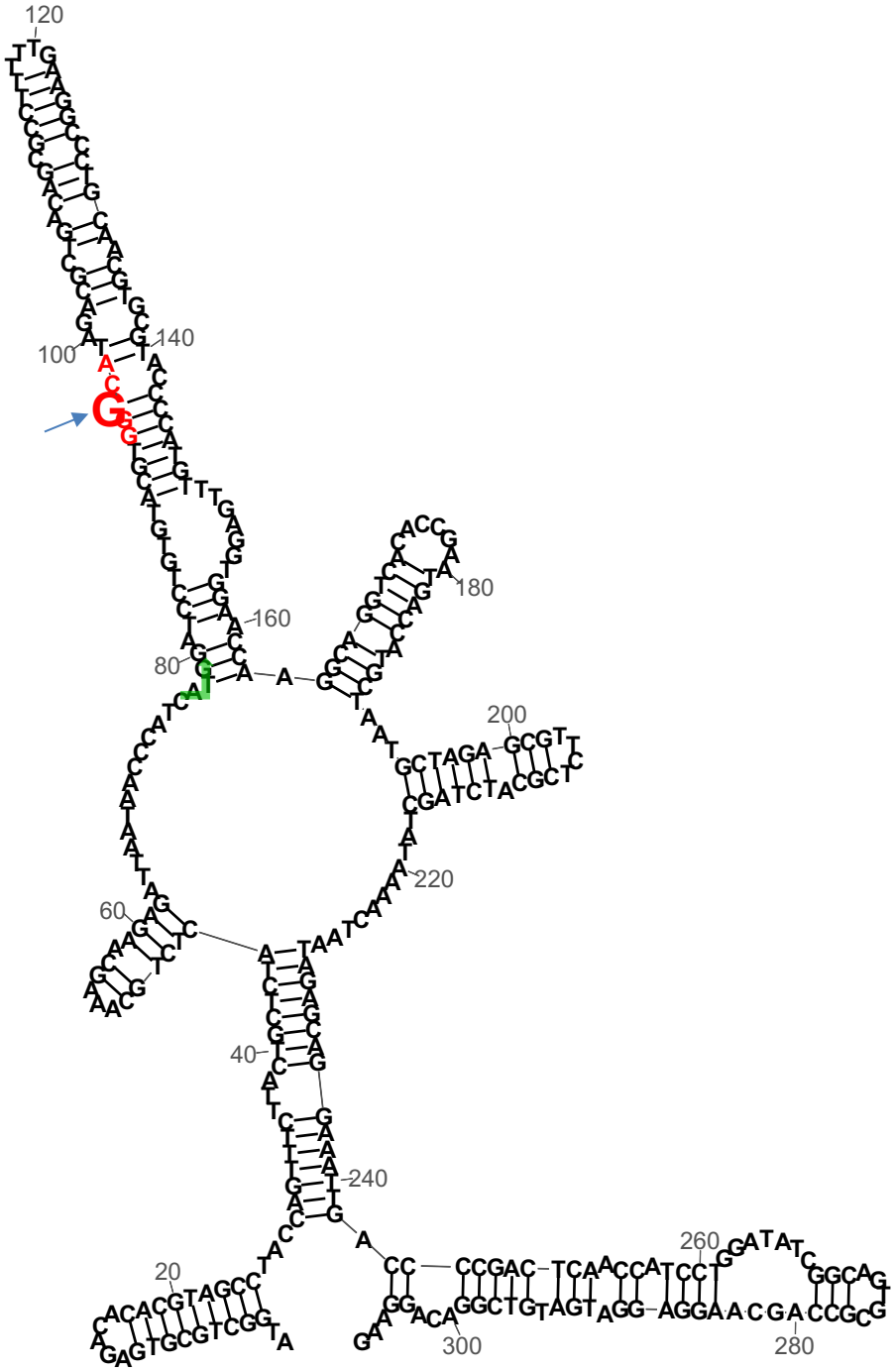

Figure 44. RNAstructure software[189] LFE folding of the 96$^{A>G}$ CHIKV RNA at 37 °C

First 307 5' nucleotides of 96$^{A>G}$ CHIKV at 37 °C at the Lowest Free Energy -113.7 kcal/mol, DRACH sequence in red with 96G in bold red indicated by the blue arrow and ATG start codon highlighted in green. Visualized using RNACanvas[233].

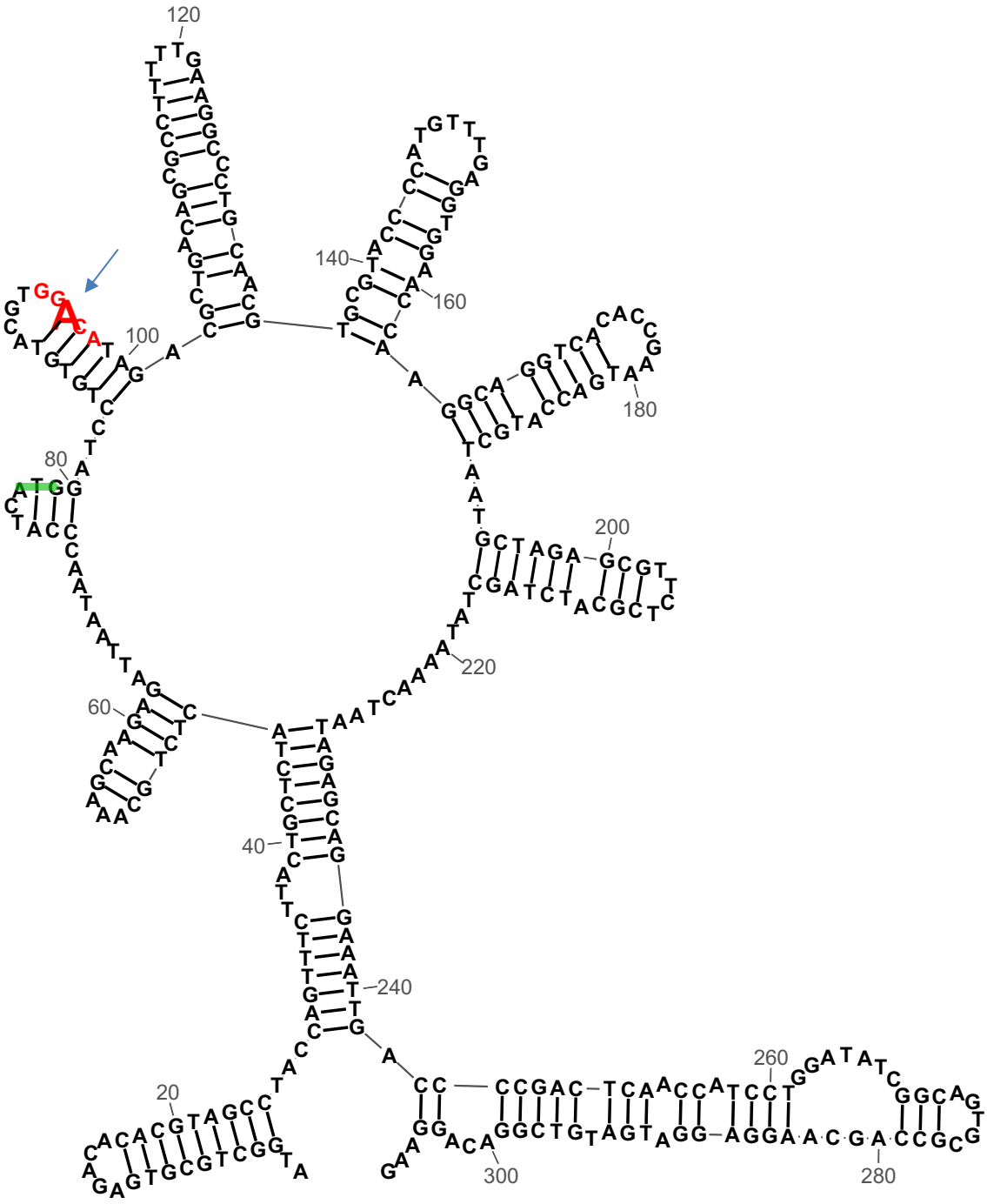

Figure 45. RNAstructure software[189] LFE folding of the WT CHIKV RNA at 28 °C

First 307 5' nucleotides of WT CHIKV at 28 °C at the Lowest Free Energy -130 kcal/mol, DRACH sequence in red with 96A in bold red indicated by the blue arrow and ATG start codon highlighted in green. Visualized using RNACanvas[233].

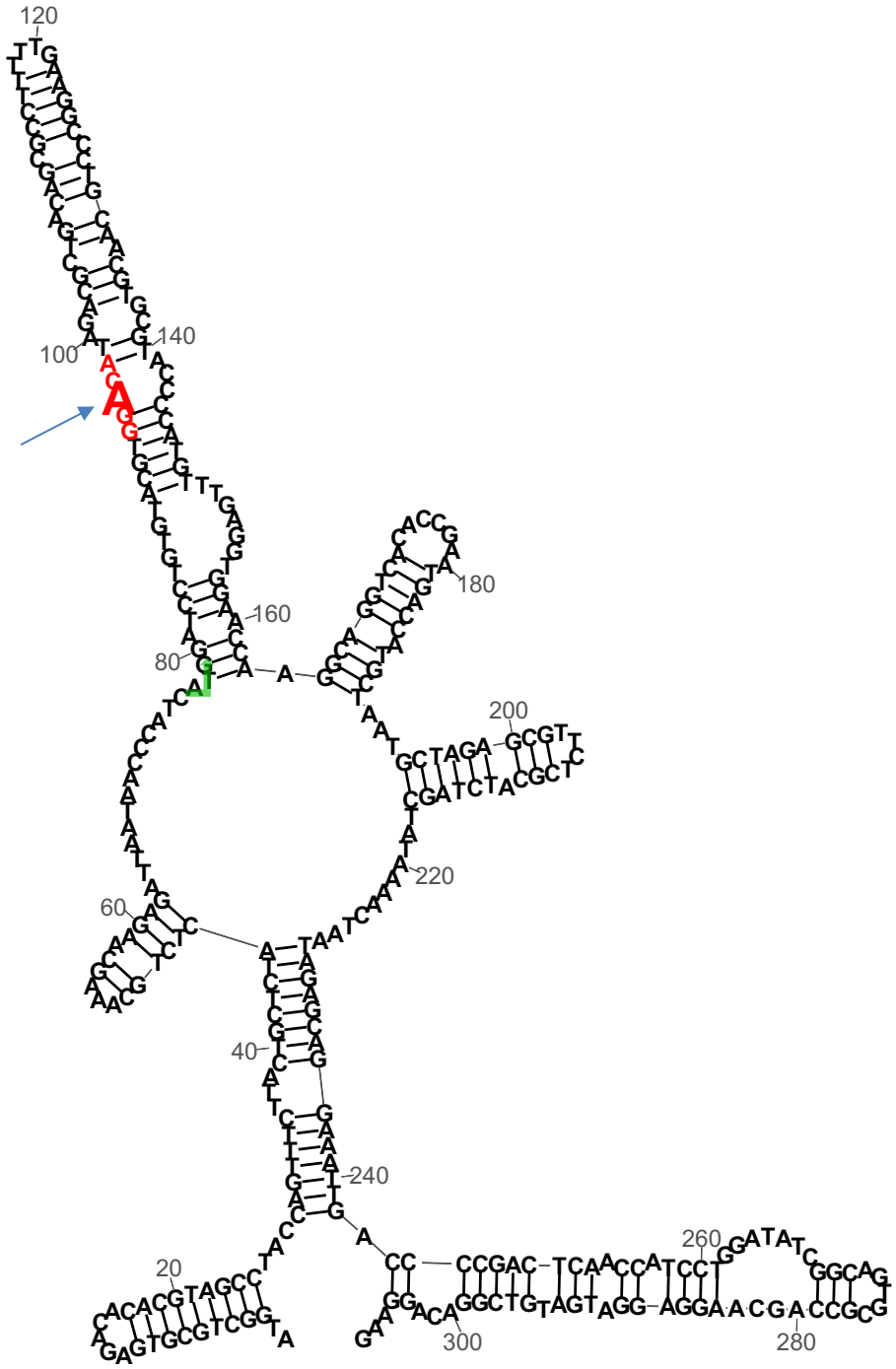

Figure 46. RNAstructure software[189] Second LFE folding of the WT CHIKV RNA at 28 °C

First 307 5' nucleotides of WT CHIKV at 28 °C at the Second Lowest Free Energy -129.4 kcal/mol, DRACH sequence in red with 96A in bold red indicated by the blue arrow and ATG start codon highlighted in green. Visualized using RNACanvas[233].

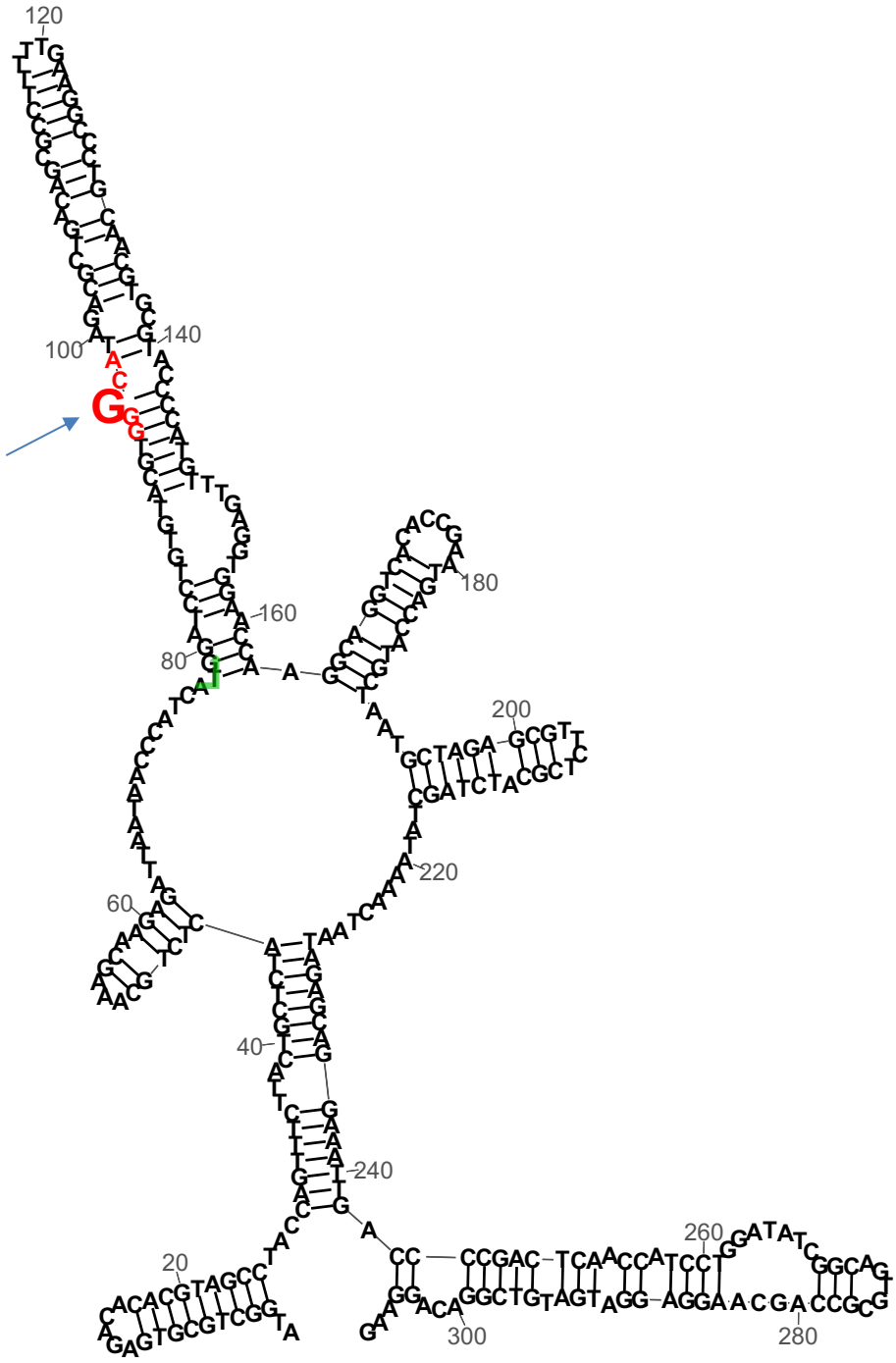

Figure 47. RNAstructure software[189] LFE folding of the 96$^{A>G}$ CHIKV RNA at 28 °C

First 307 5' nucleotides of 96$^{A>G}$ CHIKV at 28 °C at the Lowest Free Energy -133.2, DRACH sequence in red with 96A in bold red indicated by the blue arrow and ATG start codon highlighted in green. Visualized using RNACanvas[233].

4.6 Discussion

In conclusion, using the *trans* complementation replicon assay in cells treated with c3Ado showed a reduction in efficient CHIKV genome replication in both human and mosquito cells. However, in both the human and mosquito systems there must be a consideration that reduction in RNA replication was shown in the context of a 70% and 50% cell survival at the concentration of c3do used. There could also have been potential ill effects to the over overall health on those remaining surviving cells due to c3Ado treatment. These experiments also do not differentiate between a requirement for SAM dependent methylation at the level of the CHIKV sequence contained in the RNA *trans* replicon molecule or on host cellular transcripts.

Previously, potential m^6A sites in the CHIKV genome were mapped (Figure 28). In an attempt to distinguish between CHIKV and host transcript requirement for m^6A, potential m^6A sites in the CHIKV genome were targeted for site directed mutagenesis to remove the potential for m^6A methylation at those sites. The two sites chosen for investigation were at positions 96 and 11749 in the viral genome. They were both mutated independently in the ICRES plasmid from $96^{A>G}$ and $11749^{A>G}$. RNA transcribed from those mutated plasmids was transfected into both mammalian and mosquito cells. Residue 96^{A} was observed to be essential for efficient CHIKV replication in both Huh7 and C636 cells. While 11749^{A} was not important for CHIKV replication in Huh7 and C636 cells.

Further work mutating both $96^{A>G}$ and $11749^{A>G}$ in the *trans* replicon reporter plasmid showed that in Huh7 cells both the 96^{A} and 11749^{A} site were important to viral RNA replication but that the 96^{A} site likely played a greater role. In C636 cells, neither the 96^{A} nor 11749^{A} seemed to be important to viral RNA replication. Taken together with the c3Ado and the infectious virus experiments, these results suggest that an A at position 96 is important for viral genome replication. However, in mosquito cells this cannot be conclusively linked to viral RNA replication. Likely features of the RNA which

are sequence dependent, such as m^6A methylation at 96^A or possibly sequence specific structural elements are important to the replication of the CHIKV RNA. This supports the work on 5' secondary structures published by Kendall *et al.* which shows that secondary structures such as SL85 which were essential to replication in mammalian cells were not in mosquito cells after 24 hours[30]. As 96^A is in this 5' structure region it is possible that by changing the A to a G the essential SL85 was disrupted.

To better understand the functional importance of 96^A in the CHIKV genome, further work would be needed to determine the specific protein and RNA factors involved in recognition of 96^A. Work from Kim *et al.* identified that m^6A binding protein YTHDF2 was pro-viral for CHIKV and YTHDF1 and YTHDF3 were identified as antiviral[140]. Potentially, YTHDF2 could recognize $96^{A>G}$ ICRES viral RNA less well than the WT ICRES RNA or alternatively YTHDF1 and YTHDF3 could bind the $96^{A>G}$ ICRES viral RNA with higher affinity[140]. There also might be other m^6A reader proteins or other RNS binding proteins that bind that site in the CHIKV RNA and although the binding is the same regardless of methylation at that site the effect of the binding is different without methylation at that site. The work presented here looked at predominantly viral replication within a 24-hour window. It would be interesting considering the rapid reversion of $96^{A>G}$ IC RNA back to 96^A to look at earlier time points in the replication cycle. A growth curve for viral replication at earlier time points with sequencing would allow identification of when the switch to WT sequence CHIKV occurs, and if it is consistent across experiments. This could be performed using c3Ado and in WTAP knockdown cell lines to see the effect of reduced SAM dependent methylation, including m^6A has on the reversion at 96 from A to G. Looking later in the lifecycle at 48 hours would clarify if the titres of supernatant from the $96^{A>G}$ CHIKV RNA transfected BHK-21 cells return to WT levels. However, the rapid reversion and decreased viral replication of the $96^{A>G}$ virus all suggests the vital importance of an A at this proposed m^6A site, 96 nucleotides into the viral genome. This could also be due to disruption of essential base pairing for the formation SL85 as described in Kendal *et al.* [66] or the loss of m^6A methylation at this site.

The mutation from A > G at position 96 was intended to be minimally disruptive to the RNA structure, while still ensuring it could not be m^6A methylated at that site. The *in silico* analysis shown in Figure 43 through Figure 47**Error! Reference source not found.** alone cannot confirm that mutation would not have changed the structure. Given more time SHAPE of the $96^{A>G}$ and $11749^{A>G}$ mutants would confirm the structure of both RNAs and more confidentially link the reduction in viral replication and viral RNA transcription to m^6A methylation at position 96. Both *in vitro* SHAPE and *in-silico* mapping were performed on a truncated RNA molecules (nts 1-330) but the same results were seen for full-length CHIKV genome (personal communication Dr Tuplin). To take into consideration different dynamics in the cell which would influence the whole viral genome folding and unfolding in-cell SHAPE could be performed.

Chapter 5- Discussion

CHIKV is an arbovirus of emerging endemic potential which is passed between mammalian hosts by an infected mosquito's bloodmeal[3]. This virus has spread onto five continents, one hundred countries and continues to expand its geographical range along with that of its mosquito vectors [3,20]. There is currently one newly FDA-licensed vaccine but no therapeutics for CHIKV infection[7]. Patients with access to medical facilities can seek only palliative care for the debilitating symptoms of arthralgia and the virus can be found in persistent reservoirs within the body, like the liver, months and years after initial infection[203]. CHIKV has a single stranded RNA genome that is replicated by a viral replication complex and has regulatory RNA secondary structure and RNA sequence that dictates stages of the viral lifecycle. This includes from initial translation of ORF1 which contains the viral RdRp, replication of the viral RNA, and packaging of the genomic RNA into the virion which buds from the cell's plasma membrane[30,40,41,227].

The overarching question of this study was to assess the role of a post transcriptional modification, m^{6}A methylation, on CHIKV replication. m^{6}A is a reversible modification added at to the N-6 position of an adenosine, mainly at a DRACH consensus sequence motif within the transcript. The recognition of this methylation by host machinery has implications for the fate of the transcript, including but not limited to splicing, translation, and stability. Understanding the interplay of the host cell with this m^{6}A post transcriptional modification could have direct impact on the design and effectiveness of RNA therapeutics. For instance, circRNA present an interesting area of RNA therapeutic development and m^{6}A has been shown to direct translation, degradation, and influence innate immune detection of circRNA[234], [235]. Direct m^{6}A methylation of the CHIKV viral transcript, as well as other viral RNAs, has been detected in the time since this work was first undertaken. Kim *et al.* 2020 detected methylation in the first 5000 nts of CHIKV genomes isolated from mature released virions by MeRIP[156]. The area of m^{6}A detection and its relationship to virology is under constant development and as discussed in the Introduction antibody-based methods of m^{6}A detection are flawed. So to present an alternative perspective, also in the time since this PhD work was

undertaken a preprint was published on BioRxiv on October 5, 2023[195]. This work detailed ONT, MeRIP, LC-MS/MS, and protein knockdown experiments on CHIKV and DENV infected cells[195]. They conclude based on their work that m^{6}A is likely not a common feature of RNA genomes of cytoplasmic replicating viruses[195]. They claim they do not see convincing evidence of m^{6}A on the CHIKV or DENV transcripts[195]. This work has yet to undergo peer review but shows the contentious and complex nature of the field. Genomes of RNA arboviruses, ZIKV[117], as well as other cytoplasmic replicating RNA viruses including EVA71[159] and SARS-CoV-2[157] have also been reported to be m^{6}A methylated, with their replication impacted by experimental knockdown of m^{6}A within the cell. Interestingly for EVA71 the role of m^{6}A appears to be mostly proviral in Vero cells while it is antiviral for SARS-CoV-2 in Huh7 cells and ZIKV in 293T cells[117,159]. Not only RNA viruses but DNA viruses such as KSHV which have mRNA intermediates have also been shown to be directly m^{6}A methylated[127]. During both ZIKV and KSHV infection changes to m^{6}A methylation signatures across host transcripts have also been detected through MeRIP-seq methods, showing that there were changes to the epi-transcriptome following viral infection[117,127]. The aim of this study was to investigate the potential role of m^{6}A methylation on CHIKV replication and identify potentially methylated sites within the virus genome.

Chapter 3 set out to determine the role of m^{6}A knockdown within the cell on CHIKV replication. This was carried out by treating two human cell lines, shown previously to be permissive for CHIKV replication, and one mosquito cell line with a maximum non-cytotoxic dose of small molecule, c3Ado[223]. c3Ado has been used to study the role of m^{6}A in the KSHV lifecycle and works by reducing the available methyl donor SAM in the cell. m^{6}A reduction by a maximum non-cytotoxic dose of c3Ado in both Huh7 cells and C636 cells resulted in a significant reduction in viral replication. This suggested that reduction in m^{6}A methylation across RNA transcripts contained in the cell, both host or viral, led to a reduction in released virus. These results demonstrated that m^{6}A had a pro-viral impact on CHIKV replication. In human cell lines this effect appeared to be cell type specific, as RD cells did not show a significant reduction in CHIKV replication when treated with the

maximum non-cytotoxic dose of c3Ado. It is important to consider that the cells remaining after c3Ado treatment may not be as fit as untreated cells. These experiments can only shows that treatment with c3Ado at the concentration used, which was informed by cytotoxicity assay and the published literature, reduces CHIKV replication in Huh7 cells and C636 cells but not in RD cells. To ensure that this effect was not solely due to possible cytotoxic or non-m^{6}A related effects from c3Ado the next approach sought to knock down specific essential proteins in the m^{6}A process.

shRNA knockdown of m^{6}A machinery proteins: METTL3, FTO, and WTAP was performed in two human cell lines. In Huh7 cells, which were knocked down for WTAP there was a significant decrease in viral replication. Suggesting that the reduction in m^{6}A within the cell, on either host or viral transcripts, inhibits CHIKV replication. This could be down to methylation of host transcripts changing with viral infection (like for ZIKV or KSHV) or direct methylation of the CHIKV RNA genome (like for EVA71 and ZIKV). For the RD cell line there was no detectable effect of either c3Ado or FTO knockdown on CHIKV sub genomic or viral replication. This cell type variability for the role of m^{6}A in viral replication was similar for EVA71. Hao *et al.* saw a significant proviral role for m^{6}A in Vero cells; there was decreased viral titre in Vero cells knocked down for the m^{6}A reader proteins YTHDF2 and YTHDF3[159]. Suggesting a proviral relationship between these proteins and EVA71. However, when they attempted knockdowns of YTHDF1, YTHDF2, and YTHDF3 in RD cells they did not see that same effect, but rather the inverse[159]. In YTHDF1-3 knockdown RD cells there was an increase in EV71 replication, showing that there is cell type variation for m^{6}A and EV71[159]. For CHIKV there were differences between Huh7 cells and RD cells. Further work in cultured human primary or for ease and accessibility a RAW.264.7 murine monocyte/macrophage tissue culture system could be used in future assays to look at m^{6}A methylation and CHIKV replication in other cells targeted in natural infection [203],[236].

Further experiments investigating m^{6}A reduction by combining MeRIP with qRT-PCR of known methylated transcripts or northern blot of isolated RNA stained with an m^{6}A specific-antibody could help to establish that there is overall m^{6}A knockdown with c3Ado treatment or WTAP knockdown in these

systems. Use of a non-antibody based detection method like DART-seq or nanopore detection of known methylated transcripts, like SLC, from c3Ado treated and untreated cells or WTAP knockdown versus scramble knockdown cells could also help show this. However, c3Ado is an established drug in the study of m^6A methylation and the concentrations used were consistent with published literature. In addition, WTAP is an essential protein in the m^6A methyltransferase complex and its knockdown has been linked to reduced m^6A.

To determine if m^6A sites within the CHIKV genome could be detected by MeRIP. This would identify m^6A methylation within regions of the CHIKV genome and m^6A methylation of host transcripts. Firstly, potential m^6A sites in the CHIKV genome were predicted *in silico* using the SRAMP tool, which determined there were 35 predicted m^6A sites throughout the genome. These included one potential m^6A site at the 5' end of the genome 20 nts into the nsP1 coding region at position 96^A and another potential m^6A site in the 3' UTR at position 11749^A. The potential m^6A site at 96^A was consistent with the results from Kim *et al.* 2020 and was in an area of important regulatory function according to Kendall *et al.* and Madden et al [30,227].

The step-by-step optimization of MeRIP on CHIKV infected Huh7 cell RNAs was detailed. Poly(A) selection enriched CHIKV RNA and was incorporated into the workflow to isolate only CHIKV RNA and host mRNA. Ultimately, the possible issue in the MeRIP workflow could be narrowed down to addition of fragmentation of the RNA. This appeared to impact the ability for even positive control primers (SLC) to recognize the correct species in the qRT-PCR. However, MeRIP of both total and poly (A) selected non-fragmented RNA appeared to show SLC enrichment, which suggested that the MeRIP was working as intended. Similarly, non-fragmented CHIKV RNA was also shown to be enriched in these samples which suggested that the CHIKV genome was m^6A methylated.

Chapter 4 aimed to determine the role of two *in silico* predicted m^6A sites within the CHIKV RNA genome, 96^A and 11749^A. Site-directed mutagenesis of sites $96^{A>G}$ and $11749^{A>G}$ was performed. Mutating the A>G prevented m^6A methylation because m^6A requires a nitrogen at the 6 position where G

has an oxygen instead. This mutagenesis was done in both the infectious virus clone (ICRES) and the CHIKV *trans* replicon assay. In Huh7 cells the $96^{A>G}$ ICRES had significantly reduced released viral titre after 24 hours, with rapid reversion back to the wild type 96^{A}, as assessed by NGS. In C636 cells the $96^{A>G}$ ICRES prevented rescue of CHIKV 24 hours after transfection with the mutant ICRES RNA. This suggested that the specific 96^{A} site was important for viral replication in both a human and mosquito tissue culture systems. A second potential m^6A site mutant $11749^{A>G}$ ICRES was transfected into Huh7 cells and it was found that this mutant replicated to the same levels as wild type ICRES 24 hours after transfection. Viral RNA extracted from cells transfected with $11749^{A>G}$ ICRES could not be sequenced in the 3'UTR region. The workflow established in the lab only had primers available for the 5' region so reversion in those transfected cells could not be assessed. However, because the $11749^{A>G}$ ICRES and wild type ICRES replicated to the same levels, it suggested that 11749^{A} was not methylated.

Taken together the infectious CHIKV virus and *trans* replicon work in Huh7 cells suggests a pro-viral role for 96^{A} during CHIKV replication. If this is due to m^6A at that position it would be a similar pattern as seen for EV71 in Vero cells. However, the presence specifically of m^6A methylation at 96 could not be confirmed by the methods used and trialled here. Perhaps the c3Ado and WTAP knockdown work in Huh7 cells suggested that the lack of m^6A methylation at position 96 could be playing a part in negatively impacting viral replication through specifically reduced viral RNA replication. However, that cannot be confirmed all that can be said is that 96^{A} appears important for CHIKV replication. In support of the use of mutagenesis after initial detection to investigate m^6A sites, Hao *et al.* also performed mutagenesis of two sites in the helicase (3C) and the viral envelope protein (VP1) encoding regions of EV71, which they had confirmed as m^6A sites by MeRIP-seq and primer extension analysis, and found that their mutation led to a decrease in EV71 viral titre[159].

Although m^6Am was not specifically addressed in the mutagenesis conducted in this project, work by Zhang *et al.* (2022) investigated mutation of the 1^{A} position of the CHIKV RNA. When this site was modified they

observed decreased genomic and sub genomic RNA replication, which they attributed to necessary sequence specific recognition of the nsP1 protein to perform its capping process[36]. They used the *trans* replicon system outlined in Figure 32. However, their work showed the importance of 1^A to overall vRNA transcription and did not rule out the possibility of methylation at that site elsewhere in lifecycle of the viral RNA. By pairing this with methods of m^6A detection the chemistry of 1^A and possible m^6Am of the CHIKV genome could be further elucidated.

Together the work detailed in this thesis is consistent with the importance of three things to CHIKV replication in the cell. These three things are, firstly, the m^6A reaction methyl donor SAM, secondly a protein (WTAP) involved in m^6A methylation reaction, and thirdly a predicted m^6A site at position 96 in the viral genome to CHIKV replication in both Huh7 and C636 cells. This points to a potential functional role for m^6A methylation in CHIKV RNA replication in both its human and mosquito hosts. Understanding how the CHIKV RNA is treated in the cell and the dynamic changes to structure through modification has implications for designing therapeutics and effective vaccines.

List of References

1. Kariithi, H. M. *et al.* ICTV Virus Taxonomy Profile: Hytrosaviridae. *J. Gen. Virol.* **100**, 1271–1272 (2019).
2. Honório, N. A., Wiggins, K., Câmara, D. C. P., Eastmond, B. & Alto, B. W. Chikungunya virus vector competency of Brazilian and Florida mosquito vectors. *PLoS Negl. Trop. Dis.* **12**, (2018).
3. Simon, F., Savini, H. & Parola, P. Chikungunya: A Paradigm of Emergence and Globalization of Vector-Borne Diseases. *Medical Clinics of North America* vol. 92 1323–1343 (2008).
4. Gudo, E. S., Black, J. F. P. & Cliff, J. L. Chikungunya in Mozambique: A Forgotten History. *PLoS Negl. Trop. Dis.* **10**, (2016).
5. Knipe, D.M., and Howley, P. M. Fields' Virology - Sixth Edition. in *Lippincott Williams & Wilkins* (2013). doi:9781451105636.
6. Mahalingam, S., Tharmarajah, K. & Zaid, A. Chikungunya: Vaccines and therapeutics. *F1000Research* **6**, (2017).
7. Valneva Austria Gmbh. *IXCHIQ (Chikungunya Vaccine, Live) Solution for Intramuscular Injection*. *Valneva Austria Gmbh* (2023).
8. David C. Kaslow. BLA for Chikungunya Vaccine, Live, BL 125777/0. 1–2 (2023).
9. Powers, A. M. & Logue, C. H. Changing patterns of chikunya virus: Re-emergence of a zoonotic arbovirus. *Journal of General Virology* vol. 88 2363–2377 (2007).
10. Lumsden, W. H. R. An epidemic of virus disease in Southern Province, Tanganyika territory, in 1952–1953 II. General description and epidemiology. *Trans. R. Soc. Trop. Med. Hyg.* **49**, 33–57 (1955).
11. Kuno, G. A Re-Examination of the History of Etiologic Confusion between Dengue and Chikungunya. *PLoS Neglected Tropical Diseases* vol. 9 (2015).
12. Volk, S. M. *et al.* Genome-Scale Phylogenetic Analyses of Chikungunya Virus Reveal Independent Emergences of Recent Epidemics and Various Evolutionary Rates. *J. Virol.* **84**, 6497–6504 (2010).
13. Thiboutot, M. M. *et al.* Chikungunya: A potentially emerging epidemic? *PLoS Neglected Tropical Diseases* vol. 4 (2010).
14. Madariaga, M., Ticona, E. & Resurrecion, C. Chikungunya: Bending over the Americas and the rest of the world. *Brazilian Journal of Infectious Diseases* vol. 20 91–98 (2016).
15. Diallo, D. *et al.* Landscape ecology of sylvatic chikungunya virus and mosquito vectors in southeastern senegal. *PLoS Negl. Trop. Dis.* **6**, (2012).
16. Weaver, S. C. & Forrester, N. L. Chikungunya: Evolutionary history and recent epidemic spread. *Antiviral Research* vol. 120 32–39 (2015).

17. Cherian, S. S. *et al.* Evolutionary rates and timescale comparison of Chikungunya viruses inferred from the whole genome/E1 gene with special reference to the 2005-07 outbreak in the Indian subcontinent. *Infect. Genet. Evol.* **9**, 16–23 (2009).

18. Paupy, C., Delatte, H., Bagny, L., Corbel, V. & Fontenille, D. Aedes albopictus, an arbovirus vector: From the darkness to the light. *Microbes Infect.* **11**, 1177–1185 (2009).

19. Sukhralia, S. *et al.* From dengue to Zika: the wide spread of mosquito-borne arboviruses. *European Journal of Clinical Microbiology and Infectious Diseases* vol. 38 3–14 (2019).

20. CDC, C. for D. C. and P. Areas at Risk for Chikungunya. 1 https://www.cdc.gov/chikungunya/geo/index.html (2022).

21. Bettis, A. A. *et al.* The global epidemiology of chikungunya from 1999 to 2020: A systematic literature review to inform the development and introduction of vaccines. *PLoS Negl. Trop. Dis.* **16**, (2022).

22. Kaur, M. *et al.* Coinfection of chikungunya and dengue viruses: A serological study from North Western region of Punjab, India. *J. Lab. Physicians* **10**, 443–447 (2018).

23. Prudhomme, J. *et al.* The native European Aedes geniculatus mosquito species can transmit chikungunya virus. *Emerg. Microbes Infect.* **8**, 962–972 (2019).

24. Strauss, J. H. & Strauss, E. G. The alphaviruses: Gene expression, replication, and evolution. *Microbiological Reviews* vol. 58 491–562 (1994).

25. Chmielewski, D., Schmid, M. F., Simmons, G., Jin, J. & Chiu, W. Chikungunya virus assembly and budding visualized in situ using cryogenic electron tomography. *Nat. Microbiol.* (2022) doi:10.1038/s41564-022-01164-2.

26. Hulo, C. *et al.* ViralZone: A knowledge resource to understand virus diversity. *Nucleic Acids Res.* (2011) doi:10.1093/nar/gkq901.

27. Mendes, A. & Kuhn, R. J. Alphavirus nucleocapsid packaging and assembly. *Viruses* vol. 10 (2018).

28. Solignat, M., Gay, B., Higgs, S., Briant, L. & Devaux, C. Replication cycle of chikungunya: A re-emerging arbovirus. *Virology* vol. 393 183–197 (2009).

29. Kendra, J. A. *et al.* Functional and structural characterization of the chikungunya virus translational recoding signals. *J. Biol. Chem.* **293**, 17536–17545 (2018).

30. Kendall, C. *et al.* Structural and phenotypic analysis of Chikungunya virus RNA replication elements. *Nucleic Acids Res.* **47**, 9296–9312 (2019).

31. An, W., Ge, N., Cao, Y., Sun, J. & Jin, X. Recent progress on chikungunya virus research. *Virologica Sinica* vol. 32 441–453 (2017).

32. Jones, R., Bragagnolo, G., Arranz, R. & Reguera, J. Capping pores of

alphavirus nsP1 gate membranous viral replication factories. *Nature* **589**, 615–619 (2021).

33. Zhang, K. *et al.* Structural insights into viral RNA capping and plasma membrane targeting by Chikungunya virus nonstructural protein 1. *Cell Host Microbe* **29**, 757-764.e3 (2021).
34. Powers, A. M. *et al.* Evolutionary Relationships and Systematics of the Alphaviruses. *J. Virol.* **75**, 10118–10131 (2001).
35. Kallio, K., Hellström, K., Jokitalo, E. & Ahola, T. RNA Replication and Membrane Modification Require the Same Functions of Alphavirus Nonstructural Proteins. *J. Virol.* **90**, 1687–1692 (2016).
36. Zhang, K. *et al.* Molecular basis of specific viral RNA recognition and 5′-end capping by the Chikungunya virus nsP1. *Cell Rep.* **40**, 111133 (2022).
37. Rupp, J. C., Sokoloski, K. J., Gebhart, N. N. & Hardy, R. W. Alphavirus RNA synthesis and non-structural protein functions. *J. Gen. Virol.* **96**, 2483–2500 (2015).
38. Li, C. *et al.* mRNA Capping by Venezuelan Equine Encephalitis Virus nsP1: Functional Characterization and Implications for Antiviral Research. *J. Virol.* **89**, 8292–8303 (2015).
39. Mi, S., Durbin, R., Huang, H. V., Rice, C. M. & Stollar, V. Association of the sindbis virus RNA methyltransferase activity with the nonstructural protein nsP1. *Virology* **170**, 385–391 (1989).
40. Laurent, T. *et al.* Architecture of the chikungunya virus replication organelle. *Elife* **11**, 1–25 (2022).
41. Tan, Y. B. *et al.* Molecular architecture of the Chikungunya virus replication complex. *Sci. Adv.* **8**, 2022.04.08.487651 (2022).
42. Law, Y. S. *et al.* Structural insights into RNA recognition by the Chikungunya virus nsP2 helicase. *Proc. Natl. Acad. Sci. U. S. A.* **116**, 9558–9567 (2019).
43. Akhrymuk, I., Kulemzin, S. V. & Frolova, E. I. Evasion of the Innate Immune Response: the Old World Alphavirus nsP2 Protein Induces Rapid Degradation of Rpb1, a Catalytic Subunit of RNA Polymerase II. *J. Virol.* **86**, 7180–7191 (2012).
44. Göertz, G. P. *et al.* The Methyltransferase-Like Domain of Chikungunya Virus nsP2 Inhibits the Interferon Response by Promoting the Nuclear Export of STAT1. *J. Virol.* **92**, (2018).
45. Fros, J. J. *et al.* Chikungunya Virus Nonstructural Protein 2 Inhibits Type I/II Interferon-Stimulated JAK-STAT Signaling. *J. Virol.* **84**, 10877–10887 (2010).
46. Götte, B., Liu, L. & McInerney, G. M. The enigmatic alphavirus non-structural protein 3 (nsP3) revealing its secrets at last. *Viruses* (2018) doi:10.3390/v10030105.
47. Lello, L. S. *et al.* nsP4 Is a Major Determinant of Alphavirus Replicase Activity and Template Selectivity. *J. Virol.* **95**, (2021).

48. Zhang, X., Fugère, M., Day, R. & Kielian, M. Furin Processing and Proteolytic Activation of Semliki Forest Virus. *J. Virol.* **77**, 2981–2989 (2003).

49. Cho, B. *et al.* Expression and evaluation of Chikungunya virus E1 and E2 envelope proteins for serodiagnosis of chikungunya virus infection. *Yonsei Med. J.* **49**, 828–835 (2008).

50. Metz, S. W. *et al.* Functional processing and secretion of Chikungunya virus E1 and E2 glycoproteins in insect cells. *Virol. J.* **8**, (2011).

51. Scott, C. & Griffin, S. Viroporins: Structure, function and potential as antiviral targets. *Journal of General Virology* vol. 96 2000–2027 (2015).

52. Nieva, J. L., Madan, V. & Carrasco, L. Viroporins: Structure and biological functions. *Nature Reviews Microbiology* vol. 10 563–574 (2012).

53. Firth, A. E., Chung, B. Y. W., Fleeton, M. N. & Atkins, J. F. Discovery of frameshifting in Alphavirus 6K resolves a 20-year enigma. *Virol. J.* **5**, (2008).

54. Gaedigk-Nitschko, K. & Schlesinger, M. J. The sindbis virus 6K protein can be detected in virions and is acylated with fatty acids. *Virology* **175**, 274–281 (1990).

55. Snyder, J. E. *et al.* Functional Characterization of the Alphavirus TF Protein. *J. Virol.* **87**, 8511–8523 (2013).

56. Melton, J. V. *et al.* Alphavirus 6K proteins form ion channels. *J. Biol. Chem.* **277**, 46923–46931 (2002).

57. Sanz, M. A., Madan, V., Carrasco, L. & Nieva, J. L. Interfacial domains in sindbis virus 6K protein: Detection and functional characterization. *J. Biol. Chem.* **278**, 2051–2057 (2003).

58. *Viral Membrane Proteins: Structure, Function, and Drug Design*. *Viral Membrane Proteins: Structure, Function, and Drug Design* (2005). doi:10.1007/0-387-28146-0.

59. Schnierle, B. S. Cellular attachment and entry factors for chikungunya virus. *Viruses* vol. 11 (2019).

60. Thal, M. A., Wasik, B. R., Posto, J. & Hardy, R. W. Template requirements for recognition and copying by Sindbis virus RNA-dependent RNA polymerase. *Virology* (2007) doi:10.1016/j.virol.2006.08.022.

61. Fros, J. J. & Pijlman, G. P. Alphavirus infection: Host cell shut-off and inhibition of antiviral responses. *Viruses* vol. 8 (2016).

62. Laurent, T. & Carlson, L.-A. The organization of double-stranded RNA in the chikungunya virus replication organelle. *PLoS Negl. Trop. Dis.* **17**, e0011404 (2023).

63. Gantier, M. P. & Williams, B. R. G. The response of mammalian cells to double-stranded RNA. *Cytokine Growth Factor Rev.* **18**, 363–371 (2007).

64. Liu, J. & McFadden, G. SAMD9 Is an Innate Antiviral Host Factor with Stress Response Properties That Can Be Antagonized by Poxviruses. *J. Virol.* **89**, 1925–1931 (2015).

65. Dhir, A. *et al.* Mitochondrial double-stranded RNA triggers antiviral signalling in humans. *Nature* **560**, 238–242 (2018).

66. Kendall, C. *et al.* Structural and phenotypic analysis of Chikungunya virus RNA replication elements. *Nucleic Acids Res.* **47**, 9296–9312 (2019).

67. Madden, E. A. *et al.* Using SHAPE-MaP To Model RNA Secondary Structure and Identify 3′UTR Variation in Chikungunya Virus. *J. Virol.* (2020) doi:10.1128/jvi.00701-20.

68. Wilkinson, K. A., Merino, E. J. & Weeks, K. M. Selective 2′-hydroxyl acylation analyzed by primer extension (SHAPE): Quantitative RNA structure analysis at single nucleotide resolution. *Nat. Protoc.* **1**, 1610–1616 (2006).

69. Spitale, R. C., Flynn, R. A., Torre, E. A., Kool, E. T. & Chang, H. Y. RNA structural analysis by evolving SHAPE chemistry. *Wiley interdisciplinary reviews. RNA* vol. 5 867–881 (2014).

70. McGinnis, J. L., Dunkle, J. A., Cate, J. H. D. & Weeks, K. M. The mechanisms of RNA SHAPE chemistry. *J. Am. Chem. Soc.* **134**, 6617–6624 (2012).

71. Prosser, O., Stonehouse, N. J. & Tuplin, A. Inhibition of Chikungunya virus genome replication by targeting essential RNA structures within the virus genome. *Antiviral Res.* **211**, 105523 (2023).

72. Kutchko, K. M. *et al.* Structural divergence creates new functional features in alphavirus genomes. *Nucleic Acids Res.* **46**, 3657–3670 (2018).

73. Quek, X. C. *et al.* lncRNAdb v2.0: Expanding the reference database for functional long noncoding RNAs. *Nucleic Acids Res.* **43**, D168–D173 (2015).

74. Turowski, T. W. & Boguta, M. Specific Features of RNA Polymerases I and III: Structure and Assembly. *Frontiers in Molecular Biosciences* vol. 8 (2021).

75. Clancy, S. RNA splicing: introns, exons and spliceosome. *Nat. Educ.* **1**, 3–6 (2008).

76. Roundtree, I. A., Evans, M. E., Pan, T. & He, C. Dynamic RNA Modifications in Gene Expression Regulation. *Cell* vol. 169 1187–1200 (2017).

77. Ramanathan, A., Robb, G. B. & Chan, S. H. mRNA capping: Biological functions and applications. *Nucleic Acids Research* vol. 44 7511–7526 (2016).

78. Daffis, S. *et al.* 2′-O methylation of the viral mRNA cap evades host restriction by IFIT family members. *Nature* **468**, 452–456 (2010).

79. Jonkhout, N. *et al.* The RNA modification landscape in human disease.

Rna vol. 23 1754–1769 (2017).

80. Niu, Y. *et al.* N6-methyl-adenosine (m6A) in RNA: An Old Modification with A Novel Epigenetic Function. *Genomics, Proteomics and Bioinformatics* vol. 11 8–17 (2013).

81. Perry, R. P. & Kelley, D. E. Existence of methylated messenger RNA in mouse L cells. *Cell* **1**, 37–42 (1974).

82. Desrosiers, R., Friderici, K. & Rottman, F. Identification of methylated nucleosides in messenger RNA from Novikoff hepatoma cells. *Proc. Natl. Acad. Sci. U. S. A.* **71**, 3971–3975 (1974).

83. Manners, O., Baquero-Perez, B. & Whitehouse, A. m 6 A: Widespread regulatory control in virus replication. *Biochimica et Biophysica Acta - Gene Regulatory Mechanisms* vol. 1862 370–381 (2019).

84. Bokar, J. A., Rath-Shambaugh, M. E., Ludwiczak, R., Narayan, P. & Rottman, F. Characterization and partial purification of mRNA N6-adenosine methyltransferase from HeLa cell nuclei. Internal mRNA methylation requires a multisubunit complex. *J. Biol. Chem.* **269**, 17697–17704 (1994).

85. Wang, X. *et al.* Structural basis of N6-adenosine methylation by the METTL3-METTL14 complex. *Nature* **534**, 575–578 (2016).

86. Schöller, E. *et al.* Interactions, localization, and phosphorylation of the m6A generating METTL3–METTL14–WTAP complex. *Rna* **24**, 499–512 (2018).

87. Dominissini, D. *et al.* Topology of the human and mouse m6A RNA methylomes revealed by m6A-seq. *Nature* **485**, 201–206 (2012).

88. Meyer, K. D. *et al.* Comprehensive analysis of mRNA methylation reveals enrichment in 3′ UTRs and near stop codons. *Cell* **149**, 1635–1646 (2012).

89. Linder, B. *et al.* Single-nucleotide-resolution mapping of m6A and m6Am throughout the transcriptome. *Nat. Methods* **12**, 767–772 (2015).

90. Ke, S. *et al.* A majority of m6A residues are in the last exons, allowing the potential for 3' UTR regulation. *Genes Dev.* **29**, 2037–2053 (2015).

91. Uzonyi, A. *et al.* Exclusion of m6A from splice-site proximal regions by the exon junction complex dictates m6A topologies and mRNA stability. *Mol. Cell* (2023) doi:10.1016/j.molcel.2022.12.026.

92. Bokar, J. A., Shambaugh, M. E., Polayes, D., Matera, A. G. & Rottman, F. M. Purification and cDNA cloning of the AdoMet-binding subunit of the human mRNA (N6-adenosine)-methyltransferase. *Rna* **3**, 1233–1247 (1997).

93. Oerum, S., Meynier, V., Catala, M. & Tisne, C. A comprehensive review of m6A/m6Am RNA methyltransferase structures. *Nucleic Acids Research* (2021) doi:10.1093/nar/gkab378.

94. Warda, A. S. *et al.* Human METTL16 is a N 6 -methyladenosine (m 6 A) methyltransferase that targets pre-mRNAs and various non-coding

RNAs . *EMBO Rep.* **18**, 2004–2014 (2017).

95. Ping, X. L. *et al.* Mammalian WTAP is a regulatory subunit of the RNA N6-methyladenosine methyltransferase. *Cell Res.* **24**, 177–189 (2014).
96. Garcias Morales, D. & Reyes, J. L. A birds'-eye view of the activity and specificity of the mRNA m6A methyltransferase complex. *Wiley Interdiscip. Rev. RNA* **12**, (2021).
97. Schwartz, S. *et al.* Perturbation of m6A writers reveals two distinct classes of mRNA methylation at internal and 5' sites. *Cell Rep.* **8**, 284–296 (2014).
98. Liu, J. *et al.* VIRMA mediates preferential m6A mRNA methylation in 3′UTR and near stop codon and associates with alternative polyadenylation. *Cell Discov.* **4**, (2018).
99. Patil, D. P. *et al.* M6 A RNA methylation promotes XIST-mediated transcriptional repression. *Nature* **537**, 369–373 (2016).
100. Lan, T. *et al.* KIAA1429 contributes to liver cancer progression through N6-methyladenosine-dependent post-transcriptional modification of GATA3. *Mol. Cancer* **18**, (2019).
101. Meng, Y. *et al.* RBM15-mediated N6-methyladenosine modification affects COVID-19 severity by regulating the expression of multitarget genes. *Cell Death Dis.* **12**, (2021).
102. Jia, G. *et al.* N6-Methyladenosine in nuclear RNA is a major substrate of the obesity-associated FTO. *Nat. Chem. Biol.* **7**, 885–887 (2011).
103. Zheng, G. *et al.* ALKBH5 Is a Mammalian RNA Demethylase that Impacts RNA Metabolism and Mouse Fertility. *Mol. Cell* **49**, 18–29 (2013).
104. Wei, J. *et al.* Differential m 6 A, m 6 A m , and m 1 A Demethylation Mediated by FTO in the Cell Nucleus and Cytoplasm. *Mol. Cell* **71**, 973-985.e5 (2018).
105. Meyer, K. D. *et al.* 5′ UTR m6A Promotes Cap-Independent Translation. *Cell* **163**, 999–1010 (2015).
106. Coots, R. A. *et al.* m6A Facilitates eIF4F-Independent mRNA Translation. *Mol. Cell* **68**, 504-514.e7 (2017).
107. Mauer, J. *et al.* Reversible methylation of m6 Am in the 5′ cap controls mRNA stability. *Nature* **541**, 371–375 (2017).
108. Cowling, V. H. CAPAM: The mRNA Cap Adenosine N6-Methyltransferase. *Trends Biochem. Sci.* **44**, 183–185 (2019).
109. Engel, M. *et al.* The Role of m6A/m-RNA Methylation in Stress Response Regulation. *Neuron* **99**, 389-403.e9 (2018).
110. Mauer, J. *et al.* Reversible methylation of m6 Am in the 5′ cap controls mRNA stability. *Nature* (2017) doi:10.1038/nature21022.
111. Jiang, X. *et al.* The role of m6A modification in the biological functions and diseases. *Signal Transduction and Targeted Therapy* vol. 6 (2021).

112. Harper, J. E., Miceli, S. M., Roberts, R. J. & Manley, J. L. Sequence specificity of the human mRNA N6-adenosine methylase in vitro. *Nucleic Acids Res.* **18**, 5735–5741 (1990).

113. Chen, T. *et al.* M6A RNA methylation is regulated by microRNAs and promotes reprogramming to pluripotency. *Cell Stem Cell* **16**, 289–301 (2015).

114. Lin, S., Choe, J., Du, P., Triboulet, R. & Gregory, R. I. The m6A Methyltransferase METTL3 Promotes Translation in Human Cancer Cells. *Mol. Cell* **62**, 335–345 (2016).

115. Gokhale, N. S. *et al.* Altered m6A Modification of Specific Cellular Transcripts Affects Flaviviridae Infection. *Mol. Cell* **77**, 542-555.e8 (2020).

116. Gokhale, N. S. *et al.* N6-Methyladenosine in Flaviviridae Viral RNA Genomes Regulates Infection. *Cell Host Microbe* **20**, 654–665 (2016).

117. Lichinchi, G. *et al.* Dynamics of Human and Viral RNA Methylation during Zika Virus Infection. *Cell Host Microbe* **20**, 666–673 (2016).

118. Liu, N. *et al.* N6-methyladenosine alters RNA structure to regulate binding of a low-complexity protein. *Nucleic Acids Res.* **45**, 6051–6063 (2017).

119. Haussmann, I. U. *et al.* M6 A potentiates Sxl alternative pre-mRNA splicing for robust Drosophila sex determination. *Nature* **540**, 301–304 (2016).

120. Xiao, W. *et al.* Nuclear m6A Reader YTHDC1 Regulates mRNA Splicing. *Mol. Cell* **61**, 507–519 (2016).

121. Wang, X. *et al.* N 6-methyladenosine-dependent regulation of messenger RNA stability. *Nature* **505**, 117–120 (2014).

122. Ke, S. *et al.* m6A mRNA modifications are deposited in nascent pre-mRNA and are not required for splicing but do specify cytoplasmic turnover. *Genes Dev.* **31**, 990–1006 (2017).

123. Liao, S., Sun, H. & Xu, C. YTH Domain: A Family of N6-methyladenosine (m6A) Readers. *Genomics, Proteomics and Bioinformatics* vol. 16 99–107 (2018).

124. Röder, K., Barker, A. M., Whitehouse, A. & Pasquali, S. Investigating the structural changes due to adenosine methylation of the Kaposi's sarcoma-associated herpes virus ORF50 transcript. *PLoS Comput. Biol.* **18**, 1–18 (2022).

125. Xiao Wang, A. *et al.* Human YTHDF1 binds m 6 A-modified mRNAs and through interactions with initiation factors and ribosomes increases translational output from those messages. -methyladenosine Modulates Messenger RNA Translation Efficiency. *Cell* **161**, 1388–1399 (2015).

126. Zong, X. *et al.* The N6-methyladenosine RNA-binding protein YTHDF1 modulates the translation of TRAF6 to mediate the intestinal immune response. *Nucleic Acids Res.* **49**, 5537–5552 (2021).

127. Baquero-Perez, B. *et al.* The tudor SND1 protein is an m6a RNA reader essential for replication of kaposi's sarcoma-associated herpesvirus. *Elife* **8**, (2019).

128. Zhao, Y., Shi, Y., Shen, H. & Xie, W. M6A-binding proteins: The emerging crucial performers in epigenetics. *Journal of Hematology and Oncology* vol. 13 (2020).

129. Wu, B. *et al.* Molecular basis for the specific and multivariant recognitions of RNA substrates by human hnRNP A2/B1. *Nat. Commun.* **9**, (2018).

130. Roost, C. *et al.* Structure and thermodynamics of N6-methyladenosine in RNA: A spring-loaded base modification. *J. Am. Chem. Soc.* **137**, 2107–2115 (2015).

131. Bell, J. L. *et al.* Insulin-like growth factor 2 mRNA-binding proteins (IGF2BPs): Post-transcriptional drivers of cancer progression? *Cellular and Molecular Life Sciences* vol. 70 2657–2675 (2013).

132. Huang, H. *et al.* Recognition of RNA N 6 -methyladenosine by IGF2BP proteins enhances mRNA stability and translation. *Nat. Cell Biol.* **20**, 285–295 (2018).

133. Hu, X. *et al.* IGF2BP2 regulates DANCR by serving as an N6-methyladenosine reader. *Cell Death Differ.* **27**, 1782–1794 (2020).

134. Huang, H. *et al.* Publisher Correction: Recognition of RNA N 6-methyladenosine by IGF2BP proteins enhances mRNA stability and translation (Nature Cell Biology, (2018), 20, 3, (285-295), 10.1038/s41556-018-0045-z). *Nat. Cell Biol.* **22**, 1288 (2020).

135. Zaccara, S. & Jaffrey, S. R. A Unified Model for the Function of YTHDF Proteins in Regulating m6A-Modified mRNA. *Cell* **181**, 1582-1595.e18 (2020).

136. Patil, D. P., Pickering, B. F. & Jaffrey, S. R. Reading m6A in the Transcriptome: m6A-Binding Proteins. *Trends in Cell Biology* (2018) doi:10.1016/j.tcb.2017.10.001.

137. Zaccara, S., Ries, R. J. & Jaffrey, S. R. Reading, writing and erasing mRNA methylation. *Nature Reviews Molecular Cell Biology* vol. 20 608–624 (2019).

138. McIntyre, W. *et al.* Positive-sense RNA viruses reveal the complexity and dynamics of the cellular and viral epitranscriptomes during infection. *Nucleic Acids Res.* **46**, 5776–5791 (2018).

139. Liu, C. *et al.* Absolute quantification of single-base m6A methylation in the mammalian transcriptome using GLORI. *Nat. Biotechnol.* (2023) doi:10.1038/s41587-022-01487-9.

140. Kim, B. *et al.* Discovery of Widespread Host Protein Interactions with the Pre-replicated Genome of CHIKV Using VIR-CLASP. *Mol. Cell* (2020) doi:10.1016/j.molcel.2020.04.013.

141. Moore, C. B., Guthrie, E. H., Huang, M. T. H. & Taxman, D. J. Short hairpin RNA (shRNA): design, delivery, and assessment of gene knockdown. *Methods Mol. Biol.* **629**, 141–158 (2010).

142. Meyer, K. D. DART-seq: an antibody-free method for global m6A detection. *Nat. Methods* **16**, 1275–1280 (2019).

143. Xiao, Y. L. *et al.* Transcriptome-wide profiling and quantification of N 6-methyladenosine by enzyme-assisted adenosine deamination. *Nat. Biotechnol.* (2023) doi:10.1038/s41587-022-01587-6.

144. Tegowski, M., Flamand, M. N. & Meyer, K. D. scDART-seq reveals distinct m6A signatures and mRNA methylation heterogeneity in single cells. *Mol. Cell* **82**, 868-878.e10 (2022).

145. Parker, M. T. *et al.* Nanopore direct RNA sequencing maps the complexity of arabidopsis mRNA processing and m6A modification. *Elife* **9**, (2020).

146. Liu, H. *et al.* Accurate detection of m6A RNA modifications in native RNA sequences. *Nat. Commun.* **10**, (2019).

147. Price, A. M. *et al.* Direct RNA sequencing reveals m6A modifications on adenovirus RNA are necessary for efficient splicing. *Nat. Commun.* **11**, (2020).

148. Deamer, D., Akeson, M. & Branton, D. Three decades of nanopore sequencing. *Nature Biotechnology* vol. 34 518–524 (2016).

149. Jain, M., Olsen, H. E., Paten, B. & Akeson, M. The Oxford Nanopore MinION: Delivery of nanopore sequencing to the genomics community. *Genome Biol.* **17**, (2016).

150. Lorenz, D. A., Sathe, S., Einstein, J. M. & Yeo, G. W. Direct RNA sequencing enables m6A detection in endogenous transcript isoforms at base-specific resolution. *Rna* **26**, 19–28 (2020).

151. Wang, Y. *et al.* Identification of nucleoside monophosphates and their epigenetic modifications using an engineered nanopore. *Nat. Nanotechnol.* (2022) doi:10.1038/s41565-022-01169-2.

152. Kan, L. *et al.* The m 6 A pathway facilitates sex determination in Drosophila. *Nat. Commun.* **8**, (2017).

153. Liu, C., Cao, J., Zhang, H., Wu, J. & Yin, J. Profiling of Transcriptome-Wide N6-Methyladenosine (m6A) Modifications and Identifying m6A Associated Regulation in Sperm Tail Formation in Anopheles sinensis. *Int. J. Mol. Sci.* **23**, (2022).

154. Dai, Z., Etebari, K. & Asgari, S. N6-methyladenosine modification of the Aedes aegypti transcriptome and its alteration upon dengue virus infection in Aag2 cell line. *Commun. Biol.* **5**, 1–13 (2022).

155. Baquero-Perez, B., Geers, D. & Díez, J. From a to m6a: The emerging viral epitranscriptome. *Viruses* vol. 13 (2021).

156. Kim, B. *et al.* Discovery of Widespread Host Protein Interactions with the Pre-replicated Genome of CHIKV Using VIR-CLASP. *Mol. Cell* **78**, 624-640.e7 (2020).

157. Liu, J. *et al.* The m6A methylome of SARS-CoV-2 in host cells. *Cell Res.* **31**, 404–414 (2021).

158. Campos, J. H. C. *et al.* Direct RNA sequencing reveals SARS-CoV-2

m6A sites and possible differential DRACH motif methylation among variants. *Viruses* (2021) doi:10.3390/v13112108.

159. Hao, H. *et al.* N 6 -methyladenosine modification and METTL3 modulate enterovirus 71 replication. *Nucleic Acids Res.* **47**, 362–374 (2019).
160. Lichinchi, G. *et al.* Dynamics of the human and viral m6A RNA methylomes during HIV-1 infection of T cells. *Nat. Microbiol.* **1**, (2016).
161. Kennedy, E. M. *et al.* Posttranscriptional m6A Editing of HIV-1 mRNAs Enhances Viral Gene Expression. *Cell Host Microbe* **19**, 675–685 (2016).
162. Lu, W. *et al.* N6-Methyladenosine– binding proteins suppress HIV-1 infectivity and viral production. *J. Biol. Chem.* **293**, 12992–13005 (2018).
163. Tirumuru, N. *et al.* N6-methyladenosine of HIV-1 RNA regulates viral infection and HIV-1 Gag protein expression. *Elife* **5**, (2016).
164. Jurczyszak, D. *et al.* HIV protease cleaves the antiviral m6A reader protein YTHDF3 in the viral particle. *PLoS Pathog.* **16**, (2020).
165. Chen, J. *et al.* N6-methyladenosine regulates PEDV replication and host gene expression. *Virology* **548**, 59–72 (2020).
166. Courtney, D. G. *et al.* Epitranscriptomic Enhancement of Influenza A Virus Gene Expression and Replication. *Cell Host Microbe* **22**, 377-386.e5 (2017).
167. Xue, M. *et al.* Viral N 6-methyladenosine upregulates replication and pathogenesis of human respiratory syncytial virus. *Nat. Commun.* **10**, (2019).
168. Lu, M. *et al.* N 6-methyladenosine modification enables viral RNA to escape recognition by RNA sensor RIG-I. *Nat. Microbiol.* **5**, 584–598 (2020).
169. Qiu, W. *et al.* N 6-methyladenosine RNA modification suppresses antiviral innate sensing pathways via reshaping double-stranded RNA. *Nat. Commun.* **12**, (2021).
170. Dimock, K. & Stoltzfus, C. M. Sequence Specificity of Internal Methylation in B77 Avian Sarcoma Virus RNA Subunits. *Biochemistry* (1977) doi:10.1021/bi00622a021.
171. Tsai, K., Courtney, D. G. & Cullen, B. R. Addition of m6A to SV40 late mRNAs enhances viral structural gene expression and replication. *PLoS Pathog.* **14**, (2018).
172. Ye, F., Chen, E. R. & Nilsen, T. W. Kaposi's Sarcoma-Associated Herpesvirus Utilizes and Manipulates RNA N 6 -Adenosine Methylation To Promote Lytic Replication . *J. Virol.* **91**, (2017).
173. Tan, B. *et al.* Viral and cellular N6-methyladenosine and N6,2′-O-dimethyladenosine epitranscriptomes in the KSHV life cycle. *Nat. Microbiol.* **3**, 108–120 (2017).
174. Hesser, C. R., Karijolich, J., Dominissini, D., He, C. & Glaunsinger, B.

A. N6-methyladenosine modification and the YTHDF2 reader protein play cell type specific roles in lytic viral gene expression during Kaposi's sarcoma-associated herpesvirus infection. *PLoS Pathog.* **14**, (2018).

175. Lang, F. *et al.* EBV epitranscriptome reprogramming by METTL14 is critical for viral-associated tumorigenesis. *PLoS Pathog.* **15**, (2019).
176. Xia, T. *et al.* N(6)-methyladenosine-binding protein YTHDF1 suppresses EBV replication and promotes EBV RNA decay. *EMBO Rep.* **22**, (2021).
177. Imam, H. *et al.* N6-methyladenosine modification of hepatitis b virus RNA differentially regulates the viral life cycle. *Proc. Natl. Acad. Sci. U. S. A.* **115**, 8829–8834 (2018).
178. Rubio, R. M., Depledge, D. P., Bianco, C., Thompson, L. & Mohr, I. RNA m 6 A modification enzymes shape innate responses to DNA by regulating interferon β. *Genes Dev.* **32**, 1472–1484 (2018).
179. Winkler, R. *et al.* m 6 A modification controls the innate immune response to infection by targeting type I interferons. *Nat. Immunol.* **20**, 173–182 (2019).
180. T3001, T. Mix & Go E. coli Transformation Kit & Buffer Set. **INSTRUCTIO**, 0–6 (2021).
181. Therme Scientific. Thermo Scientific GeneJET Plasmid Miniprep Kit. *Manual* 1–9 (2014).
182. Müller, M. *et al.* Chikungunya virus requires cellular chloride channels for efficient genome replication. *PLoS Negl. Trop. Dis.* **13**, (2019).
183. PerkinElmer inc. ATPlite : Luminescence ATP Detection Assay system. *Protocol* 1–20 (2015).
184. Vinet, L. & Zhedanov, A. A 'missing' family of classical orthogonal polynomials. *J. Phys. A Math. Theor.* **44**, 11–12 (2011).
185. PCRBiosystems. qPCRBIO SyGreen Mix. 2 (2019).
186. Pohjala, L. *et al.* Inhibitors of alphavirus entry and replication identified with a stable Chikungunya replicon cell line and virus-based assays. *PLoS One* **6**, (2011).
187. Utt, A. *et al.* Design and Use of Chikungunya Virus Replication Templates Utilizing Mammalian and Mosquito RNA Polymerase I-Mediated Transcription. *J. Virol.* **93**, (2019).
188. Zhou, Y., Zeng, P., Li, Y. H., Zhang, Z. & Cui, Q. SRAMP: Prediction of mammalian N6-methyladenosine (m6A) sites based on sequence-derived features. *Nucleic Acids Res.* **44**, (2016).
189. Reuter, J. S. & Mathews, D. H. RNAstructure: Software for RNA secondary structure prediction and analysis. *BMC Bioinformatics* **11**, (2010).
190. Darty, K., Denise, A. & Ponty, Y. VARNA: Interactive drawing and editing of the RNA secondary structure. *Bioinformatics* (2009) doi:10.1093/bioinformatics/btp250.

191. Biolabs, N. E. Protocol for Q5 ® Site-Directed Mutagenesis Kit (E0554). 1–2 (2023).

192. Quick, J. *et al.* Multiplex PCR method for MinION and Illumina sequencing of Zika and other virus genomes directly from clinical samples. *Nat. Protoc.* **12**, 1261–1266 (2017).

193. Ferguson, J. M. *et al.* InterARTIC: An interactive web application for whole-genome nanopore sequencing analysis of SARS-CoV-2 and other viruses. *Bioinformatics* (2022) doi:10.1093/bioinformatics/btab846.

194. Bujnicki, J. M., Feder, M., Radlinska, M. & Blumenthal, R. M. Structure prediction and phylogenetic analysis of a functionally diverse family of proteins homologous to the MT-A70 subunit of the human mRNA:m6A methyltransferase. *J. Mol. Evol.* (2002) doi:10.1007/s00239-002-2339-8.

195. Baquero-Perez, B. *et al.* N 6 -methyladenosine modification is not a general trait of viral RNA genomes Contributing authors : *bioRxiv Prepr.* (2023) doi:10.1101/2023.10.13.56183.

196. Sacco, M. T., Bland, K. M. & Horner, S. M. WTAP Targets the METTL3 m 6 A-Methyltransferase Complex to Cytoplasmic Hepatitis C Virus RNA to Regulate Infection . *J. Virol.* **96**, 1–31 (2022).

197. Taraphdar, D. *et al.* Comodulation of Dengue and Chikungunya Virus Infection During a Coinfection Scenario in Human Cell Lines. *Front. Cell. Infect. Microbiol.* **12**, 1–15 (2022).

198. Troost, B. *et al.* Tomatidine, a natural steroidal alkaloid shows antiviral activity towards chikungunya virus in vitro. *Sci. Rep.* **10**, (2020).

199. NAULITA TURNIP, O. *et al.* Growth Characteristics of Chikungunya Virus Isolate from Indonesia in Various Human Cell Lines in vitro. *Microbiol. Indones.* **13**, 1–8 (2019).

200. Sakaguchi, S., Suzuki, Y., Emi, A., Wu, H. & Nakano, T. Identification of cellular inhibitors against Chikungunya virus replication by a cDNA expression cloning combined with MinION sequencing. *Biochem. Biophys. Res. Commun.* **530**, 617–623 (2020).

201. Lani, R., Teoh, B.-T., Hassandarvish, P., Sam, S.-S. & AbuBakar, S. Fisetin Modulates Toll-Like Receptor-Mediated Innate Antiviral Response in Chikungunya Virus-Infected Hepatocellular Carcinoma Huh7 Cells. *SSRN Electron. J.* 703–719 (2022) doi:10.2139/ssrn.4166520.

202. S.-D., T. *et al.* Chikungunya fever: Epidemiology, clinical syndrome, pathogenesis and therapy. *Antiviral Research* (2013).

203. Labadie, K. *et al.* Chikungunya disease in nonhuman primates involves long-term viral persistence in macrophages. *J. Clin. Invest.* **120**, 894–906 (2010).

204. Soumahoro, M. K. *et al.* Impact of Chikungunya virus infection on health status and quality of life: A retrospective cohort study. *PLoS One* **4**, (2009).

205. Sudeep, A. B., Vyas, P. B., Parashar, D. & Shil, P. Differential susceptibility & replication potential of Vero E6, BHK-21, RD, A-549, C6/36 cells & Aedes aegypti mosquitoes to three strains of chikungunya virus. *Indian J. Med. Res.* **149**, 771–777 (2019).

206. De Clercq, E. Carbocyclic adenosine analogues as S-adenosylhomocysteine hydrolase inhibitors and antiviral agents: Recent advances. *Nucleosides and Nucleotides* vol. 17 625–634 (1998).

207. Smee, D. F., Bray, M. & Huggins, J. W. Intracellular phosphorylation of carbocyclic 3-deazaadenosine, an anti-Ebola virus agent. *Antivir. Chem. Chemother.* **12**, 251–258 (2001).

208. Sedding, D. G. *et al.* 3-Deazaadenosine prevents smooth muscle cell proliferation and neointima formation by interfering with ras signaling. *Circ. Res.* **104**, 1192–1200 (2009).

209. Xu, J. *et al.* m6A methyltransferase METTL3 maintains colon cancer tumorigenicity by suppressing SOCS2 to promote cell proliferation. *Oncol. Rep.* **44**, 973–986 (2020).

210. Fustin, J. M. *et al.* XRNA-methylation-dependent RNA processing controls the speed of the circadian clock. *Cell* **155**, 793 (2013).

211. Mudgal, R., Mahajan, S. & Tomar, S. Inhibition of Chikungunya virus by an adenosine analog targeting the SAM-dependent nsP1 methyltransferase. *FEBS Lett.* **594**, 678–694 (2020).

212. Riss, T. L. *et al. Cell Viability Assays*. *Assay Guidance Manual* (2004).

213. Hongay, C. F. & Orr-Weaver, T. L. Drosophila inducer of MEiosis 4 (IME4) is required for Notch signaling during oogenesis. *Proc. Natl. Acad. Sci. U. S. A.* (2011) doi:10.1073/pnas.1111577108.

214. Ghasemi, M., Turnbull, T., Sebastian, S. & Kempson, I. The mtt assay: Utility, limitations, pitfalls, and interpretation in bulk and single-cell analysis. *Int. J. Mol. Sci.* **22**, (2021).

215. Santana-Román, M. E. *et al.* Monitoring mitochondrial function in Aedes albopictus C6/36 cell line during dengue virus infection. *Insects* **12**, (2021).

216. McIntyre, A. B. R. *et al.* Limits in the detection of m6A changes using MeRIP/m6A-seq. *Sci. Rep.* (2020) doi:10.1038/s41598-020-63355-3.

217. Merk. Magna MeRIP™ m6A Kit Transcriptome-wide Profiling of N6-Methyladenosine. *Merck Pte Ltd*.

218. Ye, F. *et al.* Trans-omics analyses revealed key epigenetic genes associated with overall survival in secondary progressive multiple sclerosis. *J. Neuroimmunol.* **364**, (2022).

219. Guo, W. *et al.* M6A methylation of DEGS2, a key ceramide-synthesizing enzyme, is involved in colorectal cancer progression through ceramide synthesis. *Oncogene* (2021) doi:10.1038/s41388-021-01987-z.

220. Ma, C. *et al.* RNA m6A methylation participates in regulation of

postnatal development of the mouse cerebellum. *Genome Biol.* (2018) doi:10.1186/s13059-018-1435-z.

221. Sharp, T. M. *et al.* Clinical Characteristics, Histopathology, and Tissue Immunolocalization of Chikungunya Virus Antigen in Fatal Cases. *Clin. Infect. Dis.* (2021) doi:10.1093/cid/ciaa837.
222. Agarwala, S. D., Blitzblau, H. G., Hochwagen, A. & Fink, G. R. RNA methylation by the MIS complex regulates a cell fate decision in yeast. *PLoS Genet.* (2012) doi:10.1371/journal.pgen.1002732.
223. Roberts, G. C. *et al.* Evaluation of a range of mammalian and mosquito cell lines for use in Chikungunya virus research. *Sci. Rep.* **7**, (2017).
224. Schwartz, S. *et al.* High-resolution mapping reveals a conserved, widespread, dynamic meiotically regulated mRNA methylation program. *Cell* (2013).
225. L, N. E. B. T. S. Monarch ® RNA Cleanup Kits Table of Contents. (2020).
226. Masotti, A. & Preckel, T. Analysis of small RNAs with the Agilent 2100 Bioanalyzer. *Nat. Methods* **3**, (2006).
227. Madden, E. A. *et al.* Using SHAPE-MaP To Model RNA Secondary Structure and Identify 3′UTR Variation in Chikungunya Virus. *J. Virol.* **94**, (2020).
228. Utt, A. *et al.* Versatile trans-replication systems for chikungunya virus allow functional analysis and tagging of every replicase protein. *PLoS One* **11**, (2016).
229. Utt, A. *et al.* Design and Use of Chikungunya Virus Replication Templates Utilizing Mammalian and Mosquito RNA Polymerase I-Mediated Transcription. *J. Virol.* (2019) doi:10.1128/jvi.00794-19.
230. Sun, K., Müller, M., Macfarlane, C., Harris, M. & Tuplin, A. A novel interaction between the 5' untranslated region of the Chikungunya virus genome and Musashi RNA binding protein is essential for efficient virus genome replication. *bioRxiv* 2023.03.29.534719 (2023).
231. Hermann, T. & Patel, D. J. RNA bulges as architectural and recognition motifs. *Structure* vol. 8 (2000).
232. Zuker, M. Mfold web server for nucleic acid folding and hybridization prediction. *Nucleic Acids Res.* **31**, 3406–3415 (2003).
233. Johnson, P. Z. & Simon, A. E. RNAcanvas: interactive drawing and exploration of nucleic acid structures. *Nucleic Acids Res.* (2023) doi:10.1093/nar/gkad302.
234. Liu, X. *et al.* Circular RNA: An emerging frontier in RNA therapeutic targets, RNA therapeutics, and mRNA vaccines. *J. Control. Release* (2022) doi:10.1016/j.jconrel.2022.05.043.
235. Zhang, L. *et al.* The role of N6-methyladenosine (m6A) modification in the regulation of circRNAs. *Molecular Cancer* (2020) doi:10.1186/s12943-020-01224-3.

236. Lidbury, B. A. *et al.* Macrophage-derived proinflammatory factors contribute to the development of arthritis and myositis after infection with an arthrogenic alphavirus. *J. Infect. Dis.* **197**, 1585–1593 (2008).

Appendix A

Supplementary Data

#	Position	Sequence context	Structural context	Score(binary)	Score(knn)		Score(spectrum)	Score(combined)	Decision
1	96	AUCAUGGAUCCUGUGUACGUGGACAUAGACGCUGACAGCCGCCUUU	N/A	0.609	0.710	0.496	0.569	m6A site	(Low confidence)
2	352	GCAGUGCGGAAGAUCCCGAGAGACUCGCCAAUUAUGCGAGAAAGC	N/A	0.659	0.583	0.466	0.578	m6A site	(Low confidence)
3	402	UCUGCCGCAGGAAAAGUCCUGGACAGAAACAUCUCUGGAAAGAUC	N/A	0.635	0.639	0.517	0.588	m6A site	(Moderate confidence)
4	429	AACAUCUCUGGAAAGAUCGGGACUUACAAGCAGUAAUGGCCCUG	N/A	0.734	0.581	0.567	0.659	m6A site	(High confidence)
5	1694	AGCGGGCGCAGGAAUAAUAGAGACUCCGAGAGGAGCUAUCAAAGU	N/A	0.629	0.659	0.470	0.567	m6A site	(Low confidence)
6	2128	GUAAGAAGGAAAGAAGCCGCAGGACUGGUUACUGGUGGGCGACUUGA	N/A	0.702	0.589	0.464	0.601	m6A site	(Moderate confidence)
7	2709	UACAACAAGCCGAUUGUAGUGGACACUACAGGCUCAACAAAACCU	N/A	0.637	0.691	0.576	0.615	m6A site	(Moderate confidence)
8	3462	GUGACUACCAGGAGGAUAGAAGACUUUAACCCUACCACCAACAUC	N/A	0.684	0.592	0.503	0.607	m6A site	(Moderate confidence)
9	3669	CCGUUAGGUGUCCGCGGAGGCGGACUACACAUACAACCUAGAGUUG	N/A	0.618	0.413	0.527	0.572	m6A site	(Low confidence)
10	3823	UGCUCGGGGUGACUCAUUGAGACUGCUCAAACCGGCGGCUCUC	N/A	0.586	0.758	0.587	0.595	m6A site	(Moderate confidence)
11	4473	AACCACCUCUUUACAGCCAUGGACUCGACGGAUGCAGACGUGGUC	N/A	0.708	0.693	0.542	0.641	m6A site	(High confidence)
12	4590	CUGGAUGAGCACAUCUCCAUAGACUGCGAUAUUGUUCGCGUGCAC	N/A	0.66	0.668	0.433	0.569	m6A site	(Low confidence)
13	5517	ACGUUCCCCAUUACAUUUGGGGACUUCAACGAAGGAGAAAUCGAA	N/A	0.665	0.700	0.502	0.601	m6A site	(Moderate confidence)
14	5571	UCUGAGCUACUAACUUUCGGAGACUUCUUACCAGGAGAAGUGGAU	N/A	0.554	0.495	0.588	0.565	m6A site	(Low confidence)
15	5902	UGAAAGCAGCAAUCAUCCAGAGACUAAAGAGGCUGUAGACUAU	N/A	0.697	0.568	0.475	0.601	m6A site	(Moderate confidence)
16	5920	AGAGACUAAAGAGAGGCUGUAGACUAUACUUAAUGUCAGAGACCC	N/A	0.584	0.85	0.615	0.610	m6A site	(Moderate confidence)
17	5963	CCCAAAAGUCCCCUACUUACCGGACUACAUAUCCCGGCGCCUGUGUA	N/A	0.633	0.656	0.533	0.594	m6A site	(Moderate confidence)
18	6321	AUGAGGGAAUUACCCACUUUGGACUCAGCAGUAUUCAACGUGGAG	N/A	0.744	0.662	0.496	0.641	m6A site	(High confidence)
19	6777	GGAGACACUGUUUUGGAAACGGACAUAGCCUCCUUUGAUAAGAGC	N/A	0.655	0.678	0.535	0.608	m6A site	(Moderate confidence)
20	6870	GGGGUGGAUCACUCCCUGCUGGACUUGAUAGAGGCUGCUUUCGGA	N/A	0.718	0.649	0.522	0.636	m6A site	(High confidence)
21	7588	AAUGGAGUUCAUCCCAACCCAAACUUUUUACAAUAGGAGGUACCA	N/A	0.599	0.579	0.545	0.576	m6A site	(Low confidence)
22	7624	GAGGUACCAGCCUCGACCCUGGACUCCGCGCCCUACUAUCCAAGU	N/A	0.680	0.698	0.529	0.621	m6A site	(High confidence)
23	8309	UCGGUGGUGACCUGGAAUAAACACAUUGUCACUAAAAUCACCCCC	N/A	0.631	0.675	0.495	0.578	m6A site	(Low confidence)
24	8552	CGCCAGCGACGCAGCACCAAGGACAACUUCAAUGUCUAUAAAGCC	N/A	0.633	0.680	0.528	0.593	m6A site	(Moderate confidence)
25	8835	GUACGAUUACUGGAACAAUGGGACACUUCAUCCUGGCCCGAUGUC	N/A	0.558	0.437	0.586	0.563	m6A site	(Low confidence)
26	9168	AUUGCGGUGGCUCAAAUGAAGACUAACUACAGACAAAGUGA	N/A	0.728	0.588	0.511	0.634	m6A site	(High confidence)
27	9282	CUCUGGUCCCGCGUAAUGCUGAACUUGGGGACCGAAAAGGAAAAA	N/A	0.660	0.806	0.483	0.597	m6A site	(Moderate confidence)
28	9744	GCAGAUGCAUCACACCGUAUGAACUGACACCAGGAGCUACCGUCC	N/A	0.700	0.58	0.368	0.561	m6A site	(Low confidence)
29	10042	CACGGUGGGAGUACCGUAUAAGACUCUAGUCAAUGACCUGGCUA	N/A	0.643	0.63	0.565	0.611	m6A site	(Moderate confidence)
30	10202	UGCGGUACAGCAGAGUGCAAGGACAAAAACCUACCUGACUACAGC	N/A	0.644	0.667	0.448	0.566	m6A site	(Low confidence)
31	10556	AAAGGUGACGUCUAUAACAUGGACUACCCGCCCUUUGGCGCAGGA	N/A	0.687	0.731	0.504	0.616	m6A site	(Moderate confidence)
32	10587	CCUUUGGCGCAGGAAGACCAGGACAAUUUGGCGAUAUCCAAAGUC	N/A	0.635	0.641	0.546	0.600	m6A site	(Moderate confidence)
33	10802	ACAAACCCGGUAAGAGCGGUGAACUGCGCCGUAGGGAAACAUGCCC	N/A	0.614	0.532	0.519	0.572	m6A site	(Low confidence)
34	10925	CCAGCCUGCACCCAUUCCUCAGACUUUGGGGCUGCCCAUUAUU	N/A	0.700	0.656	0.455	0.600	m6A site	(Moderate confidence)
35	11749	AGAAGUAGGCAUAGCAUACCGAACUCUUCCACGAUUCUCCGAACC	N/A	0.645	0.618	0.527	0.596	m6A site	(Moderate confidence)

Supplementary Figure 1. 35 Potential m^{6}A sites in CHIKV Genome.

From Cui Lab SRAMP predictor showing position, sequence context, score, and confidence level of all 35 predicted m^{6}A sites in the CHIKV genomic RNA.

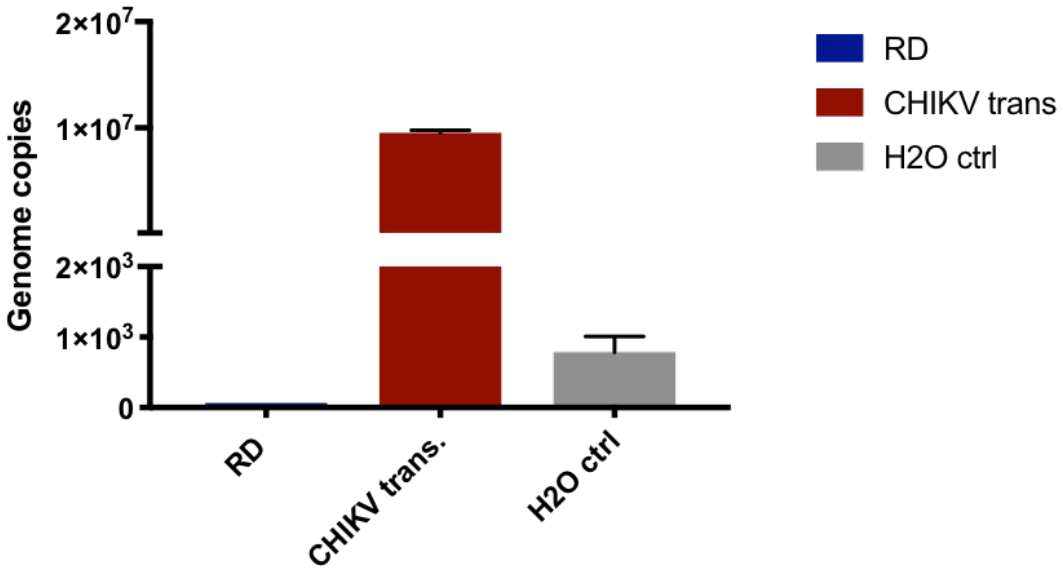

Supplementary Figure 2. RT-qPCR of total RNA extracted from CHIKV sub genomic replicon transfected RD cells prior to MeRIP.

In RD cells which had been transfected with CHIKV sub genomic RNA $1x10^4$ more genome copies detected over the not transfected control after 24 hours and qrt-PCR water control.

n=1, error bars represents standard deviation from the mean from technical replicates.

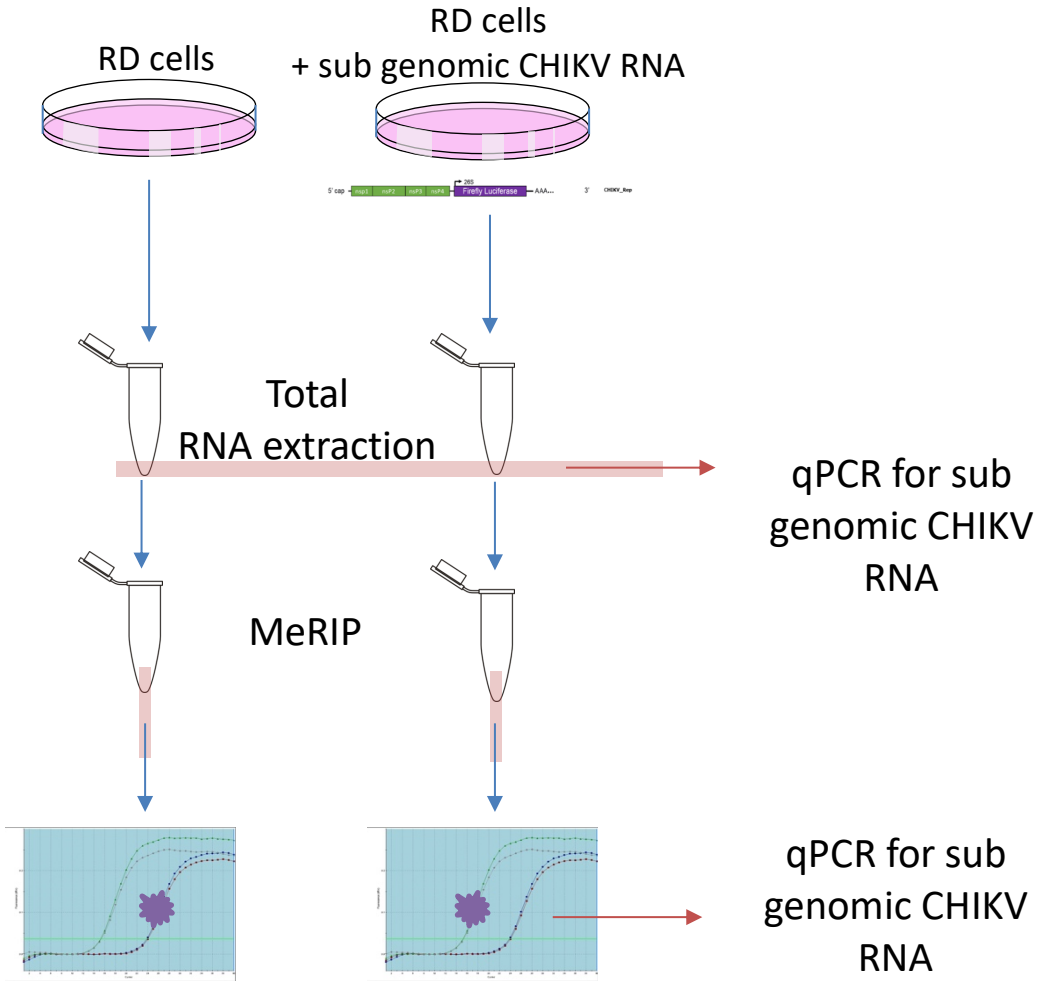

Supplementary Figure 3. m^{6}A IP initial workflow

RD cells were either transfected with CHIKV sub genomic replicon RNA or left not transfected. The cells were lysed 24 hpt. The total RNA was extracted, immunoprecipitated in an MeRIP, and underwent a CHIKV specific qRT-PCR

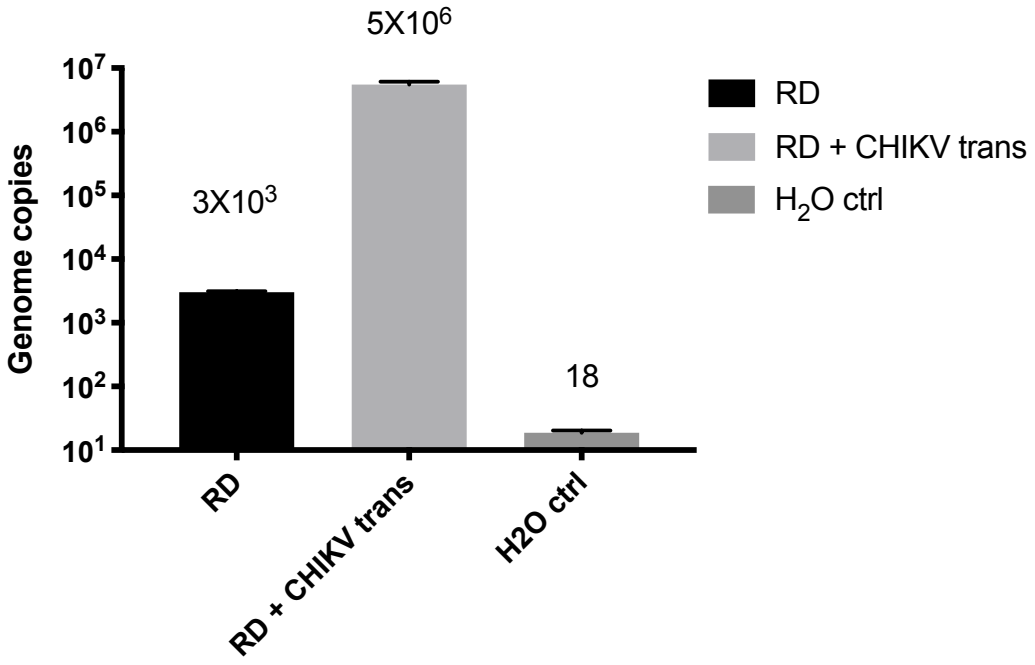

Supplementary Figure 4. CHIKV sub genomic replicon RNA was captured in an MeRIP

Total RNA from RD cells and RD cells transfected with CHIKV SGR RNA was subjected to an m^6A IP. Resulting eluent RNA from was then converted to cDNA and assessed by qRT-PCR with CHIKV specific primers. error bars show standard deviation from the mean for technical replicates, n=1

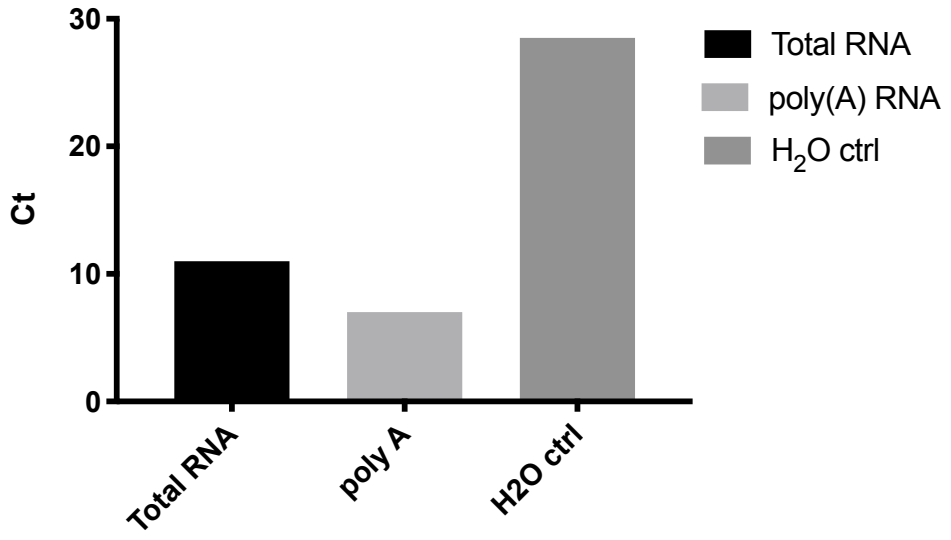

Supplementary Figure 5. qRT-PCR shows CHIKV detection enrichment with Poly(A) selection on RNA from CHIKV infected Huh7 cells

Poly(A) selected RNA requires fewer cycles to detect CHIKV RNA than for total RNA suggesting CHIKV capture and enrichment after poly(A) selection. n=1

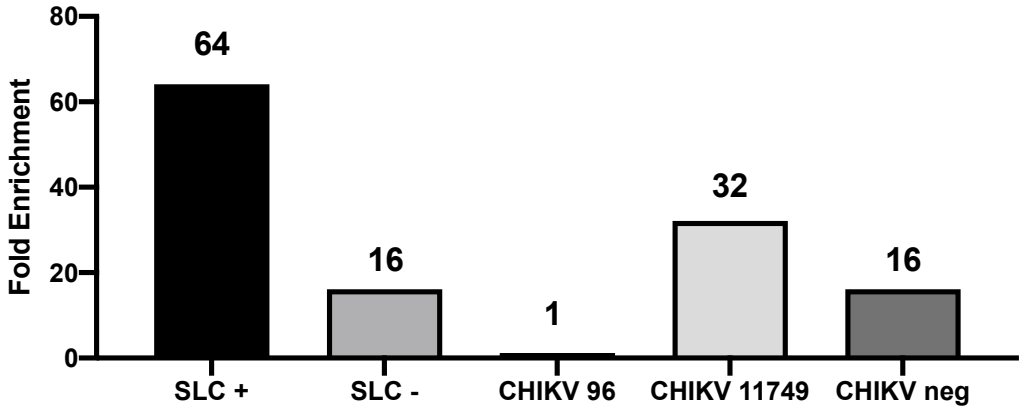

Supplementary Figure 6. MeRIP of poly(A) selected and fragmented total RNA from CHIKV infected Huh7 cells analysed by qRT-PCR SLC

SLC was used as an internal host control in regions of m^6A methylation (+) and devoid of m^6A methylation (-), CHIKV 96 were primers against amplicon including nucleotide position 96^A, CHIKV 11749 were primers against amplicon including nucleotide position 11749^A, CHIKV neg was a region in NSP2 that should not contain DRACH sites. (n=1)

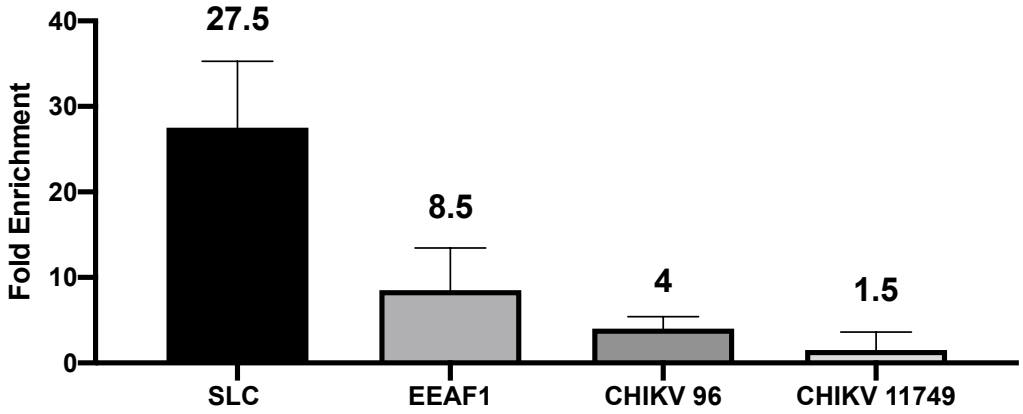

Supplementary Figure 7. MeRIP of Poly(A) selected and fragmented total RNA from CHIKV infected Huh7 cells analysed by qRT-PCR (combining both elutions from the MeRIP m^6A antibody beads).

Primers against SLC, EEAF1, HIKV 96, and CHIKV 11749 amplicons were used. Fold Enrichment rather than the IgG as the negative ($\Delta Ct_{negative}$) to calculate the fold change. error bars represent standard deviation from the mean, (n=2).

	CHIKV neg	CHIKV 96	CHIKV 11749	SLC+	SLC-
Input	**21**	**21**	**18**	**22**	**23**
IgG	**29**	**24**	**29**	**32**	**35**
Anti-m^{6}A	**25**	**24**	**24**	**26**	**31**

Supplementary Figure 8. qPCR Cq values for MERIP of 2 µg mRNA

Raw qrt-PCR Cq values from either the Input RNA samples, or RNA eluted from the IgG or anti-m^{6}A antibody coated beads. The 2 µg of RNA used in each immunoprecipitation in this experiment was poly(A) selected and fragmented prior to immunoprecipitation. The labels across the top indicate the primer sets used. For the negative control of this experiment IGG antibody coated beads were used to immunoprecipitate any nonspecific m^{6}A binding RNA fragments. Values were an average of two technical replicates.

	SLC+	SLC-	EEAF1+	EEAF1-	CHIKV 96	CHIKV 11749	CHIKV neg	GAPDH +	GAPDH -
Input	**25**	**26**	**20**	**22**	**25**	**21**	**24**	**18**	**19**
Anti-m^{6}A	**33**	**X**	**33**	**33**	**29**	**28**	**32**	**30**	**30**
H_20 (control)	**X**	**X**	**34**	**40**	**29**	**27**	**31**	**34**	**X**

Supplementary Figure 9. Cq value for 0.5 µg mRNA MeRIP

Raw qrt-PCR Cq values from either the Input RNA samples, or RNA eluted from the anti-m^{6}A antibody coated beads. The 0.5 µg of RNA used in each immunoprecipitation in this experiment was poly(A) selected and fragmented prior to immunoprecipitation. The labels across the top indicate the primer sets used. For the negative control of this experiment were SLC-, EEAF1-, and CHIKVneg. Values were an average of two technical replicates.

N1	SLC+	SLC-	EEAF1+	EEAF1-	CHIKV 96	CHIKV 11749	CHIKV neg
Input	21	23	20	18	19	18	18
Anti-m^6A	24	30	23	24	24	24	24
H_20 (control)	X	X	38	X	X	X	X
N2	SLC+	SLC-	EEAF1+	EEAF1-	CHIKV 96	CHIKV 11749	CHIKV neg
Input	22	23	21	19	22	20	20
Anti-m^6A	27	33	28	28	28	28	25
H_20 (control)	X	X	X	X	30	29	30

Supplementary Figure 10. Cq values for 4 µg mRNA MeRIP

Raw qrt-PCR Cq values from either the Input RNA samples, or RNA eluted from the anti-m^6A antibody coated beads. The 4 µg of RNA used in each immunoprecipitation in this experiment was poly(A) selected and fragmented prior to immunoprecipitation. N1 is the first independent experiment and N2 is the second independent experiment that was performed. The labels across the top indicate the primer sets used. For the negative control of this experiment were SLC-, EEAF1-, and CHIKVneg. Values were an average of two technical replicates.

	SLC+	SLC-	EEAF1+	EEAF1-	CHIKV 96	CHIKV 11749	CHIKV neg	GAPDH	GAPDH
Input	**21**	**22**	**18**	**18**	**17**	**18**	**16**	**22**	**20**
Anti-m^6A	**27**	**30**	**26**	**21**	**24**	**19**	**24**	**31**	**30**
H_20 (control)	**X**	**X**	**X**	**X**	**X**	**X**	**X**	**X**	**X**

Supplementary Figure 11. Cq value for 30 µg total RNA MeRIP

Raw qrt-PCR Cq values from either the Input RNA samples, or RNA eluted from the anti-m^6A antibody coated beads. The 30 µg of RNA used in each immunoprecipitation in this experiment was fragmented prior to immunoprecipitation. The labels across the top indicate the primer sets used. The negative control of this experiment were SLC-, EEAF1-, and CHIKVneg. Values were an average of two technical replicates.

Unfragmented Total RNA	SLC+	SLC-	CHIKV E1	GAPDH 1	GAPDH 2
Input	18	19	13	14	14
m^6A	21	21	14	18	17
IgG	31	31	25	25	25
H_20 (control)	X	X	33	X	36

Fragmented Total RNA	SLC+	SLC-	CHIKV 96	CHIKV 11749	CHIKV neg	GAPDH 1	GAPDH 2
Input	21	22	19	23	19	17	17
m^6A	27	32	27	27	28	27	26
IgG	31	31	28	27	28	25	25
H_20 (control)	X	X	29	25	32	17	X

Supplementary Figure 12. Cq values for total RNA MeRIP

Raw qrt-PCR Cq values from either the Input RNA samples, or RNA eluted from the IgG or anti-m^6A antibody coated beads. The total RNA used in each immunoprecipitation in this experiment was either fragmented to 100 nt or left unfragmented prior to immunoprecipitation. The labels across the top indicate the primer sets used.

Unfragmented polyA selected RNA	**SLC+**	**SLC-**	**CHIKV E1**	**GAPDH 1**	**GAPDH 2**
Input	**19**	**19**	**13**	**13**	**12**
m^6A	**22**	**22**	**15**	**19**	**18**
IGG	**39**	**40**	**32**	**30**	**30**
H20 (control)	**X**	**X**	**32**	**37**	**37**

Fragmented poly A selected RNA	**SLC+**	**SLC-**	**CHIKV 96**	**CHIKV 11749**	**CHIKV neg**	**GAPDH 1**	**GAPDH 2**
Input	**21**	**22**	**23**	**20**	**21**	**15**	**15**
m^6A	**29**	**34**	**28**	**28**	**32**	**27**	**28**
IGG	**35**	**40**	**30**	**26**	**32**	**30**	**30**
H20 (control)	**X**	**X**	**29**	**27**	**34**	**37**	**35**

Supplementary Figure 13. Cq values for poly(A) selected RNA

Raw qrt-PCR Cq values from either the Input RNA samples, or RNA eluted from the IgG or anti-m^6A antibody coated beads. The RNA used in each immunoprecipitation in this experiment was first poly(A) selected and then either fragmented to 100 nt or left unfragmented prior to immunoprecipitation. The labels across the top indicate the primer sets used.

A

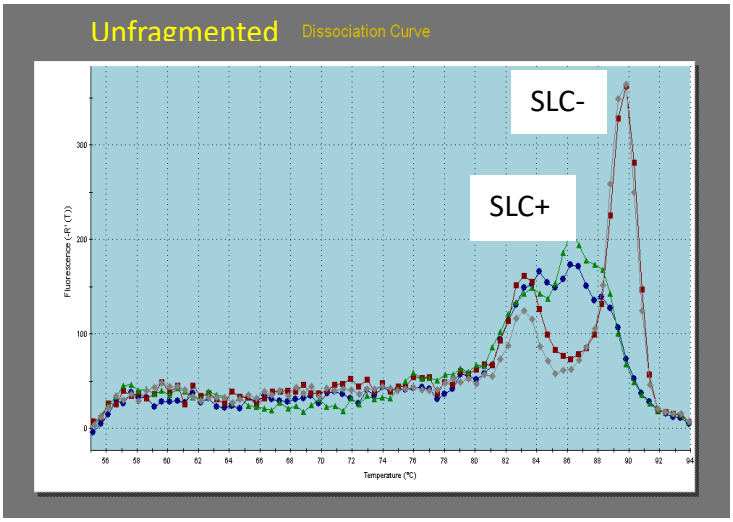

B

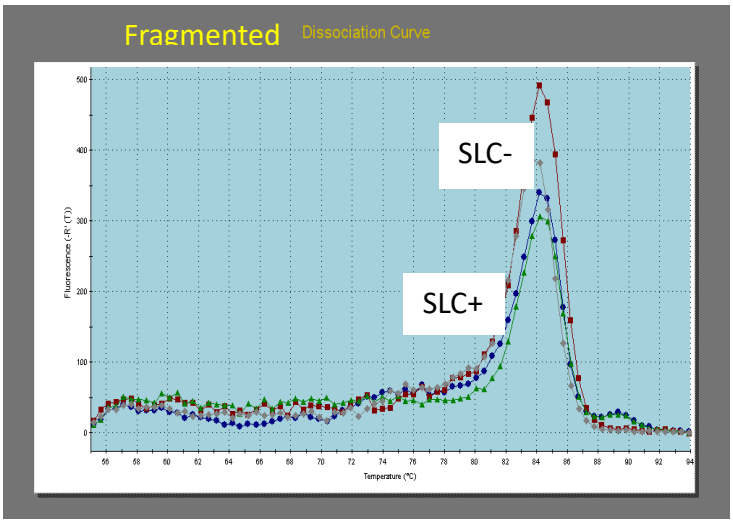

Supplementary Figure 14. Dissociation Curves for Input total RNA using SLC + and SLC- Primer sets

A. Unfragmented total RNA shows two different dissociation curves for primer set SLC + (blue and green curves, done in technical replicate) and primer set SLC – (red and grey curves, done in technical replicate).

B. Fragmented total RNA shows the same dissociation curve at 94 °C for primer set SLC + (blue and green curves, done in technical replicate) and primer set SLC – (red and grey curves, done in technical replicate).

A

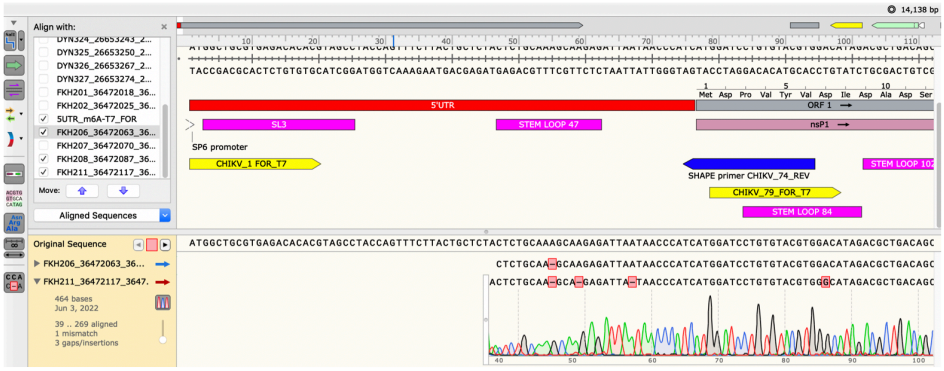

B

Supplementary Figure 15. CHIKV ICRES plasmid with A>G mutation at the 96 and 11749 position

A. Sanger sequencing read showing an example of the $^{A}96^{G}$ IC CHIKV plasmid.
B. Sanger sequencing read showing an example of the $^{A}11749^{G}$ IC CHIKV plasmid.

The colour peaks represent the corresponding base and clarity of the read.

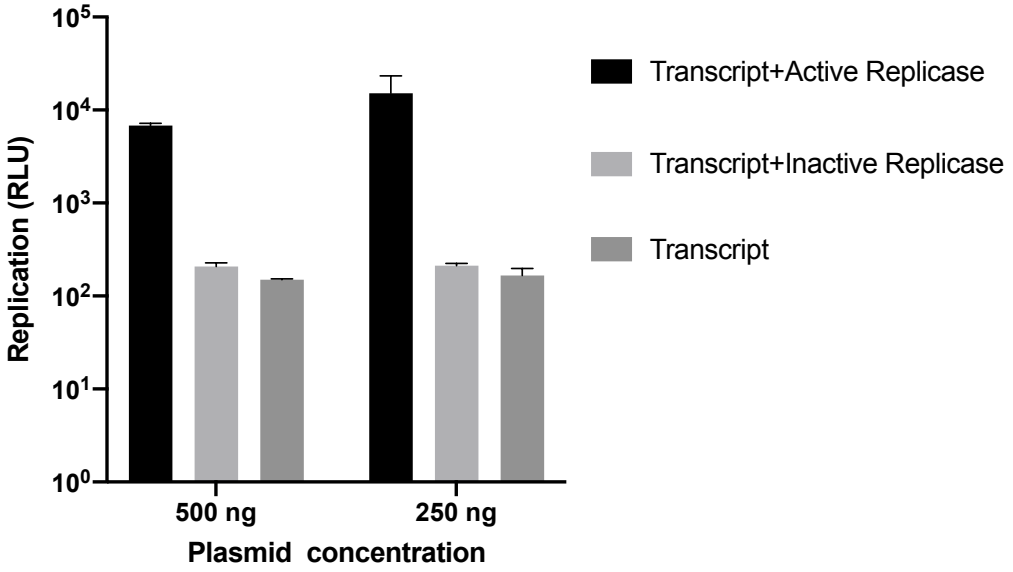

Supplementary Figure 16. Optimization of Trans-complementation Assay in C636 cells

Transfection of C636 cells with 500 ng versus 250 ng each of the transcript and replicase plasmid shows that there were similar levels of Gaussia luciferase detected for either concentration of plasmid.

N=2, Experiments were done in biological duplicate and analysed in technical duplicate, error bars represent standard deviation from the mean